Non-local interactions in Bose-Einstein Condensates

by

Abhijit Pendse

A thesis submitted in partial fulfillment for the
degree of **Doctor of Philosophy**

at the

Department of Physics

IISER PUNE

Indian Institute of Science Education and Research, Pune

February 2019

Declaration of Authorship

I, Abhijit Pendse, declare that this thesis titled, **'Non-local interactions in Bose-Einstein Condensates'** and the work presented in it are my own. I confirm that:

- This work was done wholly while in candidature for a research degree at IISER Pune.

- Where I have consulted the published work of others, this is always clearly attributed.

- Where I have quoted from the work of others, the source is always given. With the exception of such quotations, this thesis is entirely my own work.

- I have acknowledged all main sources of help.

Abstract

Bose-Einstein Condensates (BECs) are treated theoretically using the mean field Gross-Pitaevskii (GP) equation. Instead of using the local (δ-function) psueudopotential to account for the symmetric s-wave scattering between bosons, we take an extended pseudopotential to account for the finite range of inter-boson interactions. Such a pseudopotential would give corrections on top of the GP equation with local interactions. We first propose the energy functional for such correction terms added to the local GP equation. We then study the effect of finite range of interactions on the vortex solution, soliton solution and the excitation spectrum in a BEC. We see that the additional length scale emerging from the range of the inter-Boson interactions plays a significant role in the aforementioned excitations.

Acknowledgements

It is my pleasure to have this opportunity to acknowledge all the people who have made my PhD. a memorable and joyful experience. I would like to start by thanking my thesis supervisor, Dr. Arijit Bhattacharyay, from whom I have learned so much. The knowledge and teachings that I have received is too intricate a collage to be encoded into words. Nevertheless, I can say for sure that I would be forever grateful for the guidance and encouragement provided by him towards becoming an independent researcher.

My time at IISER Pune was made fun and a great learning experience by so many friends and colleagues that it would be unfair to name a few and too long a list that I am afraid it would turn out into a page full of names. I would just say that if you are reading this Acknowledgement, you know who you are and I am extremely thankful to you for being such cool friends! Outside of IISER Pune, I have had a great time with my friends from Pune University, Abdul, Deepesh, Mihir, Kaustubh and Anup. I would also like to mention my good old buddies who joined me in the much needed friendly outings. I would like to thank Gandhar, Jagdishwar and Pradyumna for this.

I owe a major part of my teaching and extra-curricular experience to DISHA, the student organization at IISER Pune which contributes to social causes, primarily by promoting scientific temper in socially-disadvantaged children through various activities. By teaching kids in DISHA I have learned a lot about the process of teaching and understanding. It has helped me a great deal in organizing my knowledge and delivering it effectively to an audience. It has also helped me gain organizational experience. DISHA has been the most engaging and fruitful part of my extra-curricular activities on campus. I would be forever indebted for the plethora of teachings in various areas received by me while working as a volunteer.

Lastly and most importantly, I would like to thank my family for the love and support extended by them. It gives me great joy to conclude my Acknowledgements by mentioning the two most encouraging and loving people in my live, my Mother and Father. Thank you for everything...

Contents

Bibliography **110**

List of Figures

Chapter 1

Introduction

The quantum revolution in 1920s brought about a change in understanding of the microscopic world. One of the major influences of quantum theory was in the field of particle statistics in that it convinced S. N. Bose at the University of Dhaka that Maxwell-Boltzmann statistics could not describe quantum particles due to Heisenberg's Uncertainty principle [1]. This led him to propose a new statistics for photons for predicting the coefficient in Planck's law [2]. Extending this idea to non-interacting particles, Einstein showed that such a statistical description predicted a macroscopic occupation of the ground state for an ideal Bose gas (gas of non-interacting particles obeying Bose statistics) below a critical temperature, a phenomenon called as Bose-Einstein Condensation (BEC) [3].

With the theoretical prediction of existence of BEC, there began search for such a phenomenon experimentally. In 1938 Fritz London proposed that BEC was the reason for superfluidity in helium-4 and also for the phenomenon of superconductivity [4]. However, as these systems were strongly interacting and as BEC was proposed in a non-interacting gas, there was much debate about the proposal by London. Hence, there was a search for a weakly interacting gas which can be cooled below the critical temperature required to achieve BEC. Due to its low interaction strength and high critical temperature, hydrogen was thought to be the most probable candidate [5]. However, even for hydrogen the critical temperature was of the order of a few hundred nanokelvin and due to limitation of cooling mechanisms at the time, this temperature was not achievable. A major step forward in the process of cooling was in the form of laser cooling in the 1970s [6–8]. From here, cooling to progressively lower temperatures was realized in atomic gases. With the final step in the form of discovery of evaporative cooling, a BEC was finally achieved in 1995 in a gas of rubidium-87 atoms [9]. The reason of it not being achieved in hydrogen

earlier will be explained in the next chapter. However, a BEC of hydrogen atoms was achieved later in 1998 [10].

While on the one hand there was technological advance in achieving BEC in a weakly interacting Bose gas, there were also major advancements in theoretical description of BEC. The most important development was the discovery of the mean-field Gross-Pitaevskii (GP) theory describing the ground state of a gas of weakly interacting bosons [11]. One of the major proposition of the GP theory was that there existed quantum coherence in the aggregate of atoms in the BEC phase and that such an aggregate may be described by a macroscopic wave-function. The GP equation that was derived is the Schrodinger equation with an added non-linear term, with the modulus squared of the wave-function describing the condensate density. This gave BECs the contemporary fame of being a *macroscopic quantum phenomenon*.

BEC being a superfluid, one of the most important excited state which can be achieved is the vortex state with quantized angular momentum [12, 13]. In superfluid helium, the quantized vortices have a very small core to be able to probe. However, the vortex core in a BEC is comparatively larger and hence can be probed. With the tunability of interactions, this core width can be further adjusted. Further, due to the non-linear nature of the GP equation, solitons may be excited in it [14, 15]. In the case of solitons too, the room for tuning the interactions and trapping is a huge plus point which allows to probe solitons under various conditions.

Due to the wide-tunability of interactions in a BEC, it has become a tool to test the quantum theory. With the advent of trapping techniques like optical lattices, BECs came to be used as analogs to condensed matter systems [16–18]. Here too, the tunability of interactions and the variety of traps that may be engineered are assets. Another important variation that may be obtained is the realization of BEC with many distinct components [19]. These *multi-component* BEC may be obtained in miscible or phase-segregated states [20]. The strength of interactions may be tuned to go from one state to another. Further, BECs are also being used as analog gravity systems [21–24]. They have also been used in atom lasers [25–28], atomic clocks [29], atom interferometer [30, 31], slowing light speed [32], atom holography [33], etc.

An important parameter in BEC is the gas parameter '$a^3 n$,' also called the diluteness parameter. The mean-field GP theory using contact interactions has had a huge success in describing many phenomenon in BEC for an extremely dilute gas with $a^3 n \ll 1$ and weak trapping. In this case, the finite range effects of the BEC do not show up [34]. However, when $a^3 n \to 1$ and/or in the presence of strong trapping, the assumption of contact interactions fail and we have to consider finite range of interactions [35, 36]. This may be accounted for as a perturbation on top of the theory with contact interactions. It

is then important to study the effect of these finite range corrections on the excitations in a BEC like vortices, solitons and small amplitude oscillation modes. It is these effects that will be addressed in this thesis.

Figure 1.1: Figure shows the December 1995 cover of 'Science' magazine which bestows the honour of '*Molecule of the year*' upon the discovery of Bose-Einstein Condensate (BEC) in rubidium-87 atoms in the same year. The cover shows an artist's conception of a BEC, where atoms in a condensate march as a group, while atoms out of the condensate move with various speeds in various directions. From *Science, Vol 270, Issue 5244, 22 December 1995.* Reprinted with permission from AAAS.

1.1   The gas parameter and the diluteness limit

The GP theory describing the dynamics of a BEC is based on certain assumptions. The most important assumption is that of the diluteness of the gas which means that the average inter-particle distance is very large as compared to the range of inter-particle interactions. In this limit, the probability of two body interactions is very high as compared to three body or higher interactions [37]. As such, the dominant interaction between the particles in a BEC is that of two-body scattering.

As BEC is the macroscopic occupation of zero-momentum ground state with very low spread in the momentum space, the average speed of the atoms in the BEC is very low. As such, an additional assumption can be made to the two body scattering mechanism.

This assumption is that the dominant scattering amplitude is the s-wave scattering amplitude [38]. This is equivalent to assuming the energy independence of the scattering process. Given a range r_0 for inter-particle interactions in a BEC with average density n, the diluteness criterion $r_0 \ll n^{-1/3}$ translates to $a \ll n^{-1/3}$ for energy independent scattering [39]. This defines the diluteness limit $a^3 n \ll 1$ for a BEC. Due to the diluteness criterion and s-wave scattering, the actual interaction potential is replaced by a δ-function pseudopotential, such that the pseudopotential preserves the strength of interactions [40]. This is because for a dilute gas the details of the inter-atomic interaction potential are not seen by the interacting particles as most of the time they are far away from each other. However, for larger values of gas parameter and/or strong trapping of BEC, we must go beyond the contact interaction pseudopotential [35, 36]. Such conditions are not artificial and BECs with high values of gas parameter have been realized experimentally [41, 42]. There have been various studies to account for the finite range effects of the interaction between particles in a BEC and they have proposed finite range corrections to the GP equation with contact interactions [35, 36]. These corrections are different from the LHY correction [43]. The effect of such corrections on the excitations in a BEC has only partially been studied to the best of our knowledge.

1.2 Energy functional of the GP theory

The GP equation may also be derived from the principle of least action. As the system is conservative, the least action principle gives a well-defined energy functional. This energy functional describes the energy cost for the BEC to be in a particular state described by a wave-function. The ground state for the BEC can then be described by minimizing this energy functional. Therefore, this energy functional is important in determining the ground state of the system. The energy functional for the GP equation with local interaction pseudopotential is well-known [44]. However, when there occur finite range corrections to the GP equation, it is essential to determine the energy functional of the GP equation with corrections. There have been studies which propose the change to the energy of the ground state of the BEC for corrections to the local GP equation up to the first order [43]. However, depending upon the system parameters, there may arise a necessity to include corrections to the local GP equations up to an arbitrary order. As such it is helpful to find corrections to the GP energy functional, given corrections to the local GP equation up to an arbitrary order. We have studied this problem and given the energy functional for corrections to the local GP equation up to an arbitrary order. In this thesis we show a term by term correspondence between the corrections to the local GP equation and the energy functional. This we have shown using simple combinatorics [45]. While this proof may seem straightforward, it is worth

noting that such a correspondence does not exist for corrections with odd symmetry and we have proved this as well. With the energy functional proposed, we have the requisite toolkit for probing the effect of correction terms to the excitations in a BEC. We particularly probe the effect of these corrections on the vortex state, solitons and excitation spectrum of a BEC.

1.3 The analogous Quantum hall effect

BECs are very popular as analogue systems to simulate phenomenon in other areas of physics with a large degree of control. One such phenomenon that may be simulated is the quantum hall effect in two dimensional electron systems subject to low temperatures and strong magnetic field [46]. This effect essentially lies in the formation of vortices in electron systems with integer or fractional filling fractions. To simulate such a system in BEC requires generation of vortices with low filling fraction. As the number of vortices increases, the length scale of fluctuations becomes of the order of distance between two vortex cores. This results in a melting transition to a vortex liquid [47]. An elementary estimate of the filling fraction where such a transition occurs can be obtained using the Lindemann criterion which historically gave a crude model for melting transition in solids [48]. Such an estimate puts the filling fraction required for melting transition at $\nu \sim 10$, where ν is the vortex filling fraction [49]. An exact diagonalization study using periodic boundary conditions estimated the filling fraction to lattice melting transition to occur at $\nu \sim 6$ [50]. As angular velocity for vortex generation is provided by rotating a BEC, such requirement of low filling fractions would take us into the regime of ultra-fast rotation. In this regime, a lot of interesting states have been proposed [51–54]. Despite this theoretical work, the goal of achieving such high rotation frequencies in trapped BEC has remained a challenge. This is mainly because of the high rotation frequencies required to achieve such states. When the frequency of rotation approaches the trap frequency, there occurs an instability due to which the condensate flies off the trap [55]. An attempt to surmount this problem has been made using a steeper trapping potential, which has helped push the angular frequency of rotation a bit above what is done using the harmonic potential [56]. In spite of this the filling fraction achievable remains around $\nu \sim 500$ [57, 58]. The low filling fractions required are still elusive.

Another method of obtaining low filling fraction in a vortex lattice may be to obtain thinner vortices. Obtaining thinner vortices will help fit more vortices in a given two dimensional area, thus achieving lower filling fractions. However, this angle has only being partially looked upon due to the dependence of the size of the vortex on the system parameters. The size of the vortex core is of the order of healing length $\xi_0 = 1/\sqrt{8\pi an}$

for a BEC with contact interactions, where a is the s-wave scattering length and n is the density of the condensate. Thus decreasing the size of the vortex means increasing the scattering length or the density of the condensate, or both. This would lead to three body losses which is not desirable. Had the dependence of the vortex width on the system parameters been the opposite, this angle of reducing the vortex width to obtain lower filling fractions would have definitely been explored. In this thesis, it is shown that in the presence of finite range corrections to the GP equation with contact interactions, a new class of vortex solution may be obtained whose width is directly proportional to the s-wave scattering length. Thus, by decreasing the scattering length we may decrease the width of such a vortex solution. This raises the possibility of obtaining thinner vortices and obtaining smaller filling fractions. We shall also propose an experimental setup to obtain such a thin vortex.

1.4 Solitons as a non-locality probe

Non-linear equations have certain characteristic excitations, one of them being the 1 dimensional soliton solutions. In the nonlinear GP equation, solitons result from the balance between the dispersive kinetic term and the focusing non-linear term [15]. Dark solitons may be obtained in a BEC with repulsive interactions, while bright solitons may be obtained in a BEC with attractive interactions. The method to generate these solitons in a BEC is by strong confinement along the radial direction in a 3 dimensional BEC, thus effectively confining it to 1D [59–61]. This is because in two and higher dimensions, there occur instabilities which lead to soliton decay. A characteristic of the soliton solution is that its length scale is of the order of the healing length ξ_0 for a BEC with contact interactions. Therefore, it is but natural to expect a change in the length scale of soliton solution upon introduction of corrections to the GP equation. It is also important to look at the effect of the correction terms on the stability of soliton solution.

An important question for the GP equation with correction is the determination of the effective range of interactions which occurs in the coefficient of correction. It is known that upon the introduction of correction to the GP equation, the healing length of the BEC gets modified [62]. This modified length captures the effect of finite range of interactions. Therefore, it is important to probe if the modified healing length shows up as the width of soliton. If it does, then by measuring the change in width of the soliton, one may measure the effective range parameter. Thus, solitons can be used as a probe to measure the effect of finite range of interactions in a BEC. In this thesis, we address the question of change in the width of the soliton solution and its stability and propose the use of soliton as a length scale probe.

1.5 The roton minimum in BEC

The elementary excitation spectrum of a superfluid gives us important information like the coherence length, and the critical velocity above which superfluidity is destroyed. BEC being a superfluid, it is important to derive its elementary excitation spectrum. BEC with contact interactions gives a phonon like dispersion relation for large wavelengths and particle like excitation spectrum for smaller wavelengths [34, 63–65]. Further, long range interactions have been known to introduce a roton minimum in the excitation spectrum [66–68]. These long range interactions in a BEC are introduced in the form of dipolar interactions [69, 70], rydberg interactions [71], spin-orbit coupling [72–74], etc. However, even in the absence of such additional long range interactions, roton minimum may be obtained using the finite range of inter-atomic interactions in a BEC. Such kind of appearance of roton minimum was first shown by Pomeau *et al.* [66]. The appearance of roton minimum in the presence of soft-core interactions has also been shown [67, 68]. The appearance of roton minimum is essential mainly for the purpose of obtaining zero energy excitations, meaning obtaining a solid order in a superfluid. This phase is also called the supersolid phase. Such a supersolid phase may be obtained by lowering the roton minimum [75, 76]. It is proposed that this be done either by increasing the range of interactions, or their strength, or both.

A multi-component BEC implies the presence of BEC with multiple species [19]. The dynamics of a component in this multi-component BEC is described by the GP equation by introducing additional terms [77]. As such, the presence of multiple components generate additional interactions. While the effect of finite range interactions on the generation and lowering of roton minimum has been studied, the effect of multiple components on the roton minimum has only partially being studied. The main issue of lowering roton minimum using the finite range of inter-boson interactions is that one needs to venture into strongly interacting BECs to lower the roton minimum [66]. This creates three body losses and hence it is important to reduce these three body losses for experimentally achieving roton lowering using just the s-wave interactions. This is where presence of multiple components in a BEC may come in handy. As the presence of multiple components generate additional interactions, the addition of multiple components may result in lowering of roton minimum at a lower value of gas parameter. We probe this angle and show that indeed this is the case.

We have thus discussed in brief the motives of the thesis and the importance of the works undertaken in the thesis. In the next chapter, we give an overview of the technical concepts that will be required to understand our works. After this technical overview, we present four chapters which will explain the works done by us. We start by rigorously deriving the energy functional for corrections to the local GP equation. We then see

effect of non-local interactions on the vortex solution in a BEC. Afterwards, we probe the effect of non-local interactions on the soliton solution in a BEC. Lastly we study the effect of finite range of interactions on the elementary excitation spectrum in a BEC for single as well as multi-component BEC. We end by presenting a conclusion and possible future works that may be undertaken based on the works presented in this thesis.

Chapter 2

General theory of Bose-Einstein Condensates

With the introduction presented in the previous chapter, let us review the general theory of Bose-Einstein Condensates (BECs) along with its experimental realization in this chapter. BEC being a statistical phenomenon characterized by macroscopic occupation of the zero momentum ground state, its theory has to be formulated using statistical methods. As we are dealing with bosons which are quantum particles, one uses Bose statistics which describes the statistical behaviour of bosons. An elementary description of a Bose gas considers a system of non-interacting bosons. This system serves two purposes; firstly it is simpler to treat than a gas of interacting bosons and second that it shows the existence of the phenomenon of BEC. From this we can build up on the theory of weakly interacting bosons, which is the condition in BECs of dilute atomic gases.

In what follows, we shall start by having a brief overview of particle statistics which will show qualitatively how the phenomenon of macroscopic occupation of ground state is unique to Bose-Einstein statistics. We shall then describe in some detail the phenomenon of BEC in a system of non-interacting bosons. Next, we will have a quick look at the density matrix representation, the concept of off-diagonal long range order (ODLRO) and the basics of scattering theory, which are essential to study a weakly interacting gas of bosons. Having set the stage with all the requisite mathematical toolkit, we shall describe in some detail the mean-field theory of weakly interacting gas of bosons. This study of BEC with weakly interacting particles will include a study of BEC with multiple components as well. After this, we shall present an analysis of BEC in traps. This is of immense importance since trapping atoms is a crucial step in obtaining a BEC. Finally, we shall present a brief overview of the most important part of the field of BEC,

the experiments. BECs were theoretically proposed way back in 1925, but the boom in study of BEC resulted from the experimental realization of BEC in atomic gases in 1995 [9, 78]. Hence, it is extremely important to study this monumental achievement and it would only be appropriate to end a chapter on the overview of BECs with the description of the experimental methods required to achieve it.

2.1 Review of particle statistics

Statistical mechanics uses tools of probability theory for the microscopic constituents of a system to predict its average macroscopic observables. Since we wish to look at the phenomenon of BEC, we shall concentrate on only one macroscopic observable, which is the average number of particles in a particular energy state. We shall see what does this average occupancy depend upon. An important point to specify here is that we will be dealing with non-interacting particles in this section. Our main aim in this section is to show how the phenomenon of macroscopic occupation of ground state is unique to Bose statistics in a system of non-interacting particles.

The particle statistics are divided into two main categories, viz., the classical statistics (for classical systems) and quantum statistics (for quantum systems). The major difference between the two being that classical particles are distinguishable and quantum particles are not. Classical systems are described by the Maxwell-Boltzmann (MB) statistics which considers an aggregate of distinguishable particles. Therefore, MB statistics doesn't apply to an aggregate of quantum particles, except in cases where the quantum nature of particles is suppressed due to thermal or other effects. However, when the condition of high temperature and/or very low density is absent, we need to consider the quantum nature of the particles. Such aggregates are described by quantum statistics. Quantum statistics are further divided into two categories as a result of the spin-statistics theorem, which states that quantum particles can either have half-integer spin or integer spin. Particles with half integer spin, the fermions, are described by the Fermi-Dirac (FD) statistics and particles with integer spin, the bosons, are described by the Bose-Einstein (BE) statistics.

In what follows, we describe these three particle statistics in short, the MB statistics, the FD statistics and the BE statistics with regards the average number of particles in each energy state.

2.1.1   Formulation of the problem

An aggregate of non-interacting particles is easy to treat statistically since the partition function for such a systems factors out. Let us start by considering an ideal gas with a discrete set of energy levels. Let the discrete energy levels be labeled by $\epsilon_1, \epsilon_2, \epsilon_3, ...$, with particle occupancy $N_1, N_2, N_3, ...$, respectively. Therefore, the energy of the system in a configuration 'R' with particular values of $N_1, N_2, N_3, ...$, the total energy of the system is $E_R = \sum_r N_r \epsilon_r$. If the system obeys particle conservation, we have an additional constraint $\sum_r N_r = N$. As mentioned before, we assume that the particles are non-interacting. The partition function of such a system can be written as

$$Z = \sum_R e^{-\beta E_R} = \sum_R e^{-\beta(N_1\epsilon_1 + N_2\epsilon_2 + ...)} \ ,$$

where the sum over 'R' implies sum over all the possible distribution of particles in different energy states. This partition function would determine the thermodynamic characteristics of the system. We are interested in the mean occupation number of an energy level ϵ_s. We shall answer this question by considering a grand-canonical ensemble to derive mean occupation number $\widehat{N_s}$ for an energy state with energy ϵ_s. This result would also hold for a canonical ensemble in the thermodynamic limit.

2.1.2   Comparison of MB, FD and BE statistics

With the description of various quantities in the system in the previous section, we now look at the behaviour of the mean occupation number $\widehat{N_s}$ for an energy level ϵ_s. It is given by the expression [79]

$$\widehat{N_s} = \frac{1}{e^{(\epsilon_s - \mu)/kT} + a}.$$

In the above expression μ is the chemical potential and 'a' is the factor which distinguishes the particle statistics and can take values $+1$ (FD), 0 (MB) and -1 (BE). The different values of a are described as follows

(**A**) The case $a = 0$ describes the MB statistics. It is worth noting here that in the limit $e^{(\epsilon_s - \mu)/kT} \gg 1$, FD and BE statistics merge to MB statistics. This is the limit where quantum effects are insignificant and the aggregate of particles can be treated classically in which case $\widehat{N_s} = e^{(\mu - \epsilon_s)/kT}$. From this expression, it can be seen that for higher temperatures, all the energy states ϵ_i are almost equally filled.

(**B**) The case $a = +1$ describes FD statistics. In this case it is worthy to note that since $e^{(\epsilon_s - \mu)/kT}$ is always positive, the mean occupation number $0 < \widehat{N_s} < 1$. This reflects Pauli's exclusion principle, which states that no two fermions can occupy the same energy state. The value of $\widehat{N_s}$ tends to its maximum value for $\epsilon_s < \mu$ and $|\epsilon_s - \mu| \gg kT$. For this limit $\widehat{N_s} \to 1$.

(**C**) The case $a = -1$ corresponds to BE statistics. This case is of interest since for $e^{(\epsilon_s - \mu)/kT} \to 1$, the mean occupation number diverges. Looking at the expression for the mean occupation number, for $\widehat{N_s}$ to remain positive, we should have $e^{(\epsilon_s - \mu)/kT} \geq 1$ and consequently $\mu < \epsilon_i$ for any i. Here, an interesting phenomenon happens when μ comes very close to the lowest energy level ϵ_0 (say). In this case $e^{(\epsilon_s - \mu)/kT} \to 1$ and the probability of occupation of the energy level ϵ_0 diverges. Thus, there occurs a macroscopic occupation of this lowest energy level of the system, which is the phenomenon of Bose-Einstein Condensation.

Fig.(2.1) shows the mean occupation number for the three statistics. As was described earlier, for high values of $(\epsilon_s - \mu)/kT$, the quantum statistics converge to the classical MB statistics. Also to note is the interesting phenomenon of divergence of mean occupation number for BE statistics.
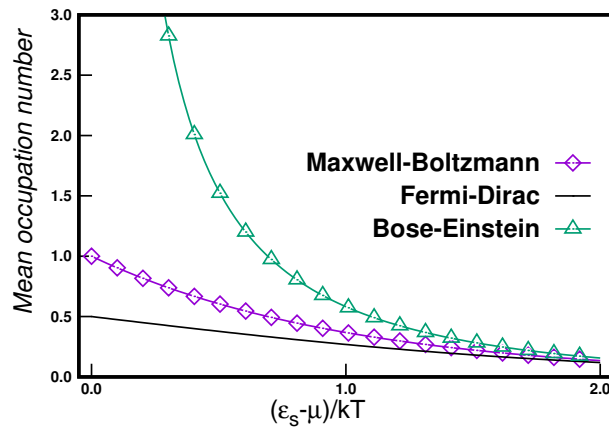
Figure 2.1: Figure shows the mean occupation number for Maxwell-Boltzmann (MB), Fermi-Dirac (FD) and Bose-Einstein (BE) statistics as a function of $(\epsilon_s - \mu)/kT$. BE statistics are distinguished by their divergence at small values of $(\epsilon_s - \mu)/kT$.

Having seen the origin of the phenomenon of Bose-Einstein Condensation qualitatively, let us have a rigorous look at this phenomenon in the next section. In the process, we would also obtain an expression for the critical temperature of BEC. Since we have seen in this section that the phenomenon of divergence of mean occupation number is unique to Bose-Einstein statistics, we shall explore in detail only the BE statistics and not MB and FD statistics.

2.2 Bose-Einstein Condensation in non-interacting gas

In the previous section we saw that the phenomenon of condensation into the ground state may be observed in a gas of non-interacting bosons. The mean occupation number was used to demonstrate the existence of this phenomenon in principal. In this section, we demonstrate the existence of BEC by a more rigorous mathematical analysis. We do this since there is an extra piece of information which we obtain by doing such an analysis. This information is the existence of a critical temperature for condensation.

The onset of BEC may be viewed crudely as being the point where the quantum wave-function of individual bosons begin to overlap. The de Broglie wavelength of a particle with momentum 'p' is given by $\lambda = h/p$, where h is the Planck's constant and λ is the de Broglie wavelength. Let these bosons occupy a volume V and be N in number in which case their density is given by $n = N/V$. The average distance between bosons in such a gas in 3 dimensions is $n^{-1/3}$. With this information, the onset of BEC can roughly be written as the point where $\lambda \sim n^{-1/3}$. Further, p can be estimated by assuming that the equipartition theorem holds and the average kinetic energy per boson at a temperature 'T' is given by $\frac{p^2}{2m} = \frac{3}{2}kT$, where '$k$' is Boltzmann's constant. Using this, the aforementioned condition for onset of condensation can be written as $\frac{h}{\sqrt{3mkT}} \sim n^{-1/3}$. Assuming that the density is held constant, there exists then a critical temperature for condensation given roughly by $T_c \sim \frac{h^2 n^{2/3}}{3mk}$.

In the derivation above for T_c, the point to note is that the regime where BEC begins to manifest depends on the de Broglie wavelength λ. For $\lambda \ll n^{-1/3}$, the Bose gas may be treated classically since the wave-function overlap is practically non-existent. This condition may also be written as $\lambda^3 n \ll 1$. Thus, we may use the parameter $\lambda^3 n$ to quantify crudely the quantum behaviour of the Bose gas. For $\lambda^3 n \sim 1$, the quantum behaviour of the Bose gas becomes significant and subsequent overlap of the wave-function may produce condensation in the ground state.

With the qualitative discussion above, let us now look at the existence of condensation temperature using quantum statistics. For a gas of bosons, the average occupation number of an energy level with energy ϵ_s is given by $\widehat{N_s} = \frac{1}{e^{(\beta\epsilon_s - \beta\mu)} - 1}$, where $\beta = 1/kT$ [80]. Therefore, the total number of particles in the boson gas is given by

$$N = \sum_{\epsilon_i} \widehat{N_i} = \sum_{\epsilon_i} \frac{1}{z^{-1}e^{\beta\epsilon_i} - 1}, \tag{2.1}$$

where we have written $e^{\beta\mu} = z$. This new parameter 'z' introduced in the above formula is called the fugacity of the gas in literature [81]. For a Bose gas occupying a large

volume 'V', the energy spectrum would be closely spaced and the summation in the above formula for N may be replaced by an integration. This small spacing between the energy levels may be viewed in an elementary fashion by considering the problem of a quantum particle in a three-dimensional infinite square well potential. As the volume of the well is increased, the spacing between the energy levels decreases. However, for doing an integral over the energy states, we need to assign a weight to each energy level using the density of states. For a non-interacting gas in 3 dimensions, the density of states is given by

$$a(\epsilon) \, d\epsilon = (2\pi V/h^3) \, (2m)^{3/2} \, \epsilon^{1/2} \, d\epsilon.$$

Note here that the subscript on ϵ is dropped since now the variation of energy levels is continuous. The above expression gives the number of states between an energy level ϵ and $\epsilon + d\epsilon$. Using $a(\epsilon)$ as the weight, we may evaluate the expression for total number of particles in a Bose gas. However, there is a problem with this approach which has to be taken into account. The expression above for the density of states attributes a zero weight to the ground state $\epsilon = 0$. Therefore, before converting the sum into an integral, we single out the $\epsilon = 0$ energy state. Thus, we have the expression for total number of particles in a Bose gas as

$$N = \frac{2\pi V}{h^3}(2m)^{3/2} \int_0^\infty \frac{\epsilon^{1/2} d\epsilon}{z^{-1}e^{\beta\epsilon} - 1} + \frac{z}{1 - z}. \tag{2.2}$$

The lower limit of the ϵ integral is kept as $\epsilon = 0$ since this won't contribute to the integral as it attributes zero weight to the level $\epsilon = 0$, as mentioned above. Before proceeding, a point to note is that the fugacity is bounded as $0 < z < 1$. The reason for the boundedness is that the chemical potential for a Bose gas is negative. This can be understood by viewing the chemical potential as the change in energy of the system due to addition of an extra particle in the system. Since there is no restriction on the occupancy of an energy level for a Bose gas, if the chemical potential is greater than or equal to 0, the entire reservoir can be emptied into the energy levels $\epsilon \leq \mu$. Therefore, for the Bose gas to be in equilibrium, $\mu < 0$. Thus, z is always between 0 and 1.

For high values of T, $z \ll 1$ and the weight of the second term in Eq.(2.2) is negligible as compared to the first term. However, as z becomes close to 1, the weight of the second term dominates and we have a divergence as seen in the previous section. Let us call the occupation number of the ground state as $N_0 = z/(1 - z)$. Therefore, the number of particles in the energy state $\epsilon > 0$, N_ϵ say, can be written as

$$N_\epsilon = N - N_0 = \frac{2\pi V(2mkT)^{3/2}}{h^3} \int_0^\infty \frac{u^{1/2}du}{z^{-1}e^u - 1} = \frac{V}{\lambda^3} g_{3/2}(z),$$

where $u = \beta\epsilon$, $\lambda = h/(2\pi mkT)^{1/2}$ and $g_\nu(z)$ are Bose-Einstein functions defined by [81]

$$g_\nu(z) = \frac{1}{\Gamma(\nu)} \int_0^\infty \frac{u^{\nu-1}du}{z^{-1}e^u - 1} = z + \frac{z^2}{2^\nu} + \frac{z^3}{3^\nu} + ...$$

As z is bounded by 1 from above and as $g_\nu(z)$ is a monotonically increasing function of z, the highest possible value of N_ϵ is given by $N_\epsilon = \frac{V}{\lambda^3} g_{3/2}(1)$. Using the definition of Bose-Einstein functions, $g_{3/2}(1)$ can be computed and its value is approximately equal to 2.612 and we shall use this value henceforth. N_ϵ is the total number of particles in all the excited state for a given volume V and temperature T at equilibrium. For a given Bose gas in equilibrium as long as the total particle number is less than this limiting value of N_ϵ, the bosons are distributed over all the excited states. However, if the total number of particles in a Bose gas exceeds this limiting value, the excess particles will be pushed into the ground state $\epsilon = 0$. Thus there occurs a macroscopic occupation of the ground state and we achieve what is called as a BEC. Therefore, the condition to achieve a BEC is given by $N > N_\epsilon$ which gives us the condition

$$N > VT^{3/2}\frac{(2\pi mk)^{3/2}}{h^3}(2.612).$$

For a Bose gas with constant density $n = N/V$ and varying temperature, we get a critical temperature for achieving BEC from the above equation as

$$T_c = \frac{h^2}{2\pi mk}(n/2.612)^{2/3}. \tag{2.3}$$

A point to note here is that the qualitative expression for T_c obtained previously using the de Broglie hypothesis has the exact same variation with respect to n and m as the above expression obtained rigorously. The equations differ in numerical factors. Thus we have obtained an expression for critical temperature below which we achieve BEC. The fraction of condensed particles N_0/N, and fraction of particles in higher excited states N_ϵ/N, as a function of T/T_c can be seen in Fig.(2.2).

Having shown the existence of BEC, let us now look at a mathematical indicator of the phenomenon, called the *off-diagonal long range order*.
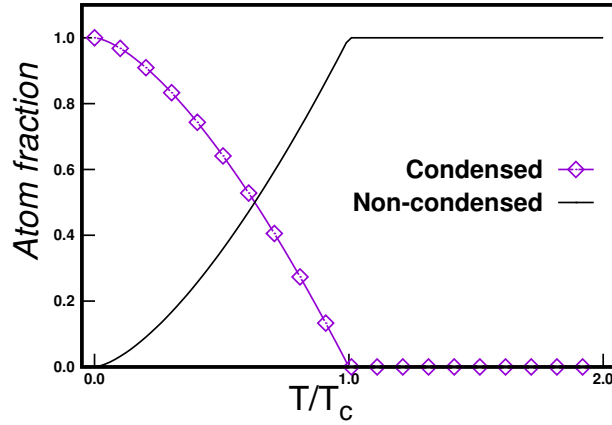
Figure 2.2: Figure shows the fraction of atoms in the BEC phase and those out of the BEC phase as a function of T/T_c.

2.3 Density matrix and Off-diagonal long range order

The phenomenon of Bose-Einstein condensation may be quantified using the density matrix. The one body density matrix for a system with wave-function $\psi(\mathbf{r})$ is defined as

$$n(\mathbf{r}, \mathbf{r}') = \left\langle \psi^*(\mathbf{r})\psi(\mathbf{r}') \right\rangle.$$

By setting $\mathbf{r} = \mathbf{r}'$, we get the diagonal density of the system $n(\mathbf{r}) = n(\mathbf{r}, \mathbf{r})$. This diagonal density gives the total number of particles in the system via the relation $N = \int d\mathbf{r} \, n(\mathbf{r})$, which reciprocally defines the normalization of the one-body density matrix.

Consider a system consisting of N bosons whose pure states are given by $\psi_l(\mathbf{r_1}, \mathbf{r_2}, ..., \mathbf{r_N})$ with energy E_l, where l is an index label on the pure state number. Then the one body density matrix for the system in a pure state is given by

$$n_l(\mathbf{r}, \mathbf{r}') = N \int d\mathbf{r}_2 .... d\mathbf{r}_N \; \psi_l^*(\mathbf{r}, \mathbf{r}_2, ..., \mathbf{r}_N) \; \psi_l(\mathbf{r}', \mathbf{r}_2, ..., \mathbf{r}_N).$$

However, a general system is in a statistical mixture of the pure states and not in a single pure state. In thermodynamic equilibrium, the one body density matrix for a general system may be written as [37]

$$n(\mathbf{r}, \mathbf{r}') = \frac{1}{Z} \sum_l e^{-E_l/kT} \; n_l(\mathbf{r}, \mathbf{r}'),$$

where Z is the partition function defined as $Z = \sum_l e^{-E_l/kT}$. Considering the particle density fixed in the thermodynamic limit, let us assume that the one body density matrix depends only on $|\mathbf{r} - \mathbf{r}'|$; let us say $|\mathbf{r} - \mathbf{r}'| = s$. With this definition, we have $n(\mathbf{r}, \mathbf{r}') =: n(s)$. This one body density matrix may be written as a Fourier transform of the one body density matrix in the momentum space as

$$n(s) = \frac{1}{V} \int d\mathbf{p}\, n(\mathbf{p})\, e^{-i\mathbf{p}.\mathbf{s}/\hbar}.$$

For a usual system, the variation $n(\mathbf{p})$ is smooth with respect to $|\mathbf{p}|$ for small momenta. Therefore, for $s \to \infty$, the phase oscillation would be very rapid and the integral would vanish. However, there is an interesting case when the momentum distribution exhibits a singular behaviour for zero-momentum states. This can be demonstrated by writing $n(\mathbf{p}) = N_0 \delta(\mathbf{p}) + \hat{n}(\mathbf{p})$, where $\hat{n}(\mathbf{p})$ gives the density matrix for particles with non-zero momentum. Considering that the density for non-zero momentum given by $\hat{n}(\mathbf{p})$ varies smoothly, the contribution of these states to the one body density vanishes for $s \to \infty$. However, due to the singular behaviour of the momentum density distribution for zero momentum states, there exists a residual density $n_0 = N_0/V$ even for $s \to \infty$. This behaviour of the one body density matrix is called the *off-diagonal long range order* (ODLRO), since it consists of elements of the density matrix with $\mathbf{r} \neq \mathbf{r}'$. The occupation number N_0 follows the condition $N_0/N < 1$ and the fraction of the total number of particles in the condensate depends on the temperature of the condensate. Above the critical temperature of condensation T_c, the condensate fraction vanishes. Note that, here we have not considered interacting bosons. However, it may be guessed that weak interactions would only shift the critical temperature and occupation number; the qualitative effect of off-diagonal long range order would remain intact [82].

The one body density matrix thus serves as an important mathematical quantifier of Bose-Einstein Condensation. Note that the macroscopic occupation of the zero-momentum state was an essential ingredient in proving the existence of ODLRO.

Having reviewed the phenomenon of BEC in a gas of non-interacting bosons, we now wish to study the effects of interactions between bosons. This is because in practice, even a dilute gas has interactions between its constituent particles. However, we will use simplifying assumptions while studying interactions. The assumption would be based on the fact that the temperature required to achieve BEC is extremely low. At such a low temperature, the bosons have extremely low energy and hence the dominant interaction mechanism would be that of s-wave scattering. Further, we will consider a dilute Bose gas which shall introduce one more simplification. It is that to the first order we may only consider pair-wise scattering between bosons since the distance between them is so

large that the probability of two body interactions is much higher than that of three and higher body interactions. However, before we implement these assumptions, let us look at two essential tools required to study a gas of interacting bosons. These tools are basic scattering theory and the representation of a Bose gas using second quantization. With this toolkit, we shall finally converge upon the protagonist of this thesis, which is the mean-field Gross-Pitaevskii theory.

2.4   Some elements of basic scattering theory

The quantum scattering problem is one of the most important problems in modern physics. In this problem one studies the effect of a potential in a certain region of space on a travelling matter wave. It is important to study this problem to understand BEC since the interaction between bosons which constitute the condensate is nothing but a scattering interaction. How to scale up the problem to study scattering between many bodies is something we would look at in the next section. But let us first have an overview of scattering between two bosons. To do this, we first formulate the problem and introduce the notations.

2.4.1   The scattering problem

Let us start by assuming that the inter-boson interaction is symmetric, i.e. dependent only on the distance between them. This interaction potential is represented in Schrodinger's equation by $V(r)$, where the scalar r denotes distance between the bosons. The Schrodinger's equation is written as

$$-\frac{\hbar^2}{2\mu}\nabla^2\,\psi(r,\theta,\phi) + V(r)\,\psi(r,\theta,\phi) = E\,\psi(r,\theta,\phi),$$

where μ is the reduced mass and ψ denotes the wave-function of the system. Given a particular form of $V(r)$, our aim is to solve the eigenvalue equation above. For simplicity, let us consider a plane wave travelling in the $z-$ direction which comes under the influence of $V(r)$ which scatters it. A part of the wave would scatter spherically and the remaining part would continue to travel in the $z-$ direction. Mathematically, therefore, the solution to this problem for large r may be written as [38]

$$\psi(r,\theta) \sim A\left\{e^{ikz} + f(\theta)\frac{e^{ikr}}{r}\right\}, \tag{2.4}$$

where k is the wave number of the incoming particle wave and $f(\theta)$ is called the scattering amplitude. The wave number is related to the energy of the incident particles as $k = \sqrt{2mE}/\hbar$. The point to note here is that in the asymptotic limit, the scattering amplitude is very important as practically all other factors are determined by the conditions before the scattering. Therefore, in effect the scattering problem is to determine $f(\theta)$ for a given $V(r)$. The asymptotic form of ψ above shall be used to determine $f(\theta)$.

The quantum scattering problem usually cannot be solved exactly for a given interaction potential. However, we can extract useful information from it. Since in BEC the scattering between bosons occurs at low temperature, we will consider low energy scattering. We shall apply perturbation techniques to calculate the forward scattering amplitude. There are two techniques which may be used, the partial wave analysis and the Born approximation. Imposing condition of consistency on expressions for forward scattering amplitude obtained using these two techniques introduces a condition on the integral of interaction potential. This expression will be useful in formulating the mean field theory of BEC [37].

2.4.2 Partial wave analysis

For a spherically symmetric potential, the solution to Schrodinger's equation is separable as $\psi(r, \theta, \phi) = R(r)Y_m^l(\theta, \phi)$, where $Y_m^l(\theta, \phi)$ is called the spherical harmonic function. The form of $R(r)$ is determined by the radial equation using $u(r) = rR(r)$ as [38]

$$-\frac{\hbar^2}{2m}\frac{d^2u(r)}{dr^2} + \left[V(r) + \frac{\hbar^2}{2m}\frac{l(l+1)}{r^2}\right]u(r) = Eu(r).$$

The solution to this equation far from the scattering region is given by [83]

$$\psi(r, \theta) = A\left[e^{ikz} + k\sum_{l=0}^{\infty}i^{l+1}(2l+1)a_l h_l^{(1)}(kr)P_l(\cos(\theta))\right], \tag{2.5}$$

where $h_l^{(1)}$ is the first spherical Hankel function, P_l is the 'l'th Legendre polynomial and a_l is called the 'l'th partial wave amplitude. Comparing it with Eq.(2.4), the scattering amplitude may be read off as

$$f(\theta) = \sum_{l=0}^{\infty}(2l+1)a_l P_l(\cos(\theta)), \tag{2.6}$$

where the large r limit for the Hankel function is taken. Thus we have obtained a series solution for scattering amplitude by breaking up the solution to the scattering problem into partial waves with different angular momentum number l.

This problem can also be viewed in term of phase shifts, meaning we may assume that scattering of a free wave from a potential only brings about change in phase of the wave. Here too, we consider the partial wave analysis in a way, meaning we assume that during scattering the angular momentum 'l' is conserved for each partial wave. The phase shift for each partial wave can then be calculated. Using this approach one gets, after solving the Schrodinger equation for an incoming wave of the form $\psi = Ae^{ikz}$, the expression [84]

$$\psi^l(r, \theta) \sim A\frac{(2l + 1)}{2ikr} \left[e^{i(kr + 2\delta_l)} - (-1)^l e^{-ikr}\right] P_l(\cos(\theta)),$$

for a specific 'l' where δ_l is the phase shift. One can compare the equation above with the expression for a particular 'l' in Eq.(2.5) to get the expression for a_l as

$$a_l = \frac{1}{2ik} \left(e^{2i\delta_l} - 1\right).$$

For low energy scattering, the most dominant partial wave is the one with $l = 0$, called the *s-wave* . Scattering considering only the $l = 0$ partial wave is called the *s*-wave scattering. From Eq.(2.6), one can see that for *s*-wave scattering, $f = a_0$. The value of a_0 can be obtained from the equation above connecting a_l with the phase shift δ_l. For low energy scattering and small phase shifts, we have $a_0 \sim \frac{\delta_0}{k}$. The final piece of puzzle is taking the limit $k \to 0$, which gives us $f = -a$, where 'a' is the s-wave scattering length, defined as

$$\lim_{k \to 0} k \, \cot[\delta_0(k)] = -\frac{1}{a} .$$

The scattering amplitude being equal to $-a$ is an important result we have obtained here and shall be used for justifying the pseudopotential approach in subsequent sections. We shall now look at the first Born approximation which shall also be used in justifying the pseudopotential approach.

2.4.3 First Born approximation

Another method to solve the scattering problem is using the Green's function approach. We start by writing the Schrodinger's equation as

$$[\nabla^2 + k^2]\psi(\mathbf{r}) = Q,$$

where $k = \sqrt{2mE}/\hbar$ and $Q = 2\mu V(r)\psi(\mathbf{r})$. Note here that we have used $\mathbf{r}$ to denote the 3D dependence of ψ. For a given Green's function $G(\mathbf{r})$, the solution of this equation would be $\psi(\mathbf{r}) = \int G(\mathbf{r} - \mathbf{r}')Q(\mathbf{r}')d^3\mathbf{r}'$. By using the usual Green's function analysis, the general solution in terms of the potential $V(r)$ may be written as [84]

$$\psi(\mathbf{r}) = \psi_0(\mathbf{r}) - \frac{\mu}{2\pi\hbar^2} \int \frac{e^{ik|\mathbf{r}-\mathbf{r}'|}}{|\mathbf{r} - \mathbf{r}'|}V(r')\psi(\mathbf{r}')d^3\mathbf{r}', \tag{2.7}$$

where $\psi_0(\mathbf{r})$ satisfies the free-particle Schrodinger equation

$$[\nabla^2 + k^2]\psi_0(\mathbf{r}) = 0.$$

As we will be dealing with BEC in dilute gases, we may assume that for the majority of time, the bosons are far away from each other. Therefore, we calculate $\psi(\mathbf{r})$ at points far away from the scattering centre. Let us assume that the scattering potential is localized about $\mathbf{r_0} = \bar{0}$, meaning it drops to zero beyond some finite range. This is a good approximation for a realistic interaction potential between bosons. So for the term in the integral in Eq.(2.7), $|\mathbf{r}| \gg |\mathbf{r}'|$ and therefore $|\mathbf{r} - \mathbf{r}'| \sim r - \hat{r}.\mathbf{r}'$. Further taking $\mathbf{k} = k\hat{r}$ we get $e^{ik|(\mathbf{r}-\mathbf{r}')|} \sim e^{ikr}e^{-i(\mathbf{k}.\mathbf{r}')}$, which in turn gives $\frac{e^{ik|(\mathbf{r}-\mathbf{r}')|}}{|(\mathbf{r}-\mathbf{r}')|} \sim \frac{e^{ikr}}{r}e^{-i(\mathbf{k}.\mathbf{r}')}$. With this Eq.(2.7) becomes

$$\psi(\mathbf{r}) = Ae^{ikz} - \frac{\mu}{2\pi\hbar^2}\frac{e^{ikr}}{r} \int e^{-i\mathbf{k}.\mathbf{r}'}V(r')\psi(\mathbf{r}') \, d^3\mathbf{r}', \tag{2.8}$$

where we have taken $\psi_0(\mathbf{r}) = Ae^{ikz}$. Now comes the Born approximation, which states that the incoming wave is not substantially altered by the interacting potential. Mathematically stating, the Born approximation states $\psi(\mathbf{r}') \sim \psi_0(\mathbf{r}') = Ae^{ik'z'} = Ae^{i\mathbf{k}'.\mathbf{r}'}$, where $\mathbf{k}' = k'\hat{z}$. By comparing with Eq.(2.4), the scattering amplitude may be read from Eq.(2.8). Using the Born approximation, the scattering amplitude may be written as

$$f(\theta, \phi) \sim -\frac{\mu}{2\pi\hbar^2} \int e^{i(\mathbf{k}'-\mathbf{k}).\mathbf{r}'}V(r') \, d^3\mathbf{r}' \tag{2.9}$$

Lastly, for low energy scattering, the exponential factor above is essentially constant over the scattering region and the above expression simplifies to

$$f(\theta,\phi) \sim -\frac{m}{4\pi\hbar^2} \int V(r')d^3\mathbf{r'}, \tag{2.10}$$

where we have replaced the effective mass $\mu = m/2$, where m is the mass of the constituent boson.

2.4.4 The pseudopotential

From the partial wave analysis, we obtained the expression for scattering amplitude as $f = -a$. Using Born approximation, we obtained $f = -\frac{m}{4\pi\hbar^2} \int V(r')d^3\mathbf{r'}$. For these two approaches to be consistent, since they represent the same phenomenon, we must have

$$\int V(r')d^3\mathbf{r'} = \frac{4\pi\hbar^2 a}{m}. \tag{2.11}$$

Therefore, we have a restriction on the interaction potential which is that its integral should be equal to $4\pi\hbar^2 a/m$. We shall denote this value by g and call it the strength of interaction. This does not however give us the exact form of the interaction potential, but gives us a measure of its strength [84]. The exact form of the potential may be complicated for actual interaction potentials, but now we have a measure of its strength.

For low energy s-wave scattering, the details of the interaction potential may not be seen by the interacting bosons. Therefore, to reproduce the essential characteristics of the interaction, we may replace the exact interaction potential by a soft *pseudopotential* [37]. The choice of the pseudopotential must satisfy the condition given by Eq.(2.11). The choice of a particular pseudopotential may give various detailed characteristics, but the argument is that the long wavelength characteristics of the interaction would be the same. This is a very important concept and will be an important ingredient of the mean-field Gross-Pitaevskii theory.

2.4.5 Feshbach resonance

From the pseudopotential approach, it is clear that the strength of the potential $g = 4\pi\hbar^2 a/m$ is an important parameter for s-wave scattering. Therefore, it is useful to have control over this parameter. Feshbach resonance is a technique to tune the s-wave scattering length, in principle between the range $(-\infty, \infty)$. This is done by using the magnetic field to lift the degeneracy of the hyperfine states [34]. Since BEC is obtained in a laboratory using gas of alkali atoms, let us look at this phenomenon for alkali atoms. Alkali atoms also present a simplified picture of Feshbach resonance [85].
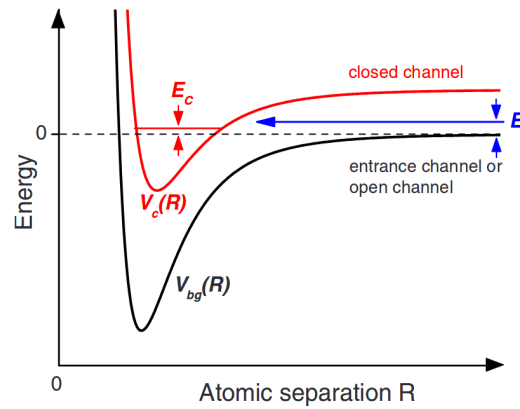
Figure 2.3: Figure shows Feshbach resonance in alkali atoms in the language of open and closed channels. A Feshbach resonance occurs when the collision energy in the open channel resonantly couples to a bound state in the closed channel [85] (*https* : //*doi.org*/10.1103/*RevModPhys*.82.1225).

The scattering process which we have considered till now does not consider the internal degrees of freedom of bosons. However, there exists interactions between the internal degrees of freedom of alkali atoms. Since alkali atoms have just one unpaired electron in the outermost shell, the interaction between its spin degree of freedom and that of the nucleus gives rise to hyperfine states which are the singlet and triplet states [86]. The difference between the energy of these states can be controlled by application of a magnetic field. Due to the hyperfine effects, the interaction potential seen by singlet and triplet states is also different . If the triplet potential (closed channel) has a bound state whose energy is equal to the asymptotic limit (in distance) for the singlet potential (entrance channel or open channel), we call this condition as a Feshbach resonance. In this case, there occurs a coupling between the singlet and triplet potential which enables tuning of the scattering length. The separation between the singlet and triplet interaction potential may be controlled by an external magnetic field. Fig.(2.3) shows the basic idea of Feshbach resonance. The s-wave scattering length varies rapidly near the point of Feshbach resonance. Thus by using an external magnetic field, the s-wave scattering length may be tuned. Experimentally, the variation of scattering length with the externally applied magnetic field is given by [37]

$$a_f = a \left(1 - \frac{\Delta}{B - B_0} \right), \tag{2.12}$$

where a_f is the tuned scattering length, B is the externally applied magnetic field, B_0 is the value of magnetic field at which resonance occurs and Δ is called the width of the resonance. Fig.(2.4) shows the variation of the scattering length near the Feshbach resonance. Feshbach resonance has become a very important tool to tune interactions

in atomic BEC which has been an important asset for applicability of BEC as analog systems [21].
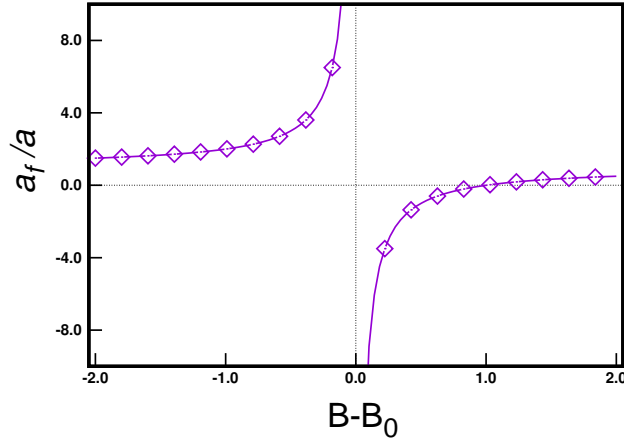
Figure 2.4: Figure shows the variation of a_f/a as a function of the difference between the externally applied magnetic field and the resonant magnetic field, given by B_0.

2.5 Bose gas using second quantization

A gas of interacting bosons may be considered using field operators in what is called the second quantized picture. The first quantization in quantum mechanics consists of replacing the Poisson brackets in classical mechanics by the quantum commutation relations. The second quantization involves replacing scalar wave-function by field operators introducing distinct commutation relations for field operators of bosons and fermions. For quantum particles (bosons or fermions), $\hat{\psi}^\dagger(\mathbf{r}, t)$ and $\hat{\psi}(\mathbf{r}, t)$ denote the creation and annihilation field operators respectively. In classical mechanics, the Hamiltonian for a conservative system may be written as the sum of kinetic and potential energy components, $H = \sum_i p_i^2/2m + V(\mathbf{r_i}, \mathbf{r_j})$. The second quantized Hamiltonian for field operators is written as [37]

$$\hat{H} = \frac{\hbar^2}{2m} \int d\mathbf{r} \, \hat{\psi}^\dagger(r) \nabla^2 \hat{\psi}(\mathbf{r}) + \int d\mathbf{r} d\mathbf{r}' \, \hat{\psi}^\dagger(r) \hat{\psi}^\dagger(r') V(\mathbf{r} - \mathbf{r}') \hat{\psi}(\mathbf{r}') \hat{\psi}(\mathbf{r}).$$

For a gas of bosons, the fields follow Bose commutation relations given by [37]

$$[\hat{\psi}(\mathbf{r}), \hat{\psi}^\dagger(\mathbf{r}')] = \delta(\mathbf{r} - \mathbf{r}'), \quad [\hat{\psi}(\mathbf{r}), \hat{\psi}(\mathbf{r}')] = 0.$$

In the Heisenberg's representation, the field operator satisfies the equation $i\hbar \frac{\partial \hat{\psi}(\mathbf{r},t)}{\partial t} = [\hat{\psi}(\mathbf{r}), \hat{H}]$. Using the Bose commutation relation and assuming that the potential $V(\mathbf{r}, \mathbf{r}')$

commutes with the field operators, we get the equation for evolution of the field operator in the presence of an external potential $V_{ext}(\mathbf{r}, t)$ as

$$i\hbar\frac{\partial\hat{\psi}(\mathbf{r}, t)}{\partial t} = \left[-\frac{\hbar^2\nabla^2}{2m} + V_{ext}(\mathbf{r}, t) + \int d\mathbf{r}' \ \hat{\psi}^\dagger(r')V(\mathbf{r} - \mathbf{r}')\hat{\psi}(\mathbf{r}')\right]\hat{\psi}(\mathbf{r}). \qquad (2.13)$$

This equation is extremely important for developing the mean field picture of BEC, giving us the Gross-Pitaevskii equation. In the next section, we will have a brief look at how we develop the mean-field theory of BEC using the Bogoliubov approximation for single and multi-component BEC. We will also have a brief look at the corrections to the local Gross-Pitaevskii equation due to finite range effects of the inter-boson interaction potential $V(\mathbf{r} - \mathbf{r}')$.

2.6   Mean field treatment of Bose-Einstein Condensates

The field operator for the many body system can be written in the diagonal form as a sum over single particle states as $\hat{\psi}(\mathbf{r}) = \sum_i \phi_i\hat{a}_i$, where a_i and $a_i^\dagger$ are the annihilation and creation operators respectively of a particle in state ϕ_i. These operators obey the commutation relations

$$[\hat{a}_i, \hat{a}_j^\dagger] = \delta_{ij} \ \ ; \ \ [\hat{a}_i, \hat{a}_j] = 0.$$

Let us consider this as the starting point to build upon for the mean field theory.

2.6.1   Bogoliubov approximation and the Gross-Pitaevskii equation

For a macroscopic occupation of the ground state which is the BEC phase, we may single out the zero momentum ground state $i = 0$ and write the field operator as $\hat{\psi}(\mathbf{r}) = \phi_0\hat{a}_0 + \sum_{i\neq 0} \phi_i\hat{a}_i$. The '*Bogoliubov approximation*' consists of replacing the creation $(a_0^\dagger)$ and annihilation (a_0) operators by the classical number, or *c-number* $\sqrt{N_0}$, where the macroscopic occupation number of particles in the condensate is represented by N_0 . Thus, the Bogoliubov approximation is equivalent to treating the macroscopic component $(\phi_0\hat{a}_0)$ of the field operator $\hat{\psi}$ as a classical field. With this approximation, the field operator may be written as

$$\hat{\psi}(\mathbf{r}) = \psi_0(\mathbf{r}) + \delta\hat{\psi}(\mathbf{r}),$$

where $\psi_0(\mathbf{r}) = \phi_0\sqrt{N_0}$ and $\delta\hat{\psi}(\mathbf{r}) = \sum_{i\neq0} \phi_i\hat{a}_i$. For a macroscopic occupation of ground state, the non-condensate part given by $\delta\hat{\psi}(\mathbf{r})$ may be neglected and the field operator $\hat{\psi}(\mathbf{r})$ may be written as a classical field [34]. This classical field given by $\psi_0(\mathbf{r})$ is called the wave-function of the condensate.

With the Bogoliubov approximation, the evolution of the field operator in Eq.(2.13) may be written as an equation for evolution of the wave-function of the condensate. This gives us the mean-field Gross-Pitaevskii (GP) equation as

$$i\hbar\frac{\partial\psi(\mathbf{r},t)}{\partial t} = \left[-\frac{\hbar^2\nabla^2}{2m} + V_{ext}(\mathbf{r},t) + \int d\mathbf{r}'\ \psi^*(\mathbf{r}',t)V(\mathbf{r}-\mathbf{r}'\psi(\mathbf{r}',t)\right]\psi(\mathbf{r},t). \quad (2.14)$$

Since ψ is a complex valued wave-function, its interpretation is that $|\psi|^2$ gives the density profile of the condensate. The chemical potential plays an important role in introducing temporal phase oscillations. It can be briefly demonstrated as follows.

The Bogoliubov approximation is equivalent to saying that the expectation value of the field operator $\langle\hat{\psi}(\mathbf{r})\rangle$ is given by the wave-function of the condensate $\psi_0(\mathbf{r})$, considering the expectation value of the part out of condensate $\langle\delta\hat{\psi}(\mathbf{r})\rangle$ is negligible. However, since field operator consists of creation and annihilation operators, only the matrix components of the form $\langle N|\hat{\psi}(\mathbf{r})|N+1\rangle$ give a non-zero value [34]. Further as the kets evolve in time as $|N\rangle \propto \sqrt{N}e^{-iE_Nt/\hbar}$, the expectation value of the field operator evolve in time as $\langle N|\hat{\psi}(\mathbf{r})|N+1\rangle \propto Ne^{-i(E_{N+1}-E_N)t/\hbar}$. In the thermodynamic limit, i.e. for large values of N, the chemical potential 'μ' may be approximated as $\mu \sim E_{N+1} - E_N$ since the chemical potential is defined as $\mu = \partial E/\partial N$. Therefore we may write $\langle\hat{\psi}(\mathbf{r})\rangle \propto Ne^{-i\mu t/\hbar}$. As we replace $\langle\hat{\psi}(\mathbf{r})\rangle$ by $\psi_0(\mathbf{r},t)$, we have

$$\psi_0(\mathbf{r},t) = \psi_0(\mathbf{r})e^{-i\mu t/\hbar}.$$

2.6.2 Interaction pseudopotential and the Local Gross-Pitaevskii Equation

Having obtained the mean-field GP equation in Eq.(2.14), there is one approximation from the scattering theory which may be used to further simplify the equation. We had seen in Sec.(2.4.4) that for low energy s-wave scattering between two bosons, the exact interaction potential may be replaced by an effective potential. This approximation may be used for a dilute BEC, which manifests at extremely low temperatures and hence low energy scales. This is because the probability of two body collisions is very high

as compared to three body or higher collisions. Therefore, we replace the interaction potential '$V(\mathbf{r} - \mathbf{r}')$' in Eq.(2.14) by an effective potential which depends on the distance between the bosons $V(|\mathbf{r} - \mathbf{r}'|)$. This turns Eq.(2.14) into

$$i\hbar\frac{\partial \psi(\mathbf{r},t)}{\partial t} = \left[-\frac{\hbar^2\nabla^2}{2m} + V_{ext}(\mathbf{r},t) + \int d\mathbf{r}' \; \psi^*(\mathbf{r}',t)V_{eff}(|\mathbf{r} - \mathbf{r}'|)\psi(\mathbf{r}',t) \right] \psi(\mathbf{r},t). \quad (2.15)$$

The only constraint on the effective potential is that it should be symmetric and its strength should be given by $g = 4\pi\hbar^2 a/m$, where a is the s-wave scattering length. The restriction on integral of the interaction potential actually gives us freedom of selecting the exact shape of the pseudopotential, the only restriction being that $\int d\mathbf{r} \; V_{eff}(|\mathbf{r} - \mathbf{r}'|) = g$. The discussion on shape in Sec.(2.4.4) applies.

Making use of the pseudopotential approach, the simplest function that can be taken is one by neglecting the range of the interaction and taking the interaction potential to be a Dirac delta function. Thus, we take in Eq.(2.15) $V_{eff}(|\mathbf{r} - \mathbf{r}'|) = g \; \delta(|\mathbf{r} - \mathbf{r}')$. We shall call the equation obtained by taking such a form of the pseudopotential as the **Local Gross-Pitaevskii Equation (LGPE)**, given by

$$i\hbar\frac{\partial \psi(\mathbf{r},t)}{\partial t} = \left[-\frac{\hbar^2\nabla^2}{2m} + V_{ext}(\mathbf{r},t) + g|\psi(\mathbf{r},t)|^2 \right] \psi(\mathbf{r},t). \quad (2.16)$$

For a BEC with average density n, the diluteness parameter of the BEC is given by $a^3 n$, which is also called as the gas parameter. The LGPE has been immensely successful in describing properties of dilute BEC with $a^3 n \ll 1$ in the presence of weak traps [83]. In such a situation, the finite range effects of the s-wave interaction may be neglected. However, for small but finite values of gas parameter and/or tight trapping, finite range effects of the inter-boson interaction potential come into play [35, 36]. In such a scenario, assuming the finite range effects of the interaction potential as perturbation on top of the LGPE gives corrections to the LGPE [45]. We shall consider such corrections to the LGPE at the end of this section.

2.6.3 Multi-component BEC

The LGPE obtained in the previous section describes the dynamics of a BEC with a single component. However, BEC with multiple components have also been realized experimentally. BEC with multiple components may be obtained by using different elements [19], isotopes of an element [87] or a particular element in different spin states [88].

The two body scattering interactions in a multi-component BEC consist of intra-species scattering and inter-species scattering. Consequently, there exist intra-species scattering lengths and inter-species scattering lengths. The inter-species scattering length is different for scattering between different species. To write a GP equation for BEC with multiple components, these interactions have to be accounted for. Such an equation may be arrived at using the same procedure as used for single component BEC in the previous sub-sections. The Hamiltonian operator in this case may be written as a sum of the intra-species and inter-species interaction as

$$
\hat{H} = \frac{\hbar^2}{2m} \sum_i \left[\int d\mathbf{r} \; \hat{\psi}_i^\dagger(\mathbf{r}) \nabla^2 \hat{\psi}_i(\mathbf{r}) \right] + \frac{1}{2} \sum_i \int d\mathbf{r} d\mathbf{r}' \; \hat{\psi}_i^\dagger(\mathbf{r}) \hat{\psi}_i^\dagger(\mathbf{r}') V^{ii}(\mathbf{r} - \mathbf{r}') \hat{\psi}_i(\mathbf{r}') \hat{\psi}_i(\mathbf{r})
$$

$$
+ \sum_{i,j}^{i \neq j} \int d\mathbf{r} d\mathbf{r}' \; \hat{\psi}_i^\dagger(\mathbf{r}) \hat{\psi}_j^\dagger(\mathbf{r}') V^{ij}(\mathbf{r} - \mathbf{r}') \hat{\psi}_i(\mathbf{r}') \hat{\psi}_j(\mathbf{r}).
$$

Using the Heisenberg equation of motion and the Bogoliubov approximation for field operators $\hat{\psi}(\mathbf{r}, t)$, the mean-field equation for evolution of wave-function of a multi-component BEC may be written as [77]

$$
i\hbar \frac{\partial \psi_i(\mathbf{r}, t)}{\partial t} = \left[-\frac{\hbar^2 \nabla^2}{2m} + V_{ext}^i(\mathbf{r}, t) + \int d\mathbf{r}' \psi_i^*(\mathbf{r}', t) V_{eff}^{ii}(|\mathbf{r} - \mathbf{r}'|) \psi_i(\mathbf{r}', t) \right.
$$

$$
\left. + \sum_{j \neq i} \int d\mathbf{r}' \psi_j^*(\mathbf{r}', t) V_{eff}^{ij}(|\mathbf{r} - \mathbf{r}'|) \psi_j(\mathbf{r}', t) \right] \psi_i(\mathbf{r}, t), \tag{2.17}
$$

where the index 'i' labels each specie of the multi-component BEC, a_{ii} is the intra-sepcies scattering length and a_{ij} is the inter-species scattering length. The multi-component BEC may exist in a homogeneous 'miscible' state with different species *mixed*, or it may exist in in a 'phase segregated' state with two or more species segregated. Whether the multi-component BEC is in a miscible state or not depends on the relative energies of the miscible phase and the segregated phase. Since the interaction energy in a BEC depends mainly on the tunable s-wave scattering length, the miscibility is decided by the intra-species and inter-species scattering length. Two components 'i' and 'j' are in a miscible phase if $a_{ij} < \sqrt{a_i a_j}$.

By using the δ-function pseudopotential used earlier for a single component BEC, wave-function evolution for a multi-component BEC can be obtained. The pseudopotential used here is of the form $V_{eff}^{ij} = g_{ij}\delta(\mathbf{r} - \mathbf{r}')$. Using this pseudopotential gives us the LGPE for multi-component BEC as

$$i\hbar\frac{\partial\psi_i(\mathbf{r},t)}{\partial t} = \left[-\frac{\hbar^2\nabla^2}{2m} + V_{ext}^i(\mathbf{r},t) + g_{ii}|\psi_i(\mathbf{r},t)|^2 + \sum_{j\neq i}g_{ij}|\psi_j(\mathbf{r},t)|^2\right]\psi_i(\mathbf{r},t). \quad (2.18)$$

As for the case of single-component BEC, this equation describes BEC for low values of gas parameter and/or weak trapping. In the absence of these conditions, the effective range of the interaction potential has to be taken into account.

In the next sub-section we shall look at the effect of finite range of interactions in the form of corrections to the LGPE.

2.6.4 Corrections to the LGPE: A Modified GP Equation

The local interaction pseudopotential gives us LGPE for single and multi-component BEC. However, for non-negligible values of gas parameter, the δ-function approximation for the pseudopotential is not good enough. This is because the interacting bosons begin to 'see' the range of the interaction potential. Due to this, there arises a need to introduce finite range effects in the system. This would introduce corrections on top of the LGPE as we shall see shortly.

The finite range effects can be accounted for up to the first order by taking an extended pseudopotential. In such a case, the simplified form of the non-linearity in LGPE will not exist. However, we may assume that even after introducing an extended pseudopotential, the variation of the wave-function in space is smooth. In such a case, we may take a Taylor expansion of the wave-function under the integral. We take the pseudopotential such that it commutes with ψ and lets us write $\psi^*\,V_{eff}\psi$ as $V_{eff}\,|\psi|^2$. We further take a spherically symmetric pseudopotential. The Taylor expansion then turns Eq.(2.15) into

$$\begin{aligned}i\hbar\frac{\partial\psi(\mathbf{r},t)}{\partial t} =& \left[-\frac{\hbar^2\nabla^2}{2m} + V_{ext}(\mathbf{r},t)\right.\\ &+ \int d(\mathbf{r}-\mathbf{r}')V_{eff}(|\mathbf{r}-\mathbf{r}'|)\left(1 + (\mathbf{r}-\mathbf{r}').\nabla_{\mathbf{r}}\right.\\ &\left.\left. + \frac{1}{2}(\mathbf{r}-\mathbf{r}').((\mathbf{r}-\mathbf{r}').\nabla_{\mathbf{r}}(\nabla_{\mathbf{r}})) + ...\right)|\psi(\mathbf{r},t)|^2\right]\\ &\times\psi(\mathbf{r},t).\end{aligned} \quad (2.19)$$

Due to the symmetric nature of the effective potential, only the even order derivatives survive after the integration. Note that we have not taken a specific form of the pseudopotential. However, the pseudopotential used should satisfy the condition

$\int V_{eff} = g = 4\pi\hbar^2 a/m$. Performing the integrals for a specific form of pseudopotential gives us the form of corrections on top of the corrections to the LGPE as

$$i\hbar\frac{\partial\psi(\mathbf{r},t)}{\partial t} = \left[-\frac{\hbar^2\nabla^2}{2m} + V_{ext}(\mathbf{r},t) + g\left(1 + \frac{1}{2}c_1\nabla^2 + \frac{1}{4!}c_2\nabla^4 + ...\right)|\psi(\mathbf{r},t)|^2\right]\psi(\mathbf{r},t),$$

(2.20)

where the coefficients $c_1, c_2, ...$ depend on the specific form of the effective potential. However note that a particular choice of the effective potential would only alter the coefficients of the correction terms; the form of the correction terms will be the same for different effective potentials. Their structure comes from the spherically symmetric nature of s-wave scattering.

The above analysis is for single component BEC. However, it can be extended to a multi-component BEC. This turns Eq.(2.17) into

$$i\hbar\frac{\partial\psi_i(\mathbf{r},t)}{\partial t} = \left[-\frac{\hbar^2\nabla^2}{2m} + V_{ext}^i(\mathbf{r},t) + g_{ii}\left(1 + \frac{1}{2}c_1^{ii}\nabla^2 + \frac{1}{4!}c_2^{ii}\nabla^4 + ...\right)|\psi_i(\mathbf{r},t)|^2 \right.$$
$$\left. + \sum_{j\neq i}g_{ij}\left(1 + \frac{1}{2}c_1^{ij}\nabla^2 + \frac{1}{4!}c_2^{ij}\nabla^4 + ...\right)|\psi_j(\mathbf{r},t)|^2\right]\psi_i(\mathbf{r},t).$$

(2.21)

An essential assumption that we have employed here is that the series of such corrections to the LGPE has a natural truncation, meaning the subsequent terms in the series fall off, either due to their coefficients decreasing or the higher order derivatives decreasing, or both. If such a truncation does not exist, the series expansion becomes meaningless. Such a case will manifest itself in Chapter(**6**) and we shall see that in such a case, rather than doing a Taylor expansion, we do the entire integral without Taylor expanding $|\psi(\mathbf{r}')|^2$.

With this, we have the requisite mean field GP theory required to theoretically analyze a BEC. Before we move on to the discussion on experimental realization of BEC in atomic gases, let us briefly review BEC in the presence of an external potential.

2.7   Interacting BEC in a trap

As we shall see in the next section, obtaining a BEC requires trapping of bosons to isolate them from the environment as interactions with the surrounding apparatus will lead to thermalization of the bosons to room temperature. This is necessary because the

transition temperature for obtaining a BEC in atomic gas is of the order of nano-Kelvin. Therefore, BECs are always obtained in the presence of an external trapping potential. The trapping is done using magnetic field to trap the atoms (bosons) based on their internal quantum structure. The most common trapping potential is the harmonic trap [89] in which the external potential is of the form $V_{ext}(\mathbf{r}) = m\omega^2 r^2/2$, where ω is the trapping frequency. Other trapping potentials are also engineered in laboratories [90], including asymmetric potentials [91].

Consider a single component BEC in the presence of a harmonic potential. Let the gas parameter be very small so that the BEC may be described by the LGPE. Since the trapping potential depends only on the radial distance, the density variation would also be radial. Let the wave-function of such a trapped BEC be given by $\psi(r) = \sqrt{n(r)}e^{-i\mu t/\hbar}$. By neglecting the kinetic energy contribution, we obtain what is known as the Thomas-Fermi (TF) density [37]. Using the LGPE given by Eq.(2.16), the TF density profile of such a BEC is given by $n_{TF}(r) = \frac{1}{g}(\mu - \frac{m\omega^2 r^2}{2})$. A plot of the trapping potential and the TF density profile is given in Fig.(2.5). As we shall see, for imaging a condensate, it is released from the trap which results in an expansion of the condensate [92]. The rate of expansion depends on the strength of the trapping; the tighter the trapping, the faster the BEC expands.
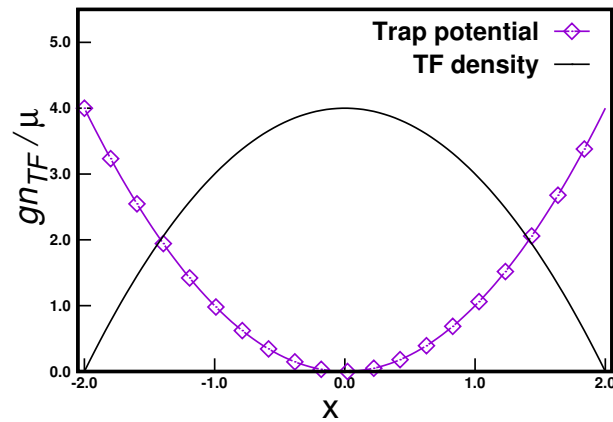
Figure 2.5: Figure shows the cross section of the TF density profile and the harmonic trapping potential along the X-axis. The density is given in units of μ/g and the distance from the centre of the trap is scaled by $(1/\omega)\sqrt{2\mu/m}$.

The very many applications that BECs find are a result of the variety of trapping potentials that can be engineered. Apart from magnetic traps, one may also engineer optical traps using counter-propagating laser beams [6]. The range of external potentials which may be engineered range from double well traps [93] to an optical lattice [18]. On top of these, BECs can be subject to several external potentials simultaneously to create solitons, vortices, etc. [34]

We thus conclude our discussion of the theoretical framework of BEC, starting from quantum statistics of non-interacting bosons and arriving at the GP equation for weakly interacting bosons and lastly looking at BEC in traps. While the theoretical framework of BEC progressed comparatively rapidly, the progress on experimental realization of the BEC took some time. Let us now look at some experimental details of BEC in atomic gases which has been one of the greatest advance in recent times in experimental physics. While the work presented in this thesis is theoretical, a description of experimental methods is necessary to put things into perspective.

2.8   Experimental realization of BEC in atomic gases

The phenomenon of BEC was theoretically discovered in 1924-25 by Satyendranath Bose, the proposer of the novel idea and Albert Einstein who worked further upon the idea [2, 3]. The lag between the discovery and its experimental realization in 1995 [9] was mainly due to technological limitations on cooling techniques for neutral atoms [28]. As any physical theory is verified by experiments, it is important to study the journey of experimental realization of BEC, along with the experimental methods used currently. This gives a perspective on the reasons for the delay between theoretical prediction and experimental realization of BEC. It also helps us understand the current limitations of the experimental setup.

The transition temperature of a non-interacting Bose gas is given by Eq.(2.3) $T_c = \frac{h^2}{2\pi mk}(n/2.612)^{2/3}$. For typical gases, this temperature is of the order of few hundred nanokelvin [34]. Thus, obtaining a BEC in laboratory involves cooling gases to such low temperatures. The journey of achieving low temperatures started with the liquefaction of helium-4 in 1908 by Kamerlingh Onnes at $\sim 4K$ [94]. After this achievement, it took a few decades for its superfluid behaviour to be detected by Kapitza in 1938 [95]. By that time the idea of Bose-Einstein condensation was already around. Fritz London was the first to propose that the superfluidity of liquid helium-4 may be a consequence of Bose-Einstein condensation of liquid helium-4 below the λ-point [4]. The experimental verification of this idea took a while [96]. However, since helium-4 is a liquid below the λ-point, strong interactions involved need to be taken into account to relate its superfluidity with BEC. Since the concept of BEC was proposed for non-interacting gases, this theory couldn't be carried over as it is to establish BEC in superfluid helium-4. As a result the experimental verification of BEC demanded a non-interacting or weakly interacting gas of particles which could be cooled below the critical temperature.

With the advent of lasers in 1960s [97], there was a renewed interest in the interaction of coherent radiation with atoms. As a consequence, there was a breakthrough in the

direction of cooling a collection of atoms using lasers in the 1970s [7]. This phenomenon was termed as laser cooling and temperatures as low as 40 kelvin were achieved using laser cooling in a gas of alkali atoms [8]. The use of alkali atoms was due to the restriction of laser frequencies available. The temperature of $40K$ was much higher than that of liquid helium, which could be cooled to about 1 K during the same time. The temperature threshold of 40 K was further reduced due to the introduction of a technique called the *Zeeman slower* which lowered the temperature threshold to a few hundred micro-kelvin [6]. This temperature was still $2 - 3$ orders of magnitude higher than the critical temperature T_c. The evaporative cooling technique was the last missing piece of the puzzle which was implemented to further cool the gas of laser cooled atoms and the first evidence of BEC in a gas of rubidium-87 atoms was achieved in 1995. A point to note here is that conventional techniques for cooling a gas of alkali atoms were not used as the atoms would condense on the walls of the container.

A vapour of dilute atomic gases is desirable to achieve BEC due to the fact that the interactions are very low and to a good approximation it could be treated as an ideal gas. Further, in a dilute gas of alkali atoms, each constituent atom may be treated as a boson due to the total atomic spin being an integer. Historically, amongst all elements, hydrogen was thought to be the most probable candidate to obtain a BEC with till the 1970s [5]. This was mainly due to two reasons. Firstly, due the inverse relation of critical temperature of condensation with the mass of bosons, the highest transition temperature for a gas of dilute atomic gases is that of hydrogen which has the lowest mass. Second, due to the small size of the hydrogen atom, and the resulting small dipole moment, hydrogen atoms react extremely weakly with each other as compared to a gas of atoms of other elements. Therefore, there was great interest in cooling hydrogen atoms to achieve BEC. Spin polarized hydrogen atoms were cooled to a temperature of millikelvin range by trapping them. However, the temperatures achievable were well above the transition temperature for achieving BEC in hydrogen.

The final stage of cooling to achieve a BEC known as 'evaporative cooling' was the final ingredient. This final stage of cooling is often popularly compared with cooling a cup of tea by blowing on its surface. By removing the energetic atoms, present as vapour on the surface of the tea, one can cool it faster. In a similar manner, evaporative cooling ejects bosons with higher energy from the trap over and over again. However, for this to happen, the atoms need to thermalize quickly due to the limited lifetime of the trap and this is where the problem with hydrogen was. Due to the low interactions between hydrogen atoms the time taken for them to thermalize in a trap was very high, thus preventing the temperature from dropping below the BEC transition temperature. Thus, in a way the very reason why hydrogen was assumed to be the best BEC candidate was the reason why hydrogen BEC could not be achieved, namely due to its low inter-atomic

interaction strength. However, this evaporative technique was perfected for rubidium-87 in 1995 and the first evidence of BEC in dilute atomic gases was reported in 1995. This was followed by observation of BEC in sodium [78], lithium [98], hydrogen [10], cesium [99], potassium [100], chromium [101], etc. The problem of cooling hydrogen was solved by using a technique called spin resonance and a hydrogen BEC was obtained in 1998.

Having given this historical perspective, we shall have a quick look at the experimental aspects. We start by giving a brief discussion of laser cooling, evaporative cooling and the trapping of neutral atoms. Then we shall see how to ascertain that the atomic gas has reached the BEC phase. In this sub-section we shall also look at the ways to image BECs and obtain their density profile. We end by briefly describing methods to excite and detect vortices, solitons and small amplitude oscillation modes in a BEC.

2.8.1   Cooling and trapping

Historically, the technique of laser cooling was developed mainly to perform better spectroscopic measurements on atoms by eliminating the thermal effects [102]. However, the importance of this technique as a step towards the critical temperature required to achieve BEC was realized in 1970s [6]. There are three aspects which are important to obtaining BEC. First is the laser cooling, second is the trapping and third is evaporative cooling. As mentioned earlier, the problem with conventional methods of cooling by using containers is that the gaseous atoms would condense on the surface of the vessel. Therefore, it is necessary to trap these gases by methods which would avoid contact with containers. The way out is trapping them in a region of space using electromagnetic effects. However, this trapping of neutral atoms in magnetic and optical traps is hindered due to the fact that neutral atoms interact only weakly with the external magnetic or electric fields. This means that the potential minimum created at the center of the trap is very shallow. As such, the atoms need to be cooled to very low temperatures for them to be contained by such traps.

Laser cooling relies on resonant absorption of photons by atoms, followed by spontaneous emission. If a photon is incident upon an atom such that the energy of the photon is exactly equal to the atomic excitation energy, the photon is absorbed by the atom and it reaches an excited state. In the meanwhile, the atom acquires momentum in the direction in which the photon was propagating. The excited atom then spontaneously emits the absorbed photon in a random direction while obtaining a recoil velocity. Suppose now that an atom is bombarded with a beam of photons with energy equal to atomic excitation in a specific direction, then with subsequent absorption of photons the atom will acquire speed in the direction of the beam. However with spontaneous emission of

the photon the average recoil velocity acquired is zero because the direction of emission is random. Thus, we can change the speed of atoms in a specific direction by making photons of specific frequency incident on them. As temperature of a gas is a measure of the average kinetic energy of its particles, slowing down the atoms in an atomic gas reduces its temperature [8]. The frequency selection required for the process of resonant absorption is provided by a laser. An important factor that has to be taken into account is the Doppler effect due to the motion of atoms and its effect on the change in frequency of incident laser which an atom *sees*. As our aim is to reduce the speed of atoms in all the directions, a gas of atoms is bombarded with laser beams from 6 directions, with one modification that the lasers are tuned such that the energy of photons is slightly lower than atomic excitation energy to account for the Doppler shift. To see how this setup works, imagine a coordinate system whose axes are aligned with the laser beams. An atom travelling in a positive X-direction will *see* the frequency of photon travelling towards it (in the negative X-direction) to be blue shifted. The detuning of the laser frequency is such that the blue shift makes the energy of the photon exactly equal to the atomic excitation energy. Note that this atom won't absorb energy from a photon travelling in the same direction (in this case, the positive X-direction) as the Doppler shift of this photon is not resonant with the atomic excitation. Thus, with subsequent absorption and spontaneous emission of laser photons, the speed of the atomic gas reduces and so does the temperature. There are however practical problems involved in this process, for example, after the atoms slow down and reach a certain speed, the detuned lasers are no longer detuned for the new Doppler shift due to the change in speed of atoms. A lucid explanation of such practical problems can be found in the excellent review by Phillips *et al.* [6] and few other reviews on the subject [28, 103]. Methods to overcome problems with laser cooling are also described in the review articles.

To obtain an aggregate of such laser cooled atoms, it is necessary to confine them in a region of space in order to avoid thermalization with surroundings. For reasons mentioned previously, containers cannot be used. As atoms are electrically neutral, their trapping is done by utilizing their magnetic and electric dipole interactions. Magnetic trapping is achieved by using spin polarized atoms. A radially symmetric magnetic field potential is engineered with the minimum of magnetic field at the center of the trap [6]. Due to the interaction of the spin polarized atoms with the magnetic field, they experience a potential well. The atoms with least energy occupy the center of the trap, with the energetic atoms being present away from the center, the distance from the center based on their energy. A similar trapping may be obtained by interaction of an electromagnetic wave with induced dipole moments in atoms. For this, a laser beam with gaussian intensity profile is used [40]. This would also produce a minimum at the centre and the atoms may be confined. However, the use of electric dipole moment has

the disadvantage that laser causes heating of atoms. Therefore, the gaussian beam has to be switched off periodically and the atoms have to be laser cooled again. This process has to be repeated to prevent loss of atoms [6] .

As the interaction of electric and magnetic dipoles with electromagnetic fields is weak, it can only confine laser cooled atoms. Furthermore, atoms in the trap have to be isolated from the surroundings as this will cause heating. A longer lifetime is achieved by trapping atoms in high vacuum. Note that due to the weak interactions of the atoms with the electromagnetic fields, strong fields need to be applied for trapping atoms. However, application of strong electromagnetic fields causes shifts in energy structure of atoms. Due to this spectroscopic measurement of atoms in a trap is largely affected. As such the trap is usually switched off before making spectroscopic measurements.

After the atoms are trapped successfully, the atoms can be further cooled by a process known as evaporative cooling [104]. Through this process, the laser cooled atoms can achieve a temperature lower than transition temperature to achieve BEC. Evaporative cooling is inspired by cooling of surfaces upon evaporation of liquids from them. Evaporation takes away energy from the system, thus cooling the system. In short, evaporative cooling may be described as follows. As mentioned above, atoms occupy regions in a trap based on their energies. The least energetic atoms occupy the trap centre with energetic atoms populating regions away from the trap center based on their energies. This distribution of atoms is crucial to perform evaporative cooling. In terms of distributions of the system, evaporative cooling involves removal of high energy tail of the distribution, thus reducing the temperature of the system. Higher energy atoms from the trap are ejected so that they leave the remaining atoms at a lower temperature. For this to happen, the atoms have to thermalize at time scales lower than the lifetime of atoms in the trap. There are several methods employed in experiments to achieve evaporative cooling. A simple method involves touching the atoms at the end of the trap with container walls, maintained at a temperature of few millikelvin [6]. Another method reduces the height of the trap, so that atoms with higher energy are ejected from the trap. However, the most popular method is the rf-method which uses the electromagnetic waves to exploit the atomic structure to selectively eject atoms from the trap [105]. The details of some of the experiments may be found in reviews by Ketterle *et al.* [103] and Tino *et al.* [106] to mention a few.

In the next section we address the question as to how does one confirm that a BEC has been achieved experimentally and how to measure subsequently the density profile and other properties of a BEC.

2.8.2 Imaging BECs

Having cooled the atoms, we need to ascertain whether we have obtained a BEC and then to measure its various properties. The most important property is the density profile of a BEC which has been used as an experimental proof of condensation. BECs are defined by the macroscopic occupation of zero energy ground state of a gas, which is the zero momentum state. Therefore, to claim evidence of achievement of a BEC, the velocity distribution of the gas has to be measured. Direct measurement of velocity distribution at such low temperatures as the BEC transition temperature is a challenge. Therefore an indirect measurement of the velocity distribution profile is done using what is known as the time of flight measurement [9]. Further, there are three popular methods of measuring the density distribution of a BEC. The most popular method is the absorption imaging where a shadow of the condensate is cast on the CCD camera [107]. The other two popular methods are phase measurement [108] and fluorescence spectroscopy [109].

As mentioned earlier, due to the trapping potential used, the trap centre is populated by atoms with lowest energy. The energy of the atoms gradually increases with distance from the trap centre. Therefore, the trapping of atoms has an additional advantage in that it converts the information regarding momentum distribution of the atoms into spatial distribution. The relative population of atoms as a function of distance from the trap centre then can ascertain the occurrence of condensation. As the atoms are released from the trap, the atoms shall expand according to their initial energy. The atoms at the centre of the trap being in their ground state would be localized even after being released from the trap, whereas the atoms away from the trap would expand more and spread out. Thus, if there is a macroscopic population of the zero momentum ground state, which would be localized near the trap centre, we may observe a spike in density of atoms even after being released from the trap. This density distribution of the atoms is then measured by utilizing the interaction of light with these atoms.

The most prevalent technique of imaging is absorption imaging. This is also the simplest technique. In this technique a resonant laser is shone upon a cloud of atoms. By 'resonant' it is meant that the laser frequency is adjusted so that it corresponds to a frequency which the atoms can absorb. By shooting the laser directly at the atom cloud and placing a CCD camera behind it, we can cast a shadow of the atomic cloud on the CCD camera. There are many caveats on the use of this technique. Firstly, for absorption imaging of atom clouds, the atoms have to be released from the trap. The reason for this is two-fold. Firstly, the magnetic field used for trapping significantly distorts the atomic structure of atoms anisotropically. Secondly, for trapped atoms, the densities are very high and as such the details of the density profile get lost while absorption

imaging. Therefore, the atoms have to be released from the trap and allowed to expand for the details of the density profile to be accessible for probing. These reasons prevent in-situ imaging of the cloud using absorption imaging. Fig.(2.6) shows the absorption images demonstrating the onset of BEC transition in the first observation of a BEC by Anderson *et al.* [9]. This shows the onset of BEC as the temperature is varied from just above the critical temperature of condensation, to the condensation temperature. The temperature of the atomic cloud is measured using its absorption image. Since the trap converts the information on momentum distribution of atoms into spatial distribution, the profile of concentration of atoms gives the momentum distribution. From this distribution, the temperature of the atomic cloud can be calculated. To note is the fact that absorption imaging is destructive since resonant absorption by atoms leads to momentum gain and consequent heating.
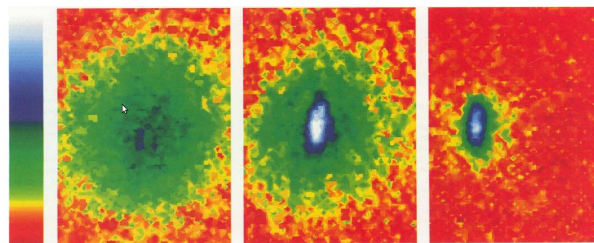
Figure 2.6: Figure shows three false colour absorption images of atomic cloud released from a trap. The image on the left shows the atomic cloud above the BEC transition temperature, the middle image is for the atomic cloud just below the transition temperature while the image on the right shows the BEC after further evaporative cooling. As can be seen, the rightmost image has the least number of atoms out of the condensate [9]. From *Science, Vol 269, Issue 5221, pp. 198-201, 14 July 1995.* Reprinted with permission from AAAS.

Another mode of interaction of light with matter is that of change of phase of the light on interaction with matter. When coherent radiation is incident upon cloud of atoms, the phase of the radiation changes and this change is proportional to the density of the atoms. However, this change of phase cannot be imaged and hence this information has to be converted to a readable density profile. This method of imaging is called 'Phase contrast imaging' [110, 111]. The information regarding the change of phase can be converted into the density profile by blocking the unscattered radiation [103]. Fig.(2.7) shows schematically the experimental setup for phase contrast imaging. Off-resonant laser radiation is incident upon the atom cloud and the unscattered radiation is blocked. The scattered radiation is then incident on a CCD camera. Due to the blocking of unscattered radiation, the intensity of radiation incident on the CCD is directly proportional to the phase shift of the laser, for small phase shifts [103]. This information about the intensity is then converted into a density profile. The main advantage of phase contrast imaging is that it allows for in-situ measurements. This is because the technique doesn't require resonant radiation to be incident on the atom cloud. As a result, the technique is non-destructive. Consequently, multiple images of

the same cloud can be taken. However, as this technique relies on the CCD camera, it suffers from slow speed of imaging. This is more of a technological limitation of the CCD. Due to the limited lifetime of a condensate in a trap, only limited number of images may be taken.
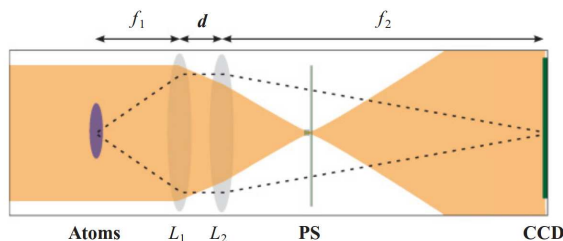
Figure 2.7: Figure shows the idea of phase contrast imaging. Trapped atoms are illuminated by coherent radiation. The interaction of coherent waves with atoms brings about a change in the phase of the wave. This combination of scattered and unscattered radiation is then passed through a lens where the unscattered radiation is focused in the focal plane. By placing an object, called the phase spot (PS) in the focal plane of non-diffracted incident radiation, the unscattered radiation is blocked. Then only the scattered radiation remains which can be read by a CCD camera to give density profile. This figure has been taken from paper by Meppelink *et al.* [111].

Lastly, fluorescence imaging is another technique to probe density of an atomic cloud. A probe beam is incident on the sample and the fluorescent radiation is measured using an imaging objective. Fig.(2.8) shows the fluorescence image of a BEC cloud [112]. In the previous two techniques, the column density along 1 direction is usually integrated. Thus, effectively 2D images of the atomic cloud are obtained. Fluorescence imaging has been proposed to obtain 3D images of the atomic cloud. However, for dense clouds only fluorescence radiation from the surface of the cloud reaches the imaging objective unscattered. Therefore, to obtain accurate 3D profile, the cloud has to be released from the trap.

Having given a brief introduction of cooling, trapping and imaging techniques, we now describe the method to obtain and image the three main types of excitations in a BEC, namely the vortices, solitons and small amplitude oscillation modes. This thesis deals mainly with the study of these excitations and as such it is useful to know how these are excited experimentally and imaged.

2.8.3 Exciting vortices in a BEC

Vortices are unique to superfluids in effectively 2D or 3D geometry. In 3D geometry, vortices appear as filaments, with interactions between vortices depending on their orientation [113]. This introduces a complex behaviour in a BEC with a bunch of vortex filaments. However in a 2D geometry, the choice of axis of rotation is confined to a
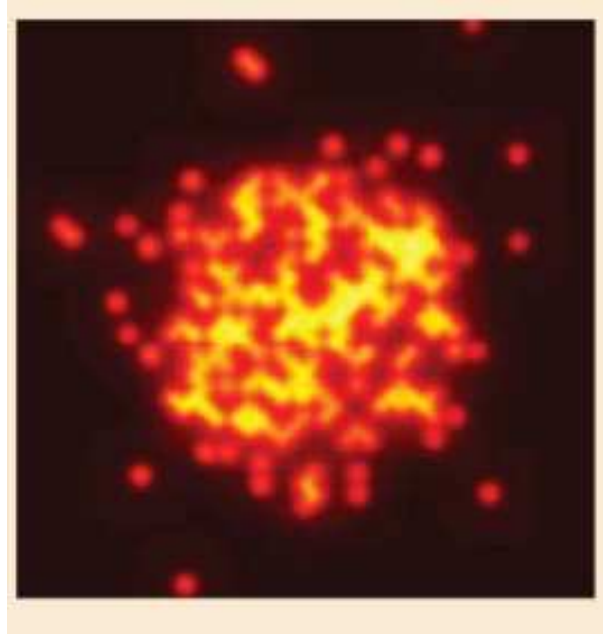
Figure 2.8: Figure shows scheme of fluorescence image of a condensed cloud. This figure has been taken from Sherson *et al.* [112].

single axis. In 2D on generation of a large number of vortices in the system, we obtain a lattice of vortices [114].

Vortices may be generated in BECs either in a deterministic manner or a stochastic manner. The category under which a certain method of vortex generation in a BEC falls is determined by the following question. Given a BEC in which we have obtained a certain configuration of vortices by a certain method, can the method be repeated to give the same configuration of vortices? If the answer is yes, then the method is called *deterministic*, or else the method is called *stochastic*. The three major techniques of exciting vortices are by stirring the condensate, phase imprinting and introducing defects in a BEC which decay as vortices. The first two methods fall under the deterministic category, while the third is a stochastic process. Further, the vortices can be imaged in a destructive manner, or by using in-situ imaging. Let us first describe briefly the methods of generation of vortices and then we will look at the imaging methods.

The first method of generating vortices consists of pumping angular momentum in the atomic cloud by stirring it. This angular momentum may be imparted either before of after the onset of condensation. A gas of BEC in a trap may be stirred by introducing anisotropy in the trap [115, 116]. This anisotropy may be introduced using a laser beam far detuned from atomic resonance. This detuning is necessary to avoid resonant absorption and hence heating. This stirring was introduced in a 2D condensate, by using two co-propagating laser beams. These lasers define a plane which contains the axis of tight confinement. By rotating this plane about the axis of tight confinement, the

condensate is stirred [57]. A variation of this technique consists of imparting angular momentum to a trapped atomic cloud before the RF cooling process. This angular momentum imparted to the thermal cloud helps nucleate vortices once it is cooled below the condensation temperature by RF cooling [117].
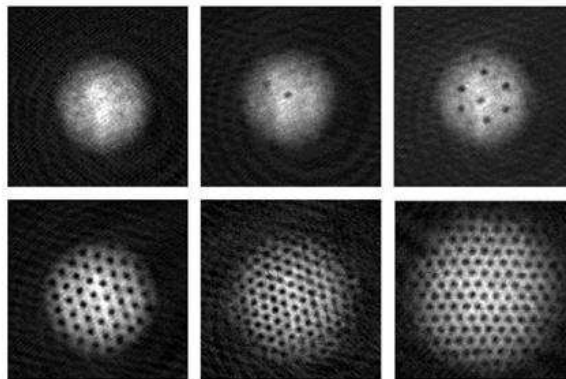
Figure 2.9: Figure shows the increase in number of vortices upon increase in frequency of rotation of the BEC and the subsequent formation of the vortex lattice. This figure has been taken from Engels *et al.* [55].

The second method consists of imprinting a phase on the condensate. This phase may be imprinted by changing the local energy of a trapped condensate [118]. The local phase of the condensate is proportional to its local energy. This energy may be varied by using a far detuned laser beam [58, 119]. Phase may also be imprinted in a BEC by using an external bias magnetic field [120].

Lastly, vortices may be generated in a BEC by inducing defects [121]. For instance, solitons are defects that are stable in 1D geometry. However, in higher dimensions, solitons suffer from snaking instability and decay into vortices [122]. Therefore, vortices may be generated in a BEC by generating 1D solitons in a 2 or 3 dimensional condensate and then waiting for them to decay into vortices. Defects can also be created by creating domains in a trapped BEC [58]. At the interface of these domains, there arises a singularity of phase which can create a soliton which can decay into vortices. This may also be done merging different condensates [123]. Further, a similar mechanism is used for generating vortices and is called the Kibble-Zurek mechanism in which the atomic gas is made to cross the BEC transition in a finite quench time [124]. This creates defects in the BEC such that domains with different phases are nucleated, consequently generating vortices.

Outlining the techniques for generating vortices in a BEC, the imaging of vortices is important in measuring their characteristics. Vortices are imaged mainly by absorption imaging. Since the length scale of the core of the vortex in a BEC is of the order of healing length, in-situ imaging using laser probes is difficult. Therefore, absorption

imaging is the most popular technique used. The condensate is released from the trap and the density profile of the expanded condensate is measured. As absorption imaging is destructive, it is mainly used for imaging deterministic vortices. However, for imaging stochastic vortices, in-situ imaging is preferable [125]. An example of the in-situ imaging technique used involves the use of a two-component BEC in which vortices are generated in one of the components. The core of these vortices are filled with atoms from the second component. The second component is then used to obtain the density profile of the vortex like a stencil [126].

Having described the nucleation and detection of vortices in a BEC, let us next have a look at the generation and imaging of solitons in an effectively 1D BEC.

2.8.4   Exciting solitons in a BEC

As discussed in the theory earlier, solitons are shape preserving waveforms which are characteristic of non-linear systems. These are characterized by dip in the density for dark solitons and a spike in the density for a bright solitons. Due to the structure of the non-linear GP equation, dark solitons are observed in a BEC with repulsive interactions, whereas bright solitons are observed in a BEC with attractive interactions. A bright soliton is essentially a particle like excitation [37]. On the other hand, dark solitons are characterized by a phase profile which changes with the depth of the central density dip [34]. Bright and dark solitons are excited in a BEC using distinct techniques. While there is one widely used technique to generate bright solitons, there are several techniques to generate dark solitons. It is important to state that solitons are stable only in 1D condensates [127]. In higher dimensions, solitons decay due to snaking instability. Therefore, solitons are excited mainly in cigar shaped condensates, i.e. the trapping along radial dimensions is extremely tight as compared to the axial direction [59].

Since attractive BECs are unstable, generating BEC in an atomic gas with attractive interactions is not feasible. On the other hand, repulsive interactions cannot sustain bright solitons. To solve these contradictory circumstances, Feshbach resonance is employed. Feshbach resonance enables to tune the strength of interactions in a BEC by modifying the s-wave scattering length, in principle from positive infinity to negative infinity. To generate bright solitons in a BEC, a BEC with repulsive interactions is generated in a magnetic trap. Feshbach resonance is then used to tune the scattering length to a weak negative value. The interactions are kept weak so as to increase the lifetime of the BEC, since attractive BECs are inherently unstable. In this way, multiple solitons may be generated [128]. The BEC is then released from the trap and solitons are imaged using absorptive or dispersive imaging [129].
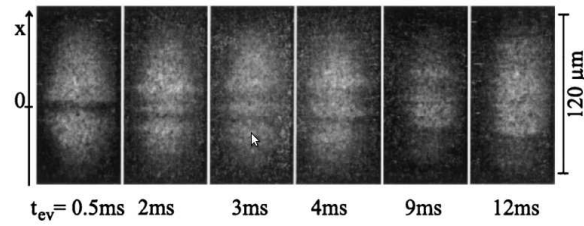
Figure 2.10: Figure shows the first absorption images of propagating solitons reported in 1999. This figure has been taken from Burger *et al.* [144].

Dark solitons are excited in a repulsive BEC using quite a few methods. After having obtained a BEC in a magnetic trap, dark solitons may be generated by density engineering method [130]. In this method, an external potential is super-imposed upon the trapping potential to create an artificial dip in density for a finite amount of time. After the external potential is turned off, a dark soliton appears in the trapped BEC. Secondly, a dark soliton can be excited by what is called the *phase-imprinting method*. In this method, a laser is shone upon one half of the BEC to imprint a phase which is the characteristic of 1D dark solitons [131]. A hybrid of the density engineering method and phase engineering method may also be used [59]. Next, solitons also appear due to defects. This was also mentioned as a vortex generation method. For example, when a BEC is generated in a double well, the condensate in each of the wells acquires a different phase. When the double well potential is turned off, the condensates merge. At their interface there is a discontinuity in the phase and solitons are generated as a result [103]. Lastly, solitons may be generated when a BEC flows past an obstacle [132]. The solitons so generated are imaged using time of flight analysis using absorptive or dispersive imaging.

2.8.5 Measuring the excitation spectrum in a BEC

The final kind of excitation which we shall be dealing in this thesis is the small amplitude oscillation mode. These excitations give us the excitation spectrum of the BEC which are important for getting knowledge about the superfluid properties of the BEC. In a trapped BEC, small amplitude modes are excited mainly using two methods. First is by perturbing the spring constant of the harmonic trapping potential [65]. After perturbing the trapping potential for a finite time, the perturbing potential is turned off and only the harmonic trapping remains. After a finite time, the harmonic trapping is turned off and the condensate is allowed to expand. This splits the atomic gas into two parts. The larger part is the condensed fraction and the smaller part are the small amplitude excitations. The separation between the centres of these two gaussians determines the wave vector. By using different frequencies to perturb the BEC, the excitation spectrum

of the BEC may be determined using this method [64]. The imaging is done either using absorptive or dispersive methods. Fig.(2.11) gives the atomic gas released after exciting small amplitude modes [63]. The condensed and the excited fractions can be clearly seen to be separated.
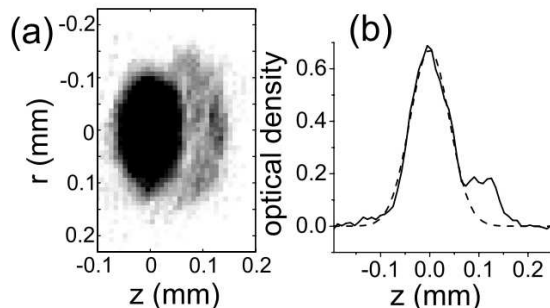
Figure 2.11: Figure shows the atomic cloud in which excitations have been induced. Part (*a*) shows the absorption image in which the condensed and excited part of the atomic cloud can be seen to be separated. Part (*b*) is a cross section of the absorption image in which the dashed line is the gaussian fit to the condensed cloud. This figure has been taken from Steinhauer *et al.* [63].

The second method of exciting small amplitude modes in a BEC is by using Bragg spectroscopy [133]. Two laser beams with almost parallel polarization and an angle between them are shone on the condensate. The detuning between the two beams can be varied using a frequency control. The angle between the lasers determines the wave vector of the mode excited in the BEC. The detuning between the lasers is then varied to obtain the Bragg resonance. The imaging here as well is done using absorptive or dispersive imaging.

Having reviewed the general theory and experimental methods in a BEC, we shall now proceed to the works done by us in what follows. We shall start with the corrections to the local GP equation and the changes to the energy functional due to these corrections. We present a proof of the exact correspondence between corrections to the GP dynamics and those to the energy functional. This non-trivial correspondence is proved rigorously. Secondly, we shall have a look at the new class of vortex solution with width of the order of the microscopic length scale of interactions in a BEC. This is qualitatively different from the vortex solution with width of the order of the healing length ξ_0. Next, we shall see the effect of the first order correction to the LGPE on the dark and bright soliton solution. Lastly, we shall have a look at the effect of finite-range of interactions between bosons on the elementary excitation spectrum in a BEC.

Chapter 3

Energy functional for the modified Gross-Pitaevskii equation

Bose-Einstein Condensates (BECs) are modeled theoretically at a mean field level using the Gross-Pitaevskii (GP) equation [34]. Since the BEC exists at a low temperature, the low energy s-wave scattering is the dominant interaction mechanism governing the system. The mean field GP theory which takes into account only the two-particle s-wave scattering as the interaction between particles captures the essential properties of a BEC. It uses a pseudopotential approach to account for inter-particle interactions. The actual inter-particle interaction potential is replaced by a soft potential. Due to the symmetric nature of s-wave scattering, the inter-particle interaction potential in GP model is replaced by a symmetric pseudopotential. The constraint is rather on the strength of the pseudopotential. To make use of this freedom, a delta-function psuedopotential is usually used which, not only simplifies calculations considerably, but also is quite effective for dilute BECs. We shall call such a model, where the pseudopotential used is a delta-function, as the *local GP equation* (LGPE). However, using a delta-function as the pseudopotential sacrifices the information that we might get from the finite range effects of the s-wave interactions. We can expect the finite range of the s-wave interactions to introduce corrections to the LGPE. These corrections can be obtained in two ways. Firstly, we can obtain the finite momentum expansion of the phase shifts [35, 36]. Another way is to replace the delta-function by an extended pseudopotential, which would have a finite width and then employing Taylor expansion [62]. We shall see that both these methods give qualitatively similar correction terms to the LGPE.

The energy functional of a system gives the total energy of a system for a certain state. This is a very important quantity since employing energy minimization to find the ground state is the central theme of variational methods. The LGPE has a well defined energy functional [34]. In a similar way, it is desirable to obtain the energy functional for the LGPE with correction terms. As we shall see, the correction terms form a series. The physical parameters of the system would dictate the order to which such a series is truncated. As such, it is desirable to obtain a general energy functional corresponding to the series of correction terms up to an arbitrary order. In this direction, it is advantageous if we can identify a pattern between each correction to the LGPE and the corresponding correction to the energy functional. This is indeed what we shall show using simple combinatorial techniques [45].

In this chapter, we start by showing how corrections to the LGPE are obtained. Then we obtain an energy functional corresponding to such corrections to the LGPE. There exists a term by term correspondence between corrections to the LGPE and corrections to the Energy functional. This is established mathematically using simple combinatorics [45].

3.1 Corrections to the local GP equation

3.1.1 The local GP equation

The mean field GP equation is of the form

$$
\begin{aligned}
i\hbar\frac{\partial\psi(\mathbf{r},t)}{\partial t} = &- \frac{\hbar^2}{2m}\nabla^2\psi(\mathbf{r},t) + V_{ext}(\mathbf{r},t)\psi(\mathbf{r},t) \\
&+ \psi(\mathbf{r},t)\int \psi^*(\mathbf{r}',t)V_{eff}(\mathbf{r}-\mathbf{r}')\psi(\mathbf{r}',t)\ d\mathbf{r}',
\end{aligned}
\tag{3.1}
$$

where $V_{ext}(\mathbf{r},t)$ is the externally applied potential, $|\psi(\mathbf{r},t)|^2$ gives the density of the BEC and $V_{eff}(\mathbf{r}-\mathbf{r}')$ is the pseudopotential which replaces the interaction potential between the bosons in the mean field GP theory. The restriction on the pseudopotential is that $\int V_{eff} = g$, where $g = 4\pi\hbar^2 a/m$ captures the interaction strength with 'a' being the s-wave scattering length. This is because in the s-wave scattering, the exact shape of the interaction potential cannot be resolved by the low energy particles. Taking advantage of this condition, one replaces the effective potential with a δ-function, thus turning Eq.(3.1) into

$$i\hbar\frac{\partial\psi(\mathbf{r},t)}{\partial t} = -\frac{\hbar^2}{2m}\nabla^2\psi(\mathbf{r},t) + V_{ext}(\mathbf{r},t)\psi(\mathbf{r},t) + g\,\psi(\mathbf{r},t)|\psi(\mathbf{r},t)|^2. \qquad (3.2)$$

We shall refer to Eq.(3.2) as the local GP equation (LGPE). The LGPE does not take into account the energy dependence of the effective interactions. It thus neglects the finite range effects of the interaction potential and the corrections to the LGPE arising thereby. Even in the low energy regime of BEC, there would arise corrections to the GP equation. These corrections can be accounted for in two ways. One, by considering a low k expansion of the scattering amplitude and second by taking an extended pseudopotential. Let us look at both these approaches and the kind of correction terms to the LGPE that they generate.

3.1.2 Corrections due to finite momentum expansion

The real part of the scattering amplitude for s-wave scattering is given by [84]

$$-\frac{m}{4\pi\hbar^2}\int\mathbf{dr}\,e^{-i\mathbf{k}\cdot\mathbf{r}}\,V_{eff}\,e^{i\mathbf{k}\cdot\mathbf{r}} = Re[f(k)], \qquad (3.3)$$

where $\mathbf{k}$ is the incoming wave-vector. The scattering amplitude has no angular dependence due to symmetric nature of s-wave scattering. As mentioned before, in the case of LGPE, the effective potential is taken to be a delta function. As we shall see, this is the zero momentum approximation in context of scattering amplitude.

In terms of phase shifts, the scattering amplitude is given by $f_l(k) = \frac{1}{k(\cot\delta_l - i)}$, where l is the angular momentum state in the partial wave expansion [84] and δ_l is the phase shift corresponding to the value of l. Since we are dealing with s-wave scattering, we shall deal with the case $l = 0$. For low values of k, we can obtain an expansion for $k\cot\delta_0$ [83] which can be written as

$$k\cot\delta_0 = -\frac{1}{a} + \frac{1}{2}r_e k^2 - Pr_e k^4 + O(k^6), \qquad (3.4)$$

where a is the s-wave scattering length, r_e is the effective range and P is a term dependent on the shape of the interaction potential. Using the equation above, the real part of scattering amplitude for $l = 0$, $f_0(k) = \frac{1}{k(\cot\delta_0 - i)}$ can be written as $Re[f_0(k)] = -a + a^2(a-\frac{r_e}{2})k^2 + O(k^4)$. We want the expression thus obtained for scattering amplitude to be consistent with Eq.(3.3), as both represent the same quantity, the scattering amplitude. For $k = 0$ in order for this expression to be consistent with Eq.(3.3), we write $V_{eff} = g\,\delta(\mathbf{r_1} - \mathbf{r_2})$, where $g = \frac{4\pi\hbar^2 a}{m}$ and $\delta(\mathbf{r_1} - \mathbf{r_2})$ is the Dirac delta function.

In order to incorporate finite values of k in the effective range expansion, the effective potential needs to be modified. Looking at Eq.(3.3), one can estimate that there need to be Laplacian and higher order derivative terms as corrections to bring in terms of the form k^{2n} in the scattering amplitude. Hence, there would arise corrections to the effective potential on top of the δ-function. These corrections are of the form

$$V_{eff} = g\delta(\mathbf{r_1} - \mathbf{r_2}) + \frac{g_2}{2} \left[\delta(\mathbf{r_1} - \mathbf{r_2})\nabla^2_{\mathbf{r_1}-\mathbf{r_2}} + \nabla^2_{\mathbf{r_1}-\mathbf{r_2}}\delta(\mathbf{r_1} - \mathbf{r_2}) \right] + O(\nabla^4_{\mathbf{r_1}-\mathbf{r_2}}).$$

Plugging this form of the effective potential in Eq.(3.1), we get corrections to the LGPE of the form [36]

$$
\begin{aligned}
i\hbar\frac{\partial\psi(\mathbf{r},t)}{\partial t} = &-\frac{\hbar^2}{2m}\nabla^2\psi(\mathbf{r},t) + V_{ext}(\mathbf{r},t)\psi(\mathbf{r},t) + g\ \psi(\mathbf{r},t)|\psi(\mathbf{r},t)|^2 \\
&+ g_2\ g\ \psi(\mathbf{r},t)\ \nabla^2|\psi(\mathbf{r},t)|^2 + O(\psi(\mathbf{r},t)\nabla^4|\psi(\mathbf{r},t)|^2),
\end{aligned}
\tag{3.5}
$$

where g_2 captures the effective range of scattering r_e via the relation $g_2 = \left(\frac{a^2}{3} - \frac{ar_e}{2}\right)$. Thus we can see that due to the effective range expansion, we get corrections to the LGPE using the finite momentum expansion of scattering amplitude.

The name 'effective range' does not imply that r_e is the width of the interaction potential, but that r_e is approximately determined by the width and the strength of the effective potential. The limit $r_e \leq 2a/3$ can be understood as follows. Consider the solution to the s-wave scattering problem given by $\psi(k,r)$, where k is the wave momentum and is small since we are considering low energy scattering. Let the solution far away from the scattering region be given by $\phi(k,r)$. In other words for large r, $\psi(k,r) = \phi(k,r)$. Then the value of effective range is given by $r_e = 2\int dr[\phi^2(0,r) - \psi^2(0,r)]$ [134]. By definition, in a region of space where the scattering potential vanishes, $\psi(k,r) = \phi(k,r)$. Now, let the scattering potential have a range r_0, such that the scattering potential is zero for $r > r_0$. In such a case, the contribution to r_e would come from the integral from 0 to r_0 since for $r > r_0$ the integrand vanishes. Further for $k = 0$, we have $\phi(0,r) = 1 - (r/a)$, where a is the s-wave scattering length [134]. Now, looking at the expression of r_e, it may be easily inferred that the maximum value of the integrand is when $\psi(0,r)$ vanishes in the region $r \leq r_0$. This situation occurs when the scattering potential is a hard sphere potential in which case the potential is infinite for $r \leq r_0$ and zero for $r > r_0$. A simple calculation with $\phi(0,r) = 1 - (r/a)$ shows that for hard sphere scattering $r_e = 2a/3$. For any other potential, the value of integrand is smaller than this limiting value and hence $r_e \leq 2a/3$. The details of this calculation may be found in the

book by Newton [134]. There is also another way to obtain such an expression using an extended pseudopotential, which we explain next.

3.1.3 Corrections using an extended psuedopotential

The corrections to the LGPE can also be obtained by considering an extended pseudopotential instead of a δ-function pseudopotential. For the symmetric s-wave scattering considered, we can take any symmetric extended pseudopotential and do a Taylor expansion of the wavefunction to obtain the series of correction terms as in Eq.(3.5). The point to note here is that as long as we wish to look at the functional dependence of the correction terms, the exact shape of the pseudopotential does not matter. Of course the shape would decide the constant terms accompanying the correction terms. However, the functional form of the correction terms doesn't change. With this in mind, let us introduce the simplest modification to the δ-function pseudopotential in the form of a rectangular barrier potential. To abide by the requirement $\int \mathbf{dr}\, V_{eff} = g$, we take

$$V_{eff}(\mathbf{r} - \mathbf{r}') = \frac{3g}{4\pi(\alpha a)^3} \quad for \ \ |\mathbf{r} - \mathbf{r}'| < \alpha a$$
$$= 0 \quad otherwise.$$

This form of the pseudopotential asserts that the range of the interaction is of the order of a, with α being the proportionality factor. As we shall see, while obtaining corrections to th LGPE using such a pseudopotential, the zeroth order term remains unaltered. This means that to zeroth order such a pseudopotential gives the same term as that given by a δ-function pseudopotential. We can use this pseudopotential in Eq.(3.1) to obtain corrections to the LGPE. Note that as V_{eff} and ψ commute, Eq.(3.1) can be written as

$$i\hbar\frac{\partial\psi(\mathbf{r},t)}{\partial t} = -\frac{\hbar^2}{2m}\nabla^2\psi(\mathbf{r},t) + V_{ext}(\mathbf{r},t)\psi(\mathbf{r},t)$$
$$+ \psi(\mathbf{r},t)\int |\psi(\mathbf{r}',t)|^2 V_{eff}(\mathbf{r} - \mathbf{r}')\,d\mathbf{r}',$$

Further, we can Taylor expand $|\psi(\mathbf{r}',t)|^2$ around $\mathbf{r} - \mathbf{r}' = 0$. Doing this gives us

$$i\hbar\frac{\partial\psi(\mathbf{r},t)}{\partial t} = -\frac{\hbar^2}{2m}\nabla^2\psi(\mathbf{r},t) + V_{ext}(\mathbf{r},t)\psi(\mathbf{r},t) + g\ \psi(\mathbf{r},t)\ |\psi(\mathbf{r},t)|^2$$
$$+ \frac{3\alpha^2 a^2}{10}g\psi(\mathbf{r},t)\nabla^2|\psi(\mathbf{r},t)|^2 + O(\psi(\mathbf{r},t)\nabla^4|\psi(\mathbf{r},t)|^2). \tag{3.6}$$

As can be seen, the equation above gives qualitatively similar terms as Eq.(3.5). Using a different form of pseudopotential, say a gaussian, would give different numerical factors accompanying the correction terms. However, the functional form of the correction terms would remain the same. To emphasize upon this point, we can take a gaussian pseudopotential and look at the correction terms arising due to such a choice. The take the width of the pseudopotential to be of the order of s-wave scattering length, we take the width of the gaussian to be 'αa' as before. Also, as for the previous pseudopotential form, we have to abide by $\int \mathbf{dr}\ V_{eff} = g$. The form we take is

$$V_{eff}(\mathbf{r} - \mathbf{r}') = \frac{g}{\pi\sqrt{2\pi}(\alpha a)}exp[-\frac{r^2}{2(\alpha a)^2}].$$

This form of the pseudopotential can again be plugged into Eq.(3.1) and the Taylor expansion procedure can be performed as done for the barrier pseudopotential. Doing this gives the equation

$$i\hbar\frac{\partial\psi(\mathbf{r},t)}{\partial t} = -\frac{\hbar^2}{2m}\nabla^2\psi(\mathbf{r},t) + V_{ext}(\mathbf{r},t)\psi(\mathbf{r},t) + g\ \psi(\mathbf{r},t)\ |\psi(\mathbf{r},t)|^2$$
$$+ \frac{3\alpha^2 a^2}{2}g\psi(\mathbf{r},t)\nabla^2|\psi(\mathbf{r},t)|^2 + O(\psi(\mathbf{r},t)\nabla^4|\psi(\mathbf{r},t)|^2). \tag{3.7}$$

This demonstrates that the form of the dynamics remains the same, apart from numerical factors leading the corrections to LGPE. Taking another form of the pseudopotential may give different numerical factors. However, the underlying phenomenon which come out of this dynamics will qualitatively remain the same.

From the above it can be seen that, by incorporating the finite range factor in the pseudopotential itself, we can understand qualitatively the origin of the correction terms to the LGPE as arising from finite range of the actual interaction potential. Note however that, even if the terms arising from both these arguments are similar in form, the reasoning behind the origin of the terms is different. In the previous subsection, the corrections arose due to consideration of finite momentum of the BEC particles. However, the corrections presented in the current subsection arise due to consideration of finite width of the interaction potential [45]. Notice here that in the limit $\alpha \to 0$, the

corrections to the LGPE above vanish. However, the limit $r_e \to 0$ does not make the correction terms vanish. The corrections vanish for $r_e \to 2a/3$.

From Eq.(3.5) and Eq.(3.6), we get the functional form of the correction terms to the LGPE. They are of the term $\psi \nabla^2 |\psi|^2$, $\psi \nabla^4 |\psi^2|$ and so on. With the addition of correction terms to the LGPE, one needs to obtain a modified energy functional to reflect these correction terms. This is of utmost importance to study energetics of BEC systems when these correction terms assume significance. With this motive, in the next section we derive an expression of energy functional to account for such corrections to the LGPE, up to any order.

3.2 Energy functional and proof of correspondence

The LGPE can be obtained from the least action principle $\delta \int L dt = 0$, where $L = \left(- i\hbar \int \psi_0^*(\mathbf{r}, t) \frac{\partial}{\partial t} \psi_0(\mathbf{r}, t) \mathbf{dr} \right) + E$. The condition of stationarity for action can then be written as $i\hbar \frac{\partial \psi_0(\mathbf{r},t)}{\partial t} = \frac{\delta E}{\delta \psi_0^*(\mathbf{r},t)}$, where E is the energy functional. For the LGPE, the energy functional can be written as [37]

$$
E = \int d\mathbf{r} \ \left(\frac{\hbar^2}{2m} |\nabla \psi_0(\mathbf{r}, t)|^2 + V_{ext}(\mathbf{r}, t) |\psi_0(\mathbf{r}, t)|^2 + \frac{g}{2} |\psi_0(\mathbf{r}, t)|^4 \right).
$$

As the energy functional may depend on derivatives of $\psi_0^*(\mathbf{r}, t)$ as well, the notation $\frac{\delta E}{\delta \psi_0^*(\mathbf{r},t)}$ implies taking derivatives of E with respect to all the derivatives of $\psi_0^*(\mathbf{r}, t)$ as present in the energy functional. Thus,

$$
\frac{\delta E}{\delta \psi_0^*(\mathbf{r}, t)} = \left[\frac{\partial}{\partial \psi_0^*(\mathbf{r}, t)} - \nabla \cdot \frac{\partial}{\partial (\nabla \psi_0^*(\mathbf{r}, t))} + \nabla^2 \frac{\partial}{\partial (\nabla^2 \psi_0^*(\mathbf{r}, t))} - ..... \right] E
$$

As for the LGPE, we wish to write down an energy functional for corrections to the LGPE. We now propose that any correction (addition) to the local GP equation of the form $\alpha \psi \nabla^l |\psi|^2$ would correspond to an addition to the energy functional of the form $\alpha \frac{|\psi|^2}{2} \nabla^l |\psi|^2$, where l is even and α is an arbitrary constant. For simplicity, we work in Cartesian coordinates, where the Laplacian can be split as $\nabla^2 = \frac{\partial^2}{\partial x^2} + \frac{\partial^2}{\partial y^2} + \frac{\partial^2}{\partial z^2}$. In the rectangular coordinate system, the derivatives with respect to x, y, z coordinates are on equal footing as regards their appearance in the operator ∇^n. In what follows, we show what happens when a correction term with even order derivative of $|\psi|^2$ with respect to the x-coordinate is added to the energy functional. This argument can then be extend to even order derivative of y and z as x, y, z are linearly independent.

Consider the term in the energy functional $G = \frac{|\psi|^2}{2}\partial_x^l|\psi|^2 = \frac{|\psi|^2}{2}\left(\sum_{n=0}^l \binom{l}{n}(\partial_x^{l-n}\psi)(\partial_x^n\psi^*)\right)$. Let us look at the functional derivative of G with respect to ψ^*.

$$
\begin{aligned}
\frac{\delta G}{\delta\psi^*} &= \left(\sum_{m=0}^l(-1)^m\partial_x^m\frac{\partial}{\partial(\partial_x^m\psi^*)}\right)\left[\frac{|\psi|^2}{2}\left(\sum_{n=0}^l\binom{l}{n}(\partial_x^{l-n}\psi)(\partial_x^n\psi^*)\right)\right] \\
&= \left(\frac{\partial}{\partial\psi^*} + \sum_{m=1}^l(-1)^m\partial_x^m\frac{\partial}{\partial(\partial_x^m\psi^*)}\right)\left[\frac{|\psi|^2}{2}\left(\sum_{n=0}^l\binom{l}{n}(\partial_x^{l-n}\psi)(\partial_x^n\psi^*)\right)\right] \\
&= \frac{\partial}{\partial\psi^*}\left[\frac{|\psi|^2}{2}\left(\sum_{n=0}^l\binom{l}{n}(\partial_x^{l-n}\psi)(\partial_x^n\psi^*)\right)\right] \\
&\quad + \sum_{m=1}^l(-1)^m\partial_x^m\frac{\partial}{\partial(\partial_x^m\psi^*)}\left[\frac{|\psi|^2}{2}\left(\sum_{n=0}^l\binom{l}{n}(\partial_x^{l-n}\psi)(\partial_x^n\psi^*)\right)\right] \\
&= \frac{\psi}{2}\partial_x^l(|\psi|^2) + \frac{1}{2}\left[\sum_{m=0}^l(-1)^m\binom{l}{m}\partial_x^m\left(|\psi|^2(\partial_x^{l-m}\psi)\right)\right],
\end{aligned}
$$

which gives

$$
\frac{\delta G}{\delta\psi^*} = \frac{\psi}{2}\partial_x^l(|\psi|^2) + \frac{1}{2}\left[\sum_{m=0}^l(-1)^m\binom{l}{m}\sum_{p=0}^m\left(\binom{m}{p}(\partial_x^p|\psi|^2)(\partial_x^{l-p}\psi)\right)\right]. \tag{3.8}
$$

Let us fix p and considering the sum over all m, look at the the second term on the right hand side in square brackets of Eq.(3.8), which becomes $\sum_{m=p}^l(-1)^m\binom{l}{m}\binom{m}{p}\partial_x^p|\psi|^2\partial_x^{l-p}\psi$. Notice the lower sum is from p and not zero. This is necessary, because to have a term with p-th derivative, the minimum necessary value for the upper limit 'm' of the inner sum in the above equation is p. Also note that $p \leq m$. Let us introduce $q = m - p$. So we have,

$$
\begin{aligned}
\sum_{m=p}^l(-1)^m\binom{l}{m}\binom{m}{p}(\partial_x^p|\psi|^2)(\partial_x^{l-p}\psi) &= \sum_{q=0}^{l-p}(-1)^{q+p}\binom{l}{q+p}\binom{q+p}{p}(\partial_x^p|\psi|^2)(\partial_x^{l-p}\psi) \\
&= \sum_{q=0}^{l-p}(-1)^{q+p}\binom{l}{p}\binom{l-p}{q}(\partial_x^p|\psi|^2)(\partial_x^{l-p}\psi) \\
&= (\partial_x^p|\psi|^2)(\partial_x^{l-p}\psi)(-1)^p\binom{l}{p}\sum_{q=0}^{l-p}(-1)^q\binom{l-p}{q},
\end{aligned}
$$

where we have used the property $\binom{l}{q+p}\binom{q+p}{p} = \binom{l}{p}\binom{l-p}{q}$. It is easy to see that $\sum_{q=0}^{l-p}(-1)^q\binom{l-p}{q}$ is nothing but the expansion of $(1-1)^{l-p}$, which is zero, except for the case when $p = l$, for which, from Eq.(3.8) we can see that, $m = l$. So, we can conclude that the term

$\frac{1}{2}\left[\sum_{m=0}^{l}(-1)^m\binom{l}{m}\sum_{p=0}^{m}\left(\binom{m}{p}(\partial_x^p|\psi|^2)(\partial_x^{l-p}\psi)\right)\right]$ on the right hand side of Eq.(3.8) is zero, except when $p = m = l$. So, we need only consider the case where $p = m = l$ in which case, Eq.(3.8) assumes the following form

$$\begin{aligned}
\frac{\delta G}{\delta \psi^*} &= \frac{\psi}{2}\partial_x^l(|\psi|^2) + \frac{1}{2}\left[(-1)^l\left(\psi(\partial_x^l|\psi|^2)\right)\right] \\
&= \left(\frac{\psi}{2}\partial_x^l|\psi|^2\right) + (-1)^l\left(\frac{\psi}{2}\partial_x^l|\psi|^2\right).
\end{aligned} \tag{3.9}$$

From this it is clear that $\frac{\delta}{\delta\psi^*}\left(\frac{|\psi|^2}{2}\partial_x^l|\psi|^2\right) = \psi\partial_x^l\left(|\psi|^2\right)$ only when l is even and that $\frac{\delta}{\delta\psi^*}\left(\frac{|\psi|^2}{2}\partial_x^l|\psi|^2\right) = 0$ if l is odd. The absence of similar correspondence between the free energy and dynamics for odd 'l' actually manifests the non-trivial nature of the present result. Since the microscopic expansion for the s-wave scattering involves only even powers of k [35, 36] and hence only even order derivatives of $|\psi|^2$, the energy functional obtained by us can be used to calculate the energy of the system where we want to consider corrections to the local GP equation. As mentioned before, this same proof can be used for even order derivatives with respect to y and z. Thus, we have proven that any correction (addition) to the local GP equation of the form $\alpha\psi\nabla^l|\psi|^2$ would correspond to an addition to the energy functional of the form $\alpha\frac{|\psi|^2}{2}\nabla^l|\psi|^2$, where l is even.

This result is very important in the sense that the energy functional is very straightforward to evaluate, simply by writing the correction terms to the local GP equation and multiplying them by $\psi^*/2$ as long as s-wave scattering prevails. Now that we have the energy functional for corrections to the local GP equation, we can use it to study the effects of the corrections on the BEC.

3.3   Discussion

In the work done presented in this chapter, we have considered the standard form of corrections to the local GP equation arising from an effective range expansion due to non-local s-wave scattering. This effective range expansion gives corrections to the local GP equation. The order of expansion at which such a modified GP equation is truncated depends on BEC parameters. These parameters may include the effective range of the inter-boson interaction potential, the average inter-particle separation, etc. These corrections should be taken into account as we approach the strongly interacting BEC limit as shown by Fu *et al.* [36] These correction terms typically are associated with the length scales in a BEC. The kinetic term in the local GP equation is represented by

a Laplacian. Since the first correction term to this local GP equation is also a Laplacian, it is the term which is popularly considered in literature which studies BEC beyond the Fermi pseudopotential. In other words, the correction term probes a length scale similar to the kinetic term apart from the coefficient. To probe smaller length scales, one needs to add higher order corrections to the GP equation.

In this chapter the key novel result discussed concerns the corrections to the local GP energy functional arising due to corrections to the local GP equation. The given rigorous combinatorial proof of the same for taking into consideration non-local corrections up to any order in derivatives of $|\psi(\mathbf{r}, t)|^2$ is of importance. The non-triviality of this correspondence is represented by the fact that such a correspondence is absent for correction terms with odd order derivatives of $|\psi(\mathbf{r}, t)|^2$. Since the correction terms, as shown by Collin *et al.*, contain only even order derivatives and not odd order ones, our result will help write energy functional for corrections up to any order. In this sense, such a correspondence is special to symmetric s-wave scattering in BECs. This correspondence can be used to study the energetics of corrections to the GP equation, beyond the Fermi pseudopotential.

The energy functional presented here is used in our further works and, as we shall see, plays an extremely important role. This is because, the variational principle used to estimate ground states of quantum systems uses energy minimization as the key condition to fix variational parameters. As such finding the correct energy functional for a given systems assumes prime importance. Our further works on single vortex state and solitons will make extensive use of the energy functional derived.

Chapter 4

Vortex solution of the MGPE

In the previous chapter we showed the series of corrections to the local Gross-Pitaevskii equation (LGPE) arising from non-local interactions and the corresponding energy functional. Having obtained this modified GP equation (MGPE) and its corresponding energy functional, we now proceed to probe its implications on excitations in a BEC. In this chapter, we use the MGPE and study its vortex solution in a BEC.

One of the most important characteristic of a superfluid is its response to an externally induced rotation. In classical fluids, any external stirring immediately produces vortex states. As the external stirring is continuously increased, the angular momentum of the fluid increases continuously. As opposed to this, when a superfluid is subjected to external stirring starting from zero, vortex states don't appear until the stirring reaches a particular frequency. At this point, a single vortex line appears in the superfluid. As the stirring frequency is increased continuously beyond this point, in contrast to a classical fluid, the angular momentum of the single vortex line does not change at all until the frequency reaches a certain value when a second single vortex line is nucleated, and so on. This is one of the signatures of a superfluid, viz., the appearance of vortices with quantized angular momentum [12]. As a BEC exhibits superfluidity, such quantized vortices appear in BECs as well.

The width of the core of a vortex in a BEC, described by the LGPE, is of the order of healing length (ξ_0) which is an important length scale of a BEC. This length scale arises as a measure of length over which the kinetic energy term and the interaction term in the LGPE equation become comparable. For a BEC with inter-particle scattering length 'a' and density n, it is given by $\xi_0 = \frac{\hbar}{\sqrt{2mgn}}$ [37]. As ξ_0 is also the length scale of vortex solution of LGPE, it is crucial to address the question as to what happens when the trap size is made to be smaller than the healing length. This would take us into the regime of strong confinement in which the corrections to the LGPE would become significant. In

this chapter we will see that in this regime one finds a new class of vortex solution whose width is of the order of length scale of microscopic interactions [135]. Thus, we show the existence of an entirely new class of vortex solution which has never been shown before to the best of our knowledge.

In what follows we discuss the vortex solution for the LGPE and the effect of corrections to the LGPE on the vortex solution.

4.1 Overview of vortex solution for local GP equation

4.1.1 Quantization of angular momentum

Let us start by discussing the appearance of quantization of angular momentum for vortex solutions to the GP equation [34, 37, 44]. This appears mainly because of two reasons, first due to the interpretation of $|\psi|^2$ as the condensate density and second due to the constraint imposed of ψ to be single valued. To see this, let us consider the LGPE given by

$$i\hbar\frac{\partial\psi(\mathbf{r},t)}{\partial t} = -\frac{\hbar^2}{2m}\nabla^2\psi(\mathbf{r},t) + V_{ext}(\mathbf{r},t)\psi(\mathbf{r},t) + g\,\psi(\mathbf{r},t)|\psi(\mathbf{r},t)|^2.$$

Multiplying the equation above with $\psi^*(\mathbf{r},t)$ and subtracting the resultant equation from its complex conjugate yields

$$i\hbar\frac{\partial|\psi(\mathbf{r},t)|^2}{\partial t} + \nabla\cdot\left[\frac{\hbar}{2mi}\Big(\psi^*(\mathbf{r},t)\nabla\psi(\mathbf{r},t) - \psi(\mathbf{r},t)\nabla\psi^*(\mathbf{r},t)\Big)\right] = 0.$$

The equation above has the form of continuity equation for the condensate density $|\psi|^2$, with velocity $\mathbf{v} = \frac{\hbar}{2mi}\frac{(\psi^*(\mathbf{r},t)\nabla\psi(\mathbf{r},t)-\psi(\mathbf{r},t)\nabla\psi^*(\mathbf{r},t))}{|\psi(\mathbf{r},t)|^2}$. Now, due to the interpretation of $|\psi(\mathbf{r},t)|^2$ to be the density of the condensate, for a radially symmetric solution any dependence of $\psi(\mathbf{r},t)$ on the angular coordinate has to be through the phase factor. Mathematically stating, the wave-function has to be of the form $\psi(\mathbf{r},t) = f(r,t)e^{is\phi}$, where s is an integer to account for the single-valuedness of the wave-function. This form of ψ ensures that the solution is radially symmetric and that the flow is only azimuthal and not radial, which are key features of a vortex solution. Writing ψ thus gives us the velocity of BEC as $\mathbf{v} = \frac{s\hbar}{m}\nabla\phi = \frac{s\hbar}{m}\frac{\hat{\phi}}{r}$. Thus, the circulation around a closed contour $\oint\vec{v_s}.\vec{dl} = 2\pi\hbar s/m$. From this, it comes out that the angular momentum of a condensate with radial symmetry is quantized in units of h.

4.1.2   The vortex solution

Having discussed the origin of quantized vortex in LGPE, let us discuss the explicit solution. We intend to find a vortex solution to the LGPE given by Eq.(3.2). We start by taking BEC in a cylindrical geometry, with strong confinement along the z- axis. As the confinement along the radial direction is weak, we neglect the external potential along radial direction as a first order approximation [58]. Doing this, we write the 2D LGPE in the absence of external potential as

$$i\hbar\frac{\partial\psi(\mathbf{r},t)}{\partial t} = -\frac{\hbar^2}{2m}\left[\frac{1}{r}\frac{\partial}{\partial r}\left(r\frac{\partial}{\partial r}\right) + \frac{1}{r^2}\frac{\partial^2}{\partial\phi^2}\right]\psi(\mathbf{r},t) + g\ \psi(\mathbf{r},t)|\psi(\mathbf{r},t)|^2.$$

We wish to obtain a stationary vortex solution. Hence, we take an ansatz of the form $\psi_0(\mathbf{r},t) = \psi_0(\mathbf{r})e^{-i\mu t/\hbar}$, where μ is the chemical potential. As seen in the previous subsection, the vortex solution shows a $\frac{1}{r}$ velocity profile. Therefore, by physical arguments, we place the constraint that the density of a vortex solution varies as a function only of radial distance from the vortex core. Therefore, placing our origin at the core of the vortex, we take the ansatz $\psi_0(\mathbf{r}) = e^{is\phi}|\psi_0(\mathbf{r})|$. Lastly, we take the density variation over a background density n, by considering $|\psi_0| = \sqrt{n}f(\eta)$, where $\eta = r/\xi_0$ and f varies from 0 at the core of the vortex, to 1 far away from the core. Using such an ansatz gives the equation for $f(\eta) \equiv f$ as

$$\frac{1}{\eta}\frac{d}{d\eta}\left(\eta\frac{d}{d\eta}f\right) + \left(1 - \frac{s^2}{\eta^2}\right)f - f^3 = 0. \tag{4.1}$$

As the velocity profile of the vortex is given by $v \propto \frac{1}{r}$, the density of BEC at the core has to go to zero, since the velocity diverges there. Whereas far away from the vortex core, the density should relax to a uniform density. The solution f should reflect such a behaviour. Since the density vanishes at the vortex core, we should have the behaviour of f near the core of the vortex to be $f \sim \eta^q$, where q is a natural number. It turns out that near the core, for a vortex with circulation 's', the ansatz $f \sim \eta^{|s|}$ is suitable [37]. This ansatz turns Eq.(4.1) to

$$|s|^2\eta^{|s|-2} - s^2\eta^{|s|-2} + \eta^{|s|} - \eta^{3|s|} = 0.$$

This choice of f near the origin is suitable as it ensures that the largest contribution near the origin of the order $\eta^{|s|-2}$ cancels out. Thus we can say that this is the approximate behaviour of the vortex solution near the origin. Unfortunately, Eq.(4.1) has no closed form solution in general. It can be solved numerically. Analytically what can be done is

that we can find an ansatz which satisfies the conditions set on f, keeping a parameter free to be minimized using the energy functional. Such a solution, even though not exact, closely resembles the numerical solution. As an example, let us consider the vortex with unit circulation, i.e. $s = 1$. For this vortex, we take ansatz as $f = \frac{\eta}{\sqrt{\alpha^2 + \eta^2}}$, where α is a free parameter to be minimized using the energy functional. As we can see, this solution satisfies the boundary conditionz on f; it goes to 0 near the core as $f \sim \eta$, is always < 1, goes from 0 at the core to 1 smoothly for $\eta \to \infty$ and its derivative goes to zero for $\eta \to \infty$. One can plug this ansatz for f in the energy functional and minimize the energy functional with respect to α. As mentioned in the previous chapter, the energy functional is given as

$$E = \int d\mathbf{r} \left(\frac{\hbar^2}{2m} |\nabla \psi_0(\mathbf{r}, t)|^2 + \frac{g}{2} |\psi_0(\mathbf{r}, t)|^4 \right).$$

Doing this, one gets $\alpha \sim \sqrt{2}$ and the ansatz becomes $f = \frac{\eta}{\sqrt{2 + \eta^2}}$. As a comparison, we can see in Fig.(4.1), the simultaneous plot of the numerical solution and the ansatz for $|s| = 1$ [34]. As one can see, the ansatz and the numerical solution approximately resemble each other.
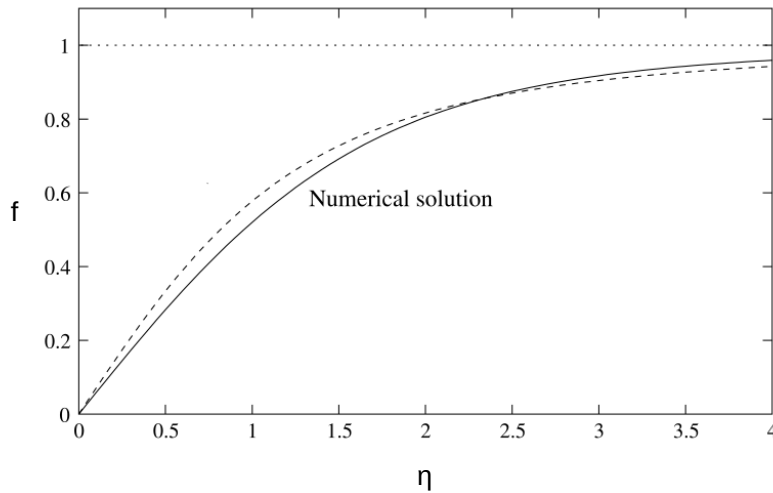
Figure 4.1: Figure shows the density profile of single vortex line using the ansatz $f = \frac{\eta}{\sqrt{2 + \eta^2}}$ (dotted line) and the numerical solution (solid line) to the LGPE. (Credits: *Bose-Einstein Condensation in dilute gases* by *Pethick and Smith.*)[34]

One can, using a suitable ansatz or numerical methods, construct the vortex solution for higher values of circulation (s).

There are a few things to note here. Firstly, the ansatz used shows the approximate behaviour of the solution quite accurately. Secondly, even though the dynamics indicates the approximate behaviour near the origin as $\sim \eta^{|s|}$, it doesn't give the value of the slope of the solution. This slope $(1/\alpha)$ has to be determined by taking an ansatz and minimizing the energy functional.

In the next section, we shall see the vortex solution for the MGPE. We shall see how the MGPE gives the slope selection from the dynamics itself. For the LGPE, the width of the vortex solution is of the order of the healing length ξ_0. For the MGPE, we get an entirely new class of vortex solution with width of the order of the microscopic length scale of interactions.

4.2 MGPE and a new class of vortex solution

Let us consider the entire series of correction to the LGPE. Re-writing this series given by Eq.(3.5), we have

$$
i\hbar\frac{\partial\psi(\mathbf{r},t)}{\partial t} = -\frac{\hbar^2}{2m}\nabla^2\psi(\mathbf{r},t) + V_{ext}(\mathbf{r},t)\psi(\mathbf{r},t) + g\,\psi(\mathbf{r},t)|\psi(\mathbf{r},t)|^2
$$
$$
+ g_2\,g\,\psi(\mathbf{r},t)\,\nabla^2|\psi(\mathbf{r},t)|^2 + O\Big(\psi(\mathbf{r},t)\nabla^4|\psi(\mathbf{r},t)|^2\Big).
$$

A point to note here is that due to the form of correction terms, one can get a continuity equation here as well using the same procedure viz., multiply the series with ψ^* and then subtract it from its complex conjugate equation. Hence, one may get quantized vortex solutions for the LGPE with correction series as well.

As for the LGPE, we wish to find the vortex solution and hence write the solution as $\psi(\mathbf{r},t) = \psi_0(r)e^{is\phi}e^{-i\mu t/\hbar}$. Then, the series of corrections to the LGPE can be written in the form

$$
-\frac{\hbar^2}{2m}\frac{1}{r}\frac{d}{dr}\Big(r\frac{d}{dr}|\psi_0(r)|\Big) + \frac{\hbar^2 s^2}{2mr^2}|\psi_0(r)| + g|\psi_0(r)|^2\psi_0(r)
$$
$$
+ g\,|\psi_0(r)|\left[g_2\frac{1}{r}\frac{d}{dr}\Big(r\frac{d}{dr}|\psi_0(r)|^2\Big) + g_4\Big(\frac{1}{r}\frac{d}{dr}\Big(r\frac{d}{dr}\Big)\Big)^2|\psi_0(r)|^2+ \right. \tag{4.2}
$$
$$
\left. ..... + g_{2l}\Big(\frac{1}{r}\frac{d}{dr}\Big(r\frac{d}{dr}\Big)\Big)^{2l}|\psi_0(r)|^2 + ...\right] = \mu|\psi_0(r)|,
$$

where g_{2l} represent the factors arising due to the strength of finite range of interactions up to different orders (l is a natural number). Due to the shape of the inter-particle

interaction potential, the strength of corrections to different orders need not be the same. Before scaling this equation as done for the LGPE, let us see if for a vortex with circulation s, if the equation above gives a $r^{|s|}$ behaviour for small r. Therefore, we plug in $\psi_0(r) = \sqrt{n}\,\beta\,r^{|s|}$ and take $\mu = gn$ in the equation above to get

$$\beta^2|s|^2 r^{|s|-2} - \beta^2|s|^2 r^{|s|-2} - 8\pi a n r^{3|s|}$$
$$+ 8\pi a n r^{|s|}\Big[1 - g_2\beta^2(2|s|)^2 r^{2|s|-2} - g_4\beta^4(2|s|)^2(2|s|-2)^2 r^{2|s|-4}$$
$$- .... - g_{2|s|}\beta^{2|s|}((2|s|)!!)^2\Big] = 0,$$

where we have multiplied throughout by $2m\sqrt{n}/\hbar^2$. Let us analyze the key feature of the above equation. In the absence of correction terms to the LGPE, terms with coefficients g_{2l} equal 0. This gives us back the LGPE, where the leading order unbalanced term in the above equation is of the form $r^{|s|}$. However, in the presence of the correction terms, we get a series of new terms. These terms are of the order $r^{3|s|-2}, r^{3|s|-4}, ..., r^{|s|}$. Note that there do not appear terms with negative power of r due to the structure of the radial derivative part of the Laplacian. The number of new terms appearing in the equation depend on $|s|$. However, now for a vortex with circulation s, we have two terms of the order $r^{|s|}$. Hence, we can make these two terms to balance each other. This means that now the leading term in the dynamics is of the form $r^{|s|+2}$. This is a better approximation than for LGPE because for the LGPE, the unbalanced term left in the equation for dynamics was the same order as the ansatz, viz., $r^{|s|}$. However, with the correction terms to the GP equation, the leading order term in the dynamics, viz., $r^{|s|+2}$ is two orders smaller than the ansatz $r^{|s|}$ for small r.

As one can see from the equation above, balancing terms of the order $r^{|s|}$ essentially means setting a constraint on β. This means that we get a selection for the slope from the dynamics itself. Furthermore, by balancing terms of the order $r^{|s|}$, we can see that the slope β is of the order of $\sim 1/\sqrt{g_{2|s|}}$. Thus, the length scale of this vortex is of the order $1/\beta \sim \sqrt{g_{2|s|}}$, which is the microscopic length scale of the non-local corrections. This shows that one may get a new class of vortex solution which arise due to the non-local correction terms to the LGPE.

With this slope selection for the core arising from the corrections to the LGPE, let us now construct a variational ansatz to obtain the full vortex solution.

4.2.1 Construction of solution

In the previous sub-section, we have not explicitly considered the form of coefficients of the correction terms to the LGPE. They were just abbreviated by g_{2l}. Let us now consider the form of these terms explicitly. This can be done by considering an extended pseudopotential as follows.

The local GP equation follows from its full non-local form

$$
\begin{aligned}
i\hbar\frac{\partial\psi_0(\mathbf{r},t)}{\partial t} = \Big(&-\frac{\hbar^2}{2m}\nabla^2 + V_{ext}(\mathbf{r},t)\Big)\psi_0(\mathbf{r},t) \\
&+ \psi_0(\mathbf{r},t)\int \mathbf{dr'}\,\psi_0^*(\mathbf{r'},t)V(\mathbf{r'}-\mathbf{r})\psi_0(\mathbf{r'},t).
\end{aligned}
\tag{4.3}
$$

Let us consider the pseudopotential approach to account for the s-wave scattering in a BEC. We consider a BEC with cylindrical symmetry. The radial size of the condensate is taken to be D, with strong confinement along the z-direction.

Under the first Born approximation, s-wave scattering can be captured by using an effective repulsive soft-potential [37, 38]. The range of this effective repulsive potential is in general of the order of the scattering length [38]. The effective potential simply sets the length scale over which the density variation is now being probed. Important to note that, although we are capturing here the interactions underlying s-wave scattering through an effective repulsive potential for the sake of simplicity, the actual potential can have bound states and, thus, can undergo Feshbach resonance [83]. To note here is the fact that the range of the pseudopotential is taken to be of the order of a and not exactly equal to a.

We take the interaction pseudopotential as $V(\mathbf{r'}-\mathbf{r}) \simeq V_{eff} = [g/(\sqrt{2\pi}a)^3]\times exp[-\frac{|\mathbf{r}-\mathbf{r'}|^2}{2a^2}]$. Following the arguments given above, the range of the V_{eff} would be of the order of s-wave scattering length and hence we set the range of V_{eff} as a. Doing a Taylor expansion of the wave-function $\psi(\mathbf{r'},\mathbf{t})$ about $\mathbf{r}$, we get

$$
\begin{aligned}
&-\frac{\hbar^2}{2m}\frac{1}{r}\frac{d}{dr}\Big(r\frac{d}{dr}|\psi_0|\Big) + \frac{\hbar^2 s^2}{2mr^2}|\psi_0| + g|\psi_0|^2\psi_0 - \mu|\psi_0| \\
&+ g|\psi_0|\Big[\frac{a^2}{2}\frac{1}{r}\frac{d}{dr}\Big(r\frac{d}{dr}|\psi_0|^2\Big) + \frac{a^4}{8}\Big(\frac{1}{r}\frac{d}{dr}\Big(r\frac{d}{dr}\Big)\Big)^2|\psi_0|^2 \\
&\qquad + ... + \frac{a^{2l}}{(2l)!!}\Big(\frac{1}{r}\frac{d}{dr}\Big(r\frac{d}{dr}\Big)\Big)^{2l}|\psi_0|^2 + ...\Big] = 0,
\end{aligned}
\tag{4.4}
$$

Considering $\mu = gn$, $\psi_0(\mathbf{r}) = \sqrt{n}f(r)$, and $f(r) = R^{|s|}$ near the origin, where $R = \beta r$, for a vortex with $|s|$ quanta of circulation, the series in square brackets in Eq.(4.4) terminates at $2|s|$-th order in derivatives as all other higher order derivatives would be zero. Thus, we get

$$\beta^2 |s|^2 R^{|s|-2} - \beta^2 |s|^2 R^{|s|-2} - 8\pi a n R^{3|s|}$$
$$+ 8\pi a n R^{|s|} \Big[1 - \frac{a^2 \beta^2}{2}(2|s|)^2 R^{2|s|-2} - \frac{a^4 \beta^4}{8}(2|s|)^2 (2|s|-2)^2 R^{2|s|-4}$$
$$- .... - \frac{a^{2|s|} \beta^{2|s|}}{(2|s|)!!}((2|s|)!!)^2 \Big] = 0.$$

The first 3 terms correspond to local GP equation and at the leading order $R^{|s|-2}$ we get the same result as is already shown. The next higher order terms are the first and the last terms in the square bracket which are in balance when $\beta = 1/a[(2|s|)!!]^{\frac{1}{2|s|}}$ giving us a selection on β. Note that, the first term in the square bracket comes from the linear term $\mu|\psi_0|$ in Eq.(4.4). Note also that, had we considered any other flat symmetric repulsive potential in the place of the Gaussian one, the Taylor expansion would only undergo change in numerical constants. Thus, the scaling behaviour of $\beta \sim 1/a$ is always there.

The natural truncation of the Taylor expansion of the interaction term, depending upon the order of the quantized vortex, is something of immense importance here. There is no need to truncate the series based on order of magnitude arguments. The structure of the core of a vortex, i.e. $f(r) = R^{|s|}$ naturally truncates the series and that is where the Taylor expansion makes perfect sense to be in use. For the kind of order parameters which do not provide such a natural truncation of the Taylor series, the Taylor expansion method cannot be used for these small scale structures where $\lambda \sim a$.

Having constructed the core with a definite selection of the length scale, we can construct a full variational solution for a vortex with $|s|$ quantum of circulation. We shall use the energy functional for series of correction terms, obtained in the previous chapter, for this purpose. To compute the free energy in what follows, we take the energy integral over R varying from 0 to D, where $r = D/\beta$ is the radial cut off. To obtain the solution, we divide the region $(0, D)$ in two parts. These regions are $(0, \alpha_{|s|})$ and $(\alpha_{|s|}, D)$. In the region $(0, \alpha_{|s|})$ we consider the vortex solution as $R^{|s|}$ (as was shown above in the analysis to obtain β) and in the region $(\alpha_{|s|}, D)$, we take the ansatz $f(R) = (1 - \lambda_{|s|} e^{-\delta_{|s|} R})$. The choice of this latter part of the solution is particularly good because it rises to unity at large R and it involves two free parameters which we can adjust to get a continuous solution. By matching of these two functions and their derivatives at $R = \alpha_{|s|}$ we obtain

$\lambda_{|s|} = (1 - (\alpha_{|s|})^{|s|}) \cdot exp[|s|(\alpha_{|s|})^{|s|}/(1 - (\alpha_{|s|})^{|s|})]$, $\delta_{|s|} = |s|/[(\alpha_{|s|})^{(1-|s|)} - \alpha_{|s|}]$ as a function of $\alpha_{|s|}$. Then, we plug in the complete solution (from 0 to D) in the energy functional (Eq.(4.4)) [45] to minimize the energy and thereby fix the position of matching $\alpha_{|s|}$.

The free energy functional corresponding to the general vortex of number of circulation $|s|$ in the solution we have chosen is [135]

$$E_v = \int_0^D \frac{2\pi R dR}{\beta^2} \Big[\frac{\hbar^2\beta^2}{2m} n\Big(\frac{df}{dR}\Big)^2 + \frac{\hbar^2\beta^2}{2m} n\frac{f^2}{R^2} + \frac{gn^2}{2}(1 - f^2)^2 + \frac{gn^2 f^2}{2}\Big\{\frac{\beta^2 a^2}{2}\frac{1}{R}\frac{d}{dR}\Big(R\frac{d}{dR}f^2\Big)$$
$$+ \frac{\beta^4 a^4}{8}\Big(\frac{1}{R}\frac{d}{dR}\Big(R\frac{d}{dR}\Big)\Big)^2 f^2 + ... + \frac{\beta^{2|s|}a^{2|s|}}{(2|s|)!!}\Big(\frac{1}{R}\frac{d}{dR}\Big(R\frac{d}{dR}\Big)\Big)^{2|s|} f^2\Big\}\Big].$$

(4.5)

We use the above mentioned prescription and evaluate the energy minimum in terms of $\alpha_{|s|}$. As we assume the diluteness limit $a^3 n \ll 1$, we can take $an \ll \beta^2$ for any $|s|$ since $\beta \sim 1/a$. Making use of this inequality and keeping terms which go as β^2 over terms which go as 'an' we get an expression for free energy as

$$E = \frac{2\pi\hbar^2 n}{m}\Big[\frac{|s|^2}{2}ln\Big(\frac{D}{\alpha_{|s|}}\Big)$$
$$+ \Big(\frac{\lambda_{|s|}^2}{8}\Big)(1 + 2\alpha_{|s|}\delta_{|s|})e^{-2\alpha_{|s|}\delta_{|s|}} + \frac{|s|\alpha_{|s|}^{2|s|}}{2}\Big].$$

The minimization of the above energy functional fixes the value of the parameter as $\alpha_{|s|} = [(1 - |s| + \sqrt{49|s|^2 - 10|s| + 1})/(12|s| - 2)]^{\frac{1}{|s|}}$. Using this $\alpha_{|s|}$, we can now evaluate $\lambda_{|s|}$ and $\delta_{|s|}$ for a given value of $|s|$, thus we determine $f(R)$ for the interval $(\alpha_{|s|}, D)$. We plot $f(R)$ for $|s| = 1, 2, 3$ in Fig.(4.2) of the variational solution obtained.

A model similar to the non-local model obtained above was used by Collin *et al.* [36] for proposing the first order correction to the LGPE. This equation was of the form

$$i\hbar\frac{\partial\psi(\mathbf{r}, t)}{\partial t} = -\frac{\hbar^2}{2m}\nabla^2\psi(\mathbf{r}, t) + g\,\psi(\mathbf{r}, t)|\psi(\mathbf{r}, t)|^2$$
$$+ g_2\,g\,\psi(\mathbf{r}, t)\,\nabla^2|\psi(\mathbf{r}, t)|^2,$$

(4.6)

where $g_2 = \Big(\frac{a^2}{3} - \frac{ar_e}{2}\Big)$, where r_e determines the effective range of interactions. Here, r_e is defined to be such that $g_2 \geq 0$. For this non-local model of Collin *et al* we have taken

$r_e = a/2$ to plot the density profile of the vortex in Fig.(4.2). The figure shows that the width of the vortices is of the order of s-wave scattering length.
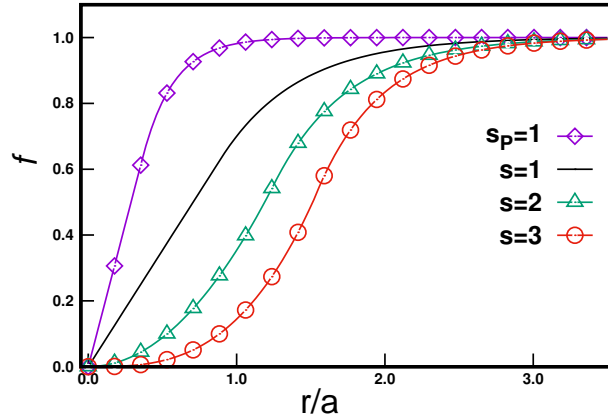
Figure 4.2: Figure shows the density profile of single vortex line for different circulations s for the generalized model and also for the microscopic interaction model by Collin *et al.* labeled by s_P for $|s| = 1$ with $r_e = a/2$.

4.3 Comparison of the solutions

Even though till now we have talked about vortex state with circulation s in general, for comparison of the two class of solutions shown above (LGPE and LGPE with correction terms), we will talk about only solutions with $|s| = 1$. This is because in BEC, vortices with higher quanta of circulation $|s| > 1$ are unstable and break down into multiple vortices with $|s| = 1$ [37]. This is due to the reason that the energy of a vortex with $|s| = q$ (E_q), where q is a natural number, is greater than energy of q vortices with $|s| = 1$ (E_1). This can be easily verified by using the energy functional of the LGPE and corrections to the LGPE upto order q. Plugging in the ansatz for vortex solution, once with $|s| = q$ and then for q vortices with $|s| = 1$, it turns out that $E_q > qE_1$. It turns out that even the contribution for interaction does not make these two energies equivalent. This is mainly due to the logarithmic nature of energy of a vortex. Hence for the purpose of comparison, we will only use vortex solution with $|s| = 1$ in this section.

Till this point, we have seen that an ansatz for the vortex solution can be constructed for the LGPE, the width of whose core is of the order of the healing length ξ_0. With the corrections to the LGPE, an ansatz for the vortex solution can be constructed whose width is of the order of the microscopic length scale governing the non-local interactions. This width is approximately of the order of a. However, there is one point which we have not analyzed till now. In the case of corrections to the LGPE, if we don't take β such that it cancels the term of the order r^1, we are left with the highest term of the order of r^1. This still vanishes as we take the limit $r \to 0$. Therefore, in the presence of

corrections to the LGPE, we need to check if an ansatz of the form $\psi_0(\eta) = \sqrt{n}\frac{r}{\sqrt{\alpha^2+r^2}}$ holds. In case if it does hold, we would need to compare the vortex solutions with width of the order of ξ_0 and a to see which solution will manifest itself in experiments. But before doing that, we review the scale selection using the LGPE energy functional in detail.

4.3.1   Scale selection from energy functional for LGPE

A scale selection for the vortex core is obtained by the variation of the grand canonical free energy functional of the LGPE (Eq.(3.2)) in general. As before, let us take the ansatz for the vortex solution to be of the form $\psi(\mathbf{r},t) = \sqrt{n}|f(r)|e^{i\phi}e^{-i\mu t/\hbar}$ with $|f(r)| = r/\sqrt{\alpha^2+r^2}$. Note that the ansatz involves r and not $\eta = r/\xi_0$. Since, this is a procedure employing energy variations, the term containing any constant phase factor of $f(r)$ is of no use. We plug this ansatz in the grand canonical energy functional of the LGPE and minimize the energy with respect to α to get a scale selection. The grand canonical energy functional of the local GP equation is [37]

$$E = \int_{-\frac{L}{2}}^{\frac{L}{2}} \int_0^{2\pi} \int_0^D \Big[\frac{\hbar^2}{2m}|\nabla\psi(\mathbf{r},t)|^2 + \frac{g}{2}(|\psi(\mathbf{r},t)| - n)^2\Big] r\, dr\, d\phi\, dz. \tag{4.7}$$

After putting the aforementioned ansatz for $\psi(\mathbf{r},t)$ in the above energy functional, we extremize it by setting $(\partial E/\partial\alpha) = 0$. This gives the following equation for $\widetilde{\alpha}$ ($\widetilde{\alpha} = \alpha/D$),

$$\widetilde{\alpha}^4[6\xi_0^2 - D^2] + \widetilde{\alpha}^2(4\xi_0^2 - D^2) + 2\xi_0^2 = 0,$$

We can find the roots of the above equation in $\widetilde{\alpha}$, which gives

$$\widetilde{\alpha}^2 = \frac{(D^2 - 4\xi_0^2) \pm \sqrt{D^4 - 32\xi_0^4}}{2(6\xi_0^2 - D^2)}.$$

For the above equation to have roots, $D^4 \geq 32\xi_0^4$. This condition is tailored in a BEC while exciting multiple vortices[114, 116, 136]. In this $D \gg \xi_0$ limit, we see that taking the $+$ sign makes the numerator $\sim 2D^2$. However, we see that there is another factor $1/[6\xi_0^2 - D^2]$, which becomes negative for $D \gg \xi_0$, in turn making $\widetilde{\alpha}^2$ negative. If we take the $-$ sign from the $\pm$, the numerator of the above equation becomes $\sim (-\xi_0^2)$,

giving $\widetilde{\alpha}^2 \sim (\xi_0^2/D^2)$ for $D \gg \xi_0$. This gives us a scale selection of $\alpha \sim \xi_0$. This is the vortex with core size of the order of healing length.

The important point to note here is that for $D^4 - 32\xi_0^4 < 0$, the solution breaks down because $\widetilde{\alpha}$ becomes complex. Now, D being a free parameter of a single vortex, it can be increased up to the system size, but in a vortex lattice, D is restricted by the position of the nearest neighbours and in what follows we are going to look at this limit after introducing the other class of solution.

4.3.2 Scale selection from energy functional for MGPE

The condition for the above mentioned class of vortex solution's breakdown appears in the context of a local GP dynamics is what we have seen so far. An important question to ask at this point is - does the leading order non-local correction to the local dynamics improve the situation? Note that we talk here only about the leading order correction since we only intend to talk about vortex with $s = 1$

Let us revisit the above variational procedure taking into consideration non-local interactions. We do that to see if there exists a vortex solution of core size ξ_0 when non-local interactions are present, despite having $D^2 < \sqrt{32}\xi_0^2$. We use g_2 to denote the strength of first order correction to the LGPE. Thus, the MGPE is of the form

$$
i\hbar\frac{\partial\psi_0(\mathbf{r},t)}{\partial t} = \Big[-\frac{\hbar^2}{2m}\nabla^2 \\
+ g\left(|\psi_0(\mathbf{r},t)|^2 + g_2\nabla^2|\psi_0(\mathbf{r},t)|^2\right)\Big]\psi_0(\mathbf{r},t),
\tag{4.8}
$$

where $g_2 \sim a^2$. Let us take Eq.(4.8) and determine the nature of vortex solution.

The energy functional for the non-local GP equation given by Eq.(4.8) is

$$
E = \int_{-\frac{L}{2}}^{\frac{L}{2}}\int_0^{2\pi}\int_0^D \Big[\frac{\hbar^2}{2m}|\nabla\psi(\mathbf{r},t)|^2 + \frac{g}{2}(|\psi(\mathbf{r},t)|^2 - n)^2 + \\
\frac{gg_2}{2}|\psi(\mathbf{r},t)|^2\nabla^2|\psi(\mathbf{r},t)|^2\Big]r\,dr\,d\phi\,dz.
\tag{4.9}
$$

We plug in the same ansatz, $|f(r)| = r/\sqrt{\alpha^2 + r^2}$ as in the previous section and check for energy functional minimization. Note that, since we do not want three body effects to dominate, it is desirable to work in the diluteness limit $a^3n \ll 1$ and hence $g_2 \ll \xi_0^2$

which can safely be considered in orders of magnitude as $g_2 \sim a^2$. The minimization condition yields

$$\widetilde{\alpha}^6(6\xi_0^2 - D^2) + \widetilde{\alpha}^4(10\xi_0^2 - 2D^2 + 4g_2)$$
$$\widetilde{\alpha}^2(6\xi_0^2 - D^2 - 4g_2) + 2\xi_0^2 = 0. \qquad (4.10)$$

The above condition is cubic in $\widetilde{\alpha}^2$. The coefficients show that the length scale dictated by g_2 would be masked by that by ξ_0, unless $g_2 \geq \xi_0^2$. However, this would take us away from the diluteness limit and into the region where three body effects would become important. Hence while we stay in the diluteness limit, the length scale dictated by ξ_0 would always dominate. Now, in the previous section, we have seen that for $D^2 < \sqrt{32}\xi_0^2$, the solution breaks down. For the same condition over most of the parameter space, one can see that all the coefficients of Eq.(4.10) are positive which denies any acceptable solution for $\widetilde{\alpha}^2$. Therefore, even the presence of non-local interaction does not help getting such a vortex solution for $D^2 < \sqrt{32}\xi_0^2$ in a system when the leading order non-local correction has been taken into account.

4.3.3 Energy comparison of solution for $|s| = 1$

The analysis above has us at somewhat of a crossroad. It seems that there are two different classes of variational solutions which satisfy the MGPE, one with width of the order of ξ_0 and one with width of the order of a. We have to ascertain which one of them shows up in experiments. To do this, let us start by analyzing the energy of the two solutions. Due to the principle of energy minimization, we may say that the solution with lesser energy shall hold.

Consider these solutions for a uniform BEC in the absence of any trap. Let us compare the grand canonical energy of the two classes of vortices, one with core size of the order of healing length (thick vortex) and other with core size of the order of s-wave scattering length (thin vortex). To do this, we use Eq.(4.9) and calculate energy of the ansatz for the thick and thin votex state presented above for $s = 1$. To the leading order then the energies of the vortex with core of size of healing length (E_{ξ_0}) and that with core size of scattering length (E_a) are given by $E_{\xi_0} \sim (\frac{\pi\hbar^2 Ln}{m})ln\left(\frac{|s|D}{\xi_0}\right)$ and $E_a \sim (\frac{\pi\hbar^2 Ln}{m})ln\left(\frac{D}{\alpha_{|s|}a}\right)$ respectively, where $\alpha_{|s|}$ is an order unity number. From these terms, we can see that if the healing length and the s-wave scattering length are of equal order, the two classes of vortices actually become comparable in energy. However, as we change the scattering length and make it smaller by keeping the density fixed, we increase the healing length.

In this case, the thick vortex with the length scale corresponding to the healing length will be energetically favoured because it is a state of lower energy.

This being said, if we desire to obtain the thin vortex solution, we would have to make the thick vortex cease to exist. To do this, one can take cue from the conditions required for the thick vortex solution to exist. As mentioned earlier, for the thick vortex solution to exist, the condition is $D^4 \geq 32\xi_0^4$. In the case $D^4 < 32\xi_0^4$, the thick vortex would cease to exist as that length scale selection is no longer present. Hence, the vortex solution existing in this regime could be a thin vortex with core size of the order of the s-wave scattering length.

Let us discuss an experimentally plausible situation where a thick vortex solution does not exist and a thin vortex state can possibly be captured [137]. Note that, the radial cut off D corresponding to a single vortex inside a vortex lattice is rather restricted and is actually much smaller than the system size. In such a situation, one can employ Feshbach mechanism off resonance to reduce the s-wave scattering length to smaller values such that $\xi_0 \sim D$ or make the packing of the vortices in the lattice so dense that the $\xi_0 \sim D$ condition is satisfied. One can reasonably expect here that the thin vortices to show up in the absence of thick vortices and some already trapped quantized angular momenta.

4.4 Thin vortex solution in a harmonic trap

Experimentally, vortex states are achieved in a BEC in a trap. Let us consider a harmonic trapping potential and show that the thin vortex solution exists here as well. Since we are talking about thin vortices only, we assume that we are in the regime where thick vortex state ceases to exist. We shall discuss a vortex solution with unit circulation, i.e. $s = 1$ using the model of MGPE as before. We consider cylindrical geometry and assume tight confinement along the z direction and use the MGPE used by Collin *et al.* This consideration would give the MGPE as

$$
\begin{aligned}
i\hbar\frac{\partial\psi_0(\mathbf{r},t)}{\partial t} = \Big[&-\frac{\hbar^2}{2m}\nabla^2 + \frac{1}{2}m\omega^2 r^2 \\
&+ g\left(|\psi_0(\mathbf{r},t)|^2 + g_2\nabla^2|\psi_0(\mathbf{r},t)|^2\right)\Big]\psi_0(\mathbf{r},t),
\end{aligned}
\tag{4.11}
$$

where ω is the trap frequency and r is the radial distance from the trap center. Due to the harmonic trapping, the ground state of the BEC is no longer one with uniform density, but would fall off away from the center of the trap. The Thomas-Fermi(TF)

density of the condensate can be evaluated by neglecting the kinetic contribution coming from the Laplacian terms. By considering $\psi_0 = \sqrt{n_{TF}}\ e^{-i\mu t/\hbar}$, we get the TF density as $n_{TF} = \frac{1}{g}(\mu - \frac{1}{2}m\omega^2 r^2)$ [37]. We wish to probe the vortex core scaling similar to the previous analysis (where we had considered a uniform background density). To this end, we consider a vortex with unit circulation ($s = 1$) at a distance d away from the trap center. If we consider a coordinate system (ρ, θ) centered at the vortex core, we would get the vortex profile near the core as $\sqrt{n_{TF}(d)}\ \beta\ \rho e^{i\theta}e^{-i\mu t/\hbar}$, where $n_{TF}(d)$ is the TF density at a distance d from the trap center. In considering a linear profile, we have assumed that the TF density of the condensate remains constant up to the first order in ρ. Also, as before we have considered here the vortex as an excited state on top of the ground state density. With respect to the coordinate system (r, ϕ) around the trap center, ρ and θ transform as $\rho = \sqrt{r^2 - 2rd\cos\phi + d^2}$ and $\theta = \tan^{-1}[r\sin\phi/(r\cos\phi - d)]$. Considering this, we can write the density profile of the vortex at a distance d from the trap center as $\psi_0(\mathbf{r},t) = \sqrt{n_{TF}(d)}\ \beta\ \sqrt{r^2 - 2rd\cos\phi + d^2}\ e^{i\tan^{-1}[\frac{r\sin\phi}{r\cos\phi - d}]}e^{-i\mu t/\hbar}$. Putting this ansatz in Eq.(4.11) gives us

$$
\begin{aligned}
\mu\sqrt{r^2 - 2rd\cos\phi + d^2} = {} & \frac{\hbar^2}{2m}\Bigg[\frac{e^{i\phi}\sqrt{r^2 - 2rd\cos\phi + d^2}}{r(d - e^{i\phi}r)} \\
& - \frac{e^{i\phi}\sqrt{r^2 - 2rd\cos\phi + d^2}}{r(d - e^{i\phi}r)}\Bigg] \\
& + \frac{1}{2}m\omega^2 r^2\sqrt{r^2 - 2rd\cos\phi + d^2} \\
& + gn_{TF}(d)\beta^2(\sqrt{r^2 - 2rd\cos\phi + d^2})^3 \\
& + 4gg_2 n_{TF}(d)\beta^2\sqrt{r^2 - 2rd\cos\phi + d^2}.
\end{aligned}
\tag{4.12}
$$

From the equation above, we can see that the terms coming from $\nabla^2\psi$ cancel each other out. We then wish to look at the remaining terms in Eq.(4.12). Since we consider ρ to be small, we go back to the (ρ, θ) coordinate system. This gives us

$$
\begin{aligned}
& \rho\Big(\mu - \frac{1}{2}m\omega^2 d^2 - gg_2 n_{TF}(d)\beta^2\Big) - \rho^2(m\omega^2 d\cos\theta) \\
& - \rho^3\Big(\frac{1}{2}m\omega^2 + gn_{TF}(d)\beta^2\Big) = 0.
\end{aligned}
$$

Up to the leading order in ρ then, we get, $[\mu - \frac{1}{2}m\omega^2 d^2 - 4gg_2 n_{TF}(d)\beta^2] = 0$. As the TF density at a distance d from the trap center is given as $n_{TF} = \frac{1}{g}(\mu - \frac{1}{2}m\omega^2 d^2)$, we get the expression for β as $\beta = 1/2\sqrt{g_2}$, same as for a BEC in the absence of a trap. While, the vortex profile far away from the core may be different from that in the uniform density

background case, the scaling of the density profile near the vortex core remains the same. This shows that the thin vortex solution obtained on top of a BEC with uniform density can be obtained for a harmonically trapped BEC as well. An anharmonic term of the order r^4 in the potential will again get absorbed by the TF density profile and will not change our result up to the scope of the present approximation.

Having obtained the core, we can now use the variational method applied in the previous section to obtain the entire vortex solution. We take the large scale cut-off width for the harmonically trapped BEC to be D and divide the radial interval $(0, D)$ into two regions as before. So long as D is bigger than the width of the actual confinement, there is no problem because the density vanishing beyond the actual width makes the integrand vanish and the integral remains the same as the one obtained considering the actual width. If the vortex is situated at a distance d from the trap center, there would in effect be three regions in the coordinates of the vortex(along a line joining the trap center to the core), viz., the region of the core $(-\alpha, \alpha)$ and the regions away from the core $(\alpha, D-d)$ and $(-(D+d), -\alpha)$. In our calculation, we write the TF density in terms of the radial coordinates of the vortex center (ϱ, θ), where $\varrho = \beta\rho$. Thus, the TF density is $n_{TF}(\varrho) = (1/g)(\mu - \frac{m\omega^2}{2}[(\varrho^2/\beta^2) + 2\varrho(d/\beta)\cos\theta + d^2])$. We take the ansatz for vortex solution of the form $\psi = f(\varrho) \, e^{i\theta}e^{-i\mu t/\hbar}$. For the interval of the core given by $(0, \alpha)$, $f = \varrho \, n_{TF}(\varrho)$. Outside the core, the ansatz is $f(\varrho) = (1 - \lambda e^{-\delta\varrho}) \, n_{TF}(\varrho)$. As before, we match the two solutions and their derivatives at $\varrho = \alpha$. Further, we minimize the energy functional with respect to α as before. Following this procedure, we numerically evaluate the parameters in the variational procedure and thus obtain the profile shown in Fig.(4.3) for the constant $m\omega^2/2\mu$ set equal to unity. Our variational method works perfectly in determining the large scale profile of the vortex.
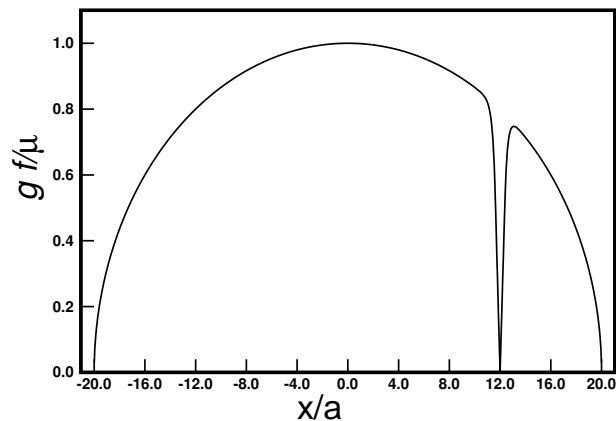
Figure 4.3: Figure shows the density profile of single vortex line in a harmonically trapped BEC situated at $d/a = 12$ from the center of the trap based on the model by Collin *et al.* for $|s| = 1$ with $r_e = a/2$.

4.5   Discussion

In this chapter, we have shown the existence of an entirely new class of thin vortex solution. We have indicated ways to realize it experimentally as well. The width of the thick vortex approximately scales as $\xi_0 = 1/(\sqrt{8\pi an})$, whereas the width of the thin vortex solution scales as $\sim a$. Thus the two class of vortex solutions differ tremendously on their dependence on a. This would be extremely important in order to manipulate their width.

Note that in arriving at the new class of vortex solution we have used here the already existing method of fixing the vortex core structure, in the presence of non-local corrections. The variational procedure then is employed to make this vortex core smoothly evolve to the uniform density far field. As opposed to Padé type approximate solution being used as a variational ansatz, which is standard, our variational analysis (practically for all vortices) is using a well determined solution of the core of the vortices at small r up to next to leading order approximation. As we have already shown in Sec.(**4.1**), at the leading order for small r near the core of a vortex, the conventional theory based on the dynamics cannot give a length scale selection and works fine for the thick vortices. However, in order to go to the sub-leading corrections, one must take the non-local correction into account which we have done and have determined the solution for the core of the vortex from the dynamics itself where the appropriate length scale shows up. Then, while making this core of the vortex recover to the uniform field, far away from the core, we have used variation to have a smooth transition. Thus, our variational approach is just not based entirely on guessed ansatz, rather, the most important part of the solution is obtained from the dynamics and then it is extrapolated to the far field smoothly using variation.

Note that the results involving higher order vortices resulting from the higher order terms of the expansion although are coming out through a general procedure, but may not all be physically accessible because of involvement of higher derivative i.e. smaller length scales. However, the first correction term should always be there since a Laplacian is already present in the local model. So, the result involving the lowest order vortex which is most stable is there.

A consistent mathematical analysis following well established methods of theoretically capturing vortex solutions, indicate here the presence of thin vortex solutions due to non-local interactions. The non-local interaction correction taken in the present context and in other previous works [35, 36] presents small length scales on top of that captured by the LGPE dynamics. The origin of such fluctuations probably lies in the quantum effects not captured by the local GP dynamics. In that sense, the dynamics of these thin vortices

would possibly manifest quantum fluctuations in the system which are required for vortex lattice melting and also important in the context of superfluid turbulence that has attracted a lot of attention lately [138]. Apart from the possible experimental situation where the thick vortex breaks down, which we have identified as a plausible situation where our thin vortex solution can be realized, a quench through the critical point and subsequent formation of vortex-antivortex pairs through Kibble-Zurek mechanism [124, 139] could also be a possible procedure to realize such a vortex. If experimentally realized, these objects can possibly demonstrate quantum fluctuations in vortices which involves rich physics.

The regime described for obtaining thin vortex solution may be realized by tuning the s-wave scattering length of a trapped BEC. Decreasing the scattering length below a certain value would take us into the regime where the condition of condensate size being $\gg \xi_0$ may be violated. Such scenarios have been achieved in experiments used to demonstrate tunability of the s-wave scattering length [140]. Such a solution may be observed experimentally by using the usual time of flight analysis. The thick and thin vortices may be distinguished based on their widths as captured by a CCD camera after expansion of the BEC cloud.

By monitoring a thin single vortex, quantum fluctuations may be monitored. The transition from a thick to thin vortex both for a single vortex solutions and a vortex lattice would require a more detailed study and we shall present such a study in our future works. We also plan to explore the phase diagram for the thick and thin vortex solution in future works.

Chapter 5

Effect of non-local interactions on soliton solution

In the previous chapter, we saw that the corrections to the LGPE give a new class of vortex solution with width of the order of length scale of microscopic interactions. Let us now move to another excited state solution of the LGPE and determine the effect of corrections to LGPE on it. The excited state solution which we wish to examine is the soliton solution.

Solitons are solitary, shape preserving travelling waveforms. These solutions are peculiar to non-linear differential equations and arise as a result of the balance between dispersion and non-linearity [15]. The discovery of solitons is attributed to John Scott Russell, who discovered a solitary dip in the Union Canal in Scotland [15]. Since then, they have been studied in a variety of systems like non-linear fluids, optical fibers and even biological systems like proteins, DNA and neurons [141–145]. As the LGPE has a kinetic term and a non-linear term, one may obtain a soliton solution [37]. The effect of the correction terms to the LGPE on the soliton solution is of interest then.

In the GP equation describing a BEC, the sign of the non-linearity depends on the attractive or repulsive nature of the inter-particle interactions. For the LGPE, one obtains bright soliton (solitary density peak) solution in an attractive BEC and dark soliton (solitary density trough) solution in a repulsive BEC [34, 37]. In BEC, solitons have been realized in trapped atomic condensates [61, 146]. These are mainly achieved by techniques like phase imprinting, density engineering, matter-wave interference method and by dragging an obstacle sufficiently fast through a condensate [59]. Solitons in BEC are of interest mainly due to the tunability by the control which atomic BEC systems provide in experiments. These control parameters include wide tunability of the s-wave

scattering length in a BEC, the availablity of trapping techniques in order to modify the external potential and the achievement of multi-component BEC [89, 147–149].

As solitons solutions for the LGPE are widely explored, the natural question to ask is whether such soliton solutions exist for the MGPE as well? Obviously one would expect the strength corrections to the LGPE to play a role if the soliton solutions exist. One straightforward observation might be the change in width of the soliton. The width of soliton of the LGPE is of the order of the healing length ξ_0. Qualitatively speaking, ξ_0 appears as the length scale since soliton solution arises due to the balance of kinetic and interaction terms. Then for a MGPE, one may expect to see a change in the length scale of soliton. The extent of modification of length scale as compared to ξ_0 would depend on the strength of the corrections to LGPE. Thus, the soliton solution might help us probe the strength of the correction terms to the LGPE. Therefore, a complete characterization of the soliton solution of the MGPE becomes essential. Apart from the change in width, it might also show some change in stability due to change in energy.

It appears that an equation similar the MGPE is used to describe a weakly non-local Kerr medium in optics [150]. Although the form of the non-locality is similar, the origin of the non-locality is quite different in optics and BEC. Exact soliton solutions in the case of non-local Kerr medium have been obtained and studied, and are found to be stable [151]. However, to our knowledge, the implications of these solutions in a non-local BEC along with the stability considerations have not been studied. Further, Sivan *et al.* have proposed a quantifier of soliton stability [152]. In light of this stability quantifier proposed, the effect of the non-local term to the stability of soliton solution in a BEC is of interest. In this chapter we present a detailed analysis of the soliton solution of the MGPE in order to systematically demonstrate the role of microscopic interaction on such typical nonlinear states.

We start by briefly describing the well known soliton solution in a local GP equation in Sec.(5.1). Then, in Sec.(5.2), the MGPE to be used is introduced. In Sec.(5.3) we use the soliton solutions previously obtained by Krolikowski *et al.* [151] and study the bright soliton solution for the case of non-local BEC. In Sec.(5.4) the same is done for a dark soliton in a non-local BEC. We end with a discussion on the scope of the soliton solutions in a non-local BEC.

5.1 Soliton solution in LGPE

Let us briefly review the well-known soliton solution in the LGPE [34, 37]. As done for the vortex solution, we assume the trapping to be weak as a first approximation

and hence neglect it. The GP equation with contact interactions in the absence of an external potential then is given by

$$i\hbar\frac{\partial\psi(\mathbf{r},\mathbf{t})}{\partial t} = -\frac{\hbar^2}{2m}\nabla^2\psi(\mathbf{r},\mathbf{t}) \pm \mathbf{g}|\psi(\mathbf{r},\mathbf{t})|^{\mathbf{2}}\psi(\mathbf{r},\mathbf{t}),$$ (5.1)

where the $+$ sign in the final term indicates a BEC with repulsive interactions and $-$ sign indicates one with attractive interactions. Here, 'm' is the mass of the boson, $g = 4\pi\hbar^2 a/m$ is the inter-boson interaction strength and 'a' is the s-wave scattering length. In the absence of the non-linear term, one would get a dispersive system such that any local disturbance in the system would disperse. The non-linearity counters this dispersion and leads to creation of localized structures like soliton [15]. We want to look at 1D soliton solutions of this equation. Therefore, we assume that $\psi(\mathbf{r},t)$ varies only along 1 direction. Let that direction be the z-direction. This can be achieved in experiment, by strong harmonic confinement in the radial direction. With such a confinement in place, consider the form of the solution as $\psi(\mathbf{r},t) = \sqrt{n_0}f(z,t)$, where n_0 is the uniform density of the BEC far away from the soliton center. The localized soliton solution has the boundary conditions $|f| \to 0$, $df/dz \to 0$ as $z \to \pm\infty$ for a bright soliton. For dark soliton, the conditions are $|f| \to 1$, $df/dz \to 0$ as $z \to \pm\infty$. For a solution obeying these boundary conditions, one can see from Eq.(5.1) that for an attractive BEC, one gets a bright soliton solution, whereas a dark soliton solution is obtained for a repulsive BEC. The exact bright soliton solution is given by

$$\psi(z,t) = \sqrt{n_0}\,\mathrm{sech}[(z-vt)/\sqrt{2}\xi_0]\,e^{\frac{it}{2\hbar}(\mu-4mv^2)}\,e^{\frac{2imvz}{\hbar}},$$

where v is the soliton speed and $\xi_0 = \hbar/\sqrt{2mgn}$ is the healing length. One can see that the bright soliton density far away from the soliton centre falls off to 0. The bright soliton moves along the z-direction like a particle.

For a BEC with repulsive inter-boson interactions, one can obtain an exact dark soliton solution given by

$$\psi(z,t) = \sqrt{n_0}\left[i\frac{v}{c} + \sqrt{1-\frac{v^2}{c^2}}\tanh\left(\frac{z-vt}{\sqrt{2}\xi_0}\sqrt{1-\frac{v^2}{c^2}}\right)\right],$$

where $c = \sqrt{gn_0/m}$ is the speed of sound in BEC, v is the soliton speed and n_0 is the uniform density far away from the soliton centre. Unlike the bright soliton where the density far from the soliton centre tends to zero, the density in a dark soliton heals to

a uniform density far away from the soliton centre. Also, the dark soliton has a phase which depends both on the co-moving coordinate $(z - vt)/\xi_0$ and the speed v of the soliton. Note that, soliton width in both cases scales as ξ_0.

As mentioned before, ξ_0 appears as the length scale of solitons as it arises from a balance between the kinetic and non-linear terms. We shall next look at the origin of ξ_0 using small amplitude oscillations around uniform density ground states in the LGPE. Having done this, it would be interesting to see the length scale modification arising due to corrections to the LGPE. Using the same method of small amplitude oscillations, we determine the length scale modification due to corrections to the LGPE as well in what follows. However, before looking at the healing length and modified healing length, we briefly revisit the MGPE used.

5.2 The MGPE

In this section, we consider corrections to the LGPE as a perturbation series in decreasing order of strength along the series. Therefore to the leading order, we only consider the first order correction to the LGPE. We call this equation, as before, the MGPE. The MGPE, in the absence of an external potential, is given by

$$
\begin{aligned}
i\hbar\frac{\partial\psi(\mathbf{r},t)}{\partial t} = & -\frac{\hbar^2}{2m}\nabla^2\psi(\mathbf{r},t) \pm g|\psi(\mathbf{r},t)|^2\psi(\mathbf{r},t) \\
& \pm g\,g_2\psi(\mathbf{r},t)\nabla^2|\psi(\mathbf{r},t)|^2,
\end{aligned}
\tag{5.2}
$$

where the $+$ sign implies a BEC with repulsive interactions and $-$ sign implies a BEC with attractive interactions. The effective range of the interactions is captured by g_2. We use the expression for g_2 used by Fu *et al.* and Collin *et al.*, given as $g_2 = \left(\frac{a^2}{3} - \frac{ar_e}{2}\right)$ [35, 36]. The energy functional of the MGPE is given by [45]

$$
F = \int \vec{dr} \left[\frac{\hbar^2}{2m}|\nabla\psi(\mathbf{r},t)|^2 \pm \frac{g}{2}|\psi(\mathbf{r},t)|^4 \pm \frac{gg_2}{2}|\psi(\mathbf{r},t)|^2\nabla^2|\psi(\mathbf{r},t)|^2 \right].
\tag{5.3}
$$

Henceforth, we use $\gamma = 2g_2/\xi_0^2$ as a non-locality parameter to compactify equations. Also, instead of using $\mu = gn_0$, as is the case for ground state condensate, we use $\mu = \alpha\,gn_0$, where 'α' is a factor that takes into account the change in the chemical potential due to the presence of soliton in the BEC. Having defined the MGPE, we shall now compare the length scales arising due to small amplitude oscillations about the uniform density ground state in LGPE and MGPE.

5.2.1   Healing length and the modified healing length

Let us look at how one may obtain the healing length of the LGPE. We then extend the analysis to find out a modified length scale for the MGPE.

We start by considering a uniform density ground state for a BEC in the absence of external potential term. We then consider small amplitude oscillations around the uniform density ground state of the form, $\psi(\mathbf{r}, t) = (\sqrt{n_0} + u e^{i\mathbf{k}.\mathbf{r}} e^{-i\omega t} + v e^{-i\mathbf{k}.\mathbf{r}} e^{i\omega t}) e^{-i\mu t/\hbar}$. Here, u and v are constants. By plugging in this form of ψ in the LGPE and equating modes with $(e^{i\omega t})$ and those with $(e^{-i\omega t})$ separately, we obtain the following set of equations

$$\hbar\omega u = \frac{\hbar^2 k^2}{2m} u \pm gn(u+v)$$
$$-\hbar\omega v = \frac{\hbar^2 k^2}{2m} v \pm gn(u+v),$$

where the $+$ sign is for repulsive interactions and $-$ sign is for attractive interactions. Writing them in a matrix form, we have

$$\begin{pmatrix} -\hbar\omega + \frac{\hbar^2 k^2}{2m} \pm gn & \pm gn \\ \pm gn & \hbar\omega + \frac{\hbar^2 k^2}{2m} \pm gn \end{pmatrix} \begin{pmatrix} u \\ v \end{pmatrix} = \begin{pmatrix} 0 \\ 0 \end{pmatrix}.$$

For a solution of this system to exist, the determinant of square matrix on the LHS has to be zero. Setting this condition gives the dispersion relation for small amplitude oscillations as $\omega = \pm k \sqrt{\pm \frac{gn}{m} + \frac{\hbar^2 k^2}{4m^2}}$ for the LGPE. The value of k for which the dispersion relation turns from phonon-like ($\omega \sim k$) to particle-like ($\omega \sim k^2$) is $\sim \xi_0$. Since an attractive BEC is unstable, the dispersion relation becomes imaginary for small k. Nevertheless, one can define the healing length to be the length scale when magnitude of the phonon-like ($\omega \sim k$) term becomes comparable to the magnitude of the particle-like term ($\omega \sim k^2$). This is to say that the healing length is the length scale where kinetic and interaction terms become equivalent. Doing this, we get the healing length as $\xi_0 = \hbar/\sqrt{2mgn}$. This length scale shows up as width of the soliton solution for LGPE.

A similar analysis can be done for the MGPE to obtain the spectrum of elementary excitations which comes out to be $\omega = \pm k \sqrt{\pm \frac{gn}{m} + \left(\frac{\hbar^2}{4m^2} \mp \frac{gg_2 n}{m}\right) k^2}$ [62]. The length scale of phonon-particle transition of elementary excitation spectrum can be found by equating the magnitude of terms which go as k and the term which goes as k^2. This length scale turns out to be $\xi = \xi_0 \sqrt{1 \mp \gamma}/\sqrt{2}$. Let us call this as the modified healing length. As ξ_0 shows up as the length scale of soliton solution of LGPE, one may expect ξ to show up as the length scale of the soliton solution of MGPE. However, note here

that the form of the correction term to the LGPE appears as somewhat of a mix of the kinetic and interaction term. Hence, the soliton solution of the MGPE may not exactly scale as ξ, but one would expect that the width would show qualitatively similar behaviour as ξ. The nature of change in the healing length indicates that there has to be a broadening of the width of the bright soliton in the presence of non-local interactions (due to sign of γ being negative). On the other hand, the width of the dark soliton would decrease in the presence of non-local interactions. In other words, the widening of the width of a bright soliton and shrinking of the dark soliton would be a proof of existence of non-local interactions and corresponding change in the healing length. In what follows, we will see that the length scale of the soliton solution of MGPE indeed qualitatively scales as ξ.

5.3   Bright soliton in an attractive MGPE

A bright soliton solution can be obtained in an attractive BEC. This corresponds to a self-focussing nonlinearity with non-locality for an optical medium, for which exact implicit solutions were obtained by Krolikowski *et al.* [151]. The solutions obtained shall be used to see the behaviour of bright solitons in a BEC in what follows. The 1D MGPE for an attractive BEC can be written as

$$
\begin{aligned}
i\hbar\frac{\partial \psi(z,t)}{\partial t} = &- \frac{\hbar^2}{2m}\frac{\partial^2 \psi(z,t)}{\partial z^2} - g|\psi(z,t)|^2\psi(z,t) \\
&- g\,g_2\psi(z,t)\frac{\partial^2}{\partial z^2}|\psi(z,t)|^2,
\end{aligned}
\tag{5.4}
$$

where g is taken to be positive and the attractive nature of BEC is expressed by putting a minus sign in the equation itself. Notice that since g is positive, so is a in the above equation. This is to say that a physically is negative, but the negative sign is taken out of a and written explicitly in the equation.

Let us consider here a system with finite size which is very large as compared to the soliton width and the healing length. Let N be the number of bosons in the system and V be its volume. For the state with uniform density, the density for the major part of the volume would be $n_0 = N/V$, barring the healing at the boundaries. This healing is neglected in the analysis that follows, since the system size is taken to be large as compared to the healing length. To obtain a bright soliton solution, moving with a speed v, the z coordinate is scaled as $\rho = (z - vt)/(\xi_0\sqrt{2})$, where $\xi_0 = \hbar/\sqrt{2mgn_0}$. Further, we write $\psi(z,t) = \sqrt{n_0}f(\rho)e^{\frac{it}{2\hbar}(\alpha gn_0 - 4mv^2)}e^{\frac{i2mvz}{\hbar}}$ where n_0 is the uniform density in the
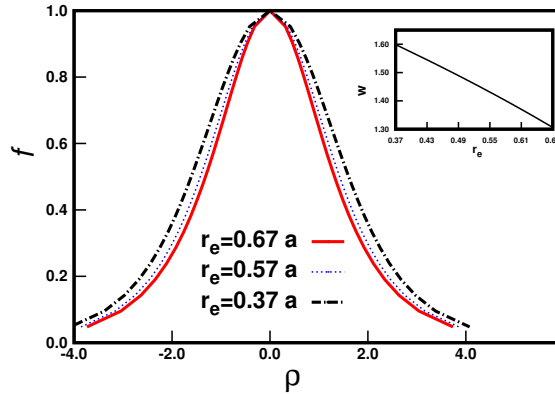
Figure 5.1: The figure shows the density profile of the bright soliton for different values of r_e and $\alpha = 1$. The inset shows the variation of the width of bright soliton with variation in r_e(in units of a) for $\nu = 0.1$.

absence of soliton and α is the factor which accounts for the presence of soliton in the system. This turns the above equation to

$$\frac{\partial^2 f}{\partial \rho^2} + 2(|f|^2 - \frac{\alpha}{2})f + \frac{g_2}{\xi_0^2}f\frac{\partial^2|f|^2}{\partial \rho^2} = 0. \tag{5.5}$$

This equation can be integrated once, to give

$$\left(\frac{df}{d\rho}\right)^2 = \frac{(\alpha - f^2)f^2}{1 + 2\left(\frac{g_2}{\xi_0^2}\right)f^2} . \tag{5.6}$$

As seen previously from the boundary conditions, the bright soliton has a central peak and the derivative of the solution at the centre is 0. This information can be plugged in the equation above to obtain the central peak density of the bright soliton. To do this, we set $df/d\rho = 0$ for $\rho = 0$ which gives the peak density as $f^2(0) = \alpha$. The factor α is evaluated by evaluating the energy functional (F) and then from dF/dN. This means that the central density of the soliton would depend on number of particles (N) and volume (V) of the system.

A further integral of the above equation leads to the implicit soliton solution [151]

$$\pm \rho = \tanh^{-1}\left(\sigma/\sqrt{\alpha}\right) + \sqrt{\gamma}\tan^{-1}\left(\sigma\sqrt{\gamma}\right), \tag{5.7}$$

where, $\gamma = 2g_2/\xi_0^2$ and $\sigma^2 = \frac{\alpha - f^2}{1 + \gamma f^2}$. In this implicit solution, there appear square roots of α and γ which may have $+$ or $-$ sign. However, for the solution to exist, it is essential that only the $+$ or the $-$ square root of γ are considered consistently. For the root of α, only the $+$ square root can be taken for the solution to exist, otherwise the sign

preceding the $\tanh^{-1}$ term would become negative. Since there are two instances when γ appears on the RHS, taking different sign for two $'\gamma's$ would imply a change of sign between the $\tanh^{-1}$ and $\tan^{-1}$ terms. This implicit expression would no longer be a solution of Eq.(5.5) as can be verified by differentiating it twice.

We can obtain the density profile of the bright soliton from the implicit Eq.(5.7). For simplicity, we consider the density profile for $\alpha = 1$. By definition of $\psi(z,t)$, we have $|\psi(z,t)|^2 = n_0 \, f^2(\rho)$. By the boundary conditions set on the density profile of the bright soliton, $f(\rho)$ goes from 1 at $\rho = 0$, to 0 as $\rho \to \pm\infty$. Therefore, varying the value of $f(\rho)$ from $(0,1]$ in Eq.(5.7) gives us the density profile of the bright soliton. Fig.(5.1) shows this profile for $U = 0$ and different values of r_e, where $U = v/(c\sqrt{2})$. The inset shows variation of width with respect to r_e for $U = 0$. From this we can see the effect of non-locality on the width of the bright soliton. For $U = 0$, the width of the bright soliton decreases if we increase r_e.

Using the bright soliton solution in Eq.(5.7), the energy for a bright soliton on top of the uniform density state can be evaluated using the expression for energy functional in Eq.(5.3). Here too we set $\alpha = 1$ for simplicity. Since the integrand involves second derivative of $|f|^2$, it is convenient to change the integration variable from $\rho \to f$. This can be done using Eq.(5.6) giving $d\rho = df \frac{\sqrt{1+\gamma f^2}}{f\sqrt{1-f^2}}$. Also, using Eq.(5.6), one can find $d^2|f|^2/d\rho^2 = 2 \times [(df/d\rho)^2 + f(d^2f/d\rho^2)]$. Further subtracting the energy of the uniform density state from this integral gives the soliton energy. This gives the expression for energy integral as

$$
E = \frac{gn^2}{2} - \sqrt{2}\xi_0 gn^2 \int_0^1 \left\{ \left[\frac{f^2(1-f^2)}{1+\gamma f^2} + (2f^2 - 1 - f^4) \right. \right.
$$
$$
\left. \left. - \frac{\gamma}{2}\left(\frac{2f^4 - 3f^6 - \gamma f^8}{1+\gamma f^2}\right) + 8U^2 f^2 \right] \times \frac{\sqrt{1+\gamma f^2}}{f\sqrt{1-f^2}} \right\} df.
$$

Fig.(5.2) shows the variation of energy with respect to γ for certain values of U. This figure shows that the effect of the non-locality in an attractive BEC is to decrease the magnitude of energy of the soliton as compared to the uniform density state for a fixed speed.

Having determined the energy of soliton solution as a function of γ, we now compare the widths of these solutions as a function of γ. To do this, we first define the width of the soliton solution. We define the width of the bright soliton to be the ρ where the soliton density falls to half of its peak density. Substituting $f^2 = 1/2$ in Eq.(5.7), we take $r_e = \beta a$ giving $\gamma = 2g_2/\xi_0^2 = 16\pi\nu(\frac{1}{3} - \frac{\beta}{2})$. Here, β is a constant proportionality
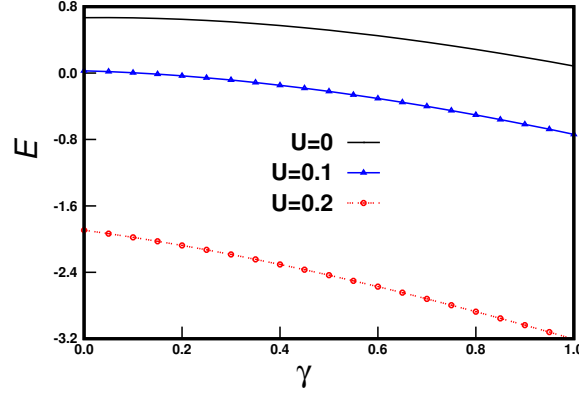
Figure 5.2: The figure shows the variation of the energy over the ground state uniform density of the bright soliton with change in γ, where $\gamma = 2g_2/\xi_0^2$ for some values of U and $\alpha = 1$.

factor. Thus, one obtains, in Fig.(5.3), a plot of the width of the bright soliton as a function of ν for different values of r_e. Note that, the width is independent of the speed v of the soliton. By definition of g_2, $r_e \sim 0.67$ corresponds to $g_2 = 0$. In Fig.(5.3), one can see that $r_e = 0.67a$ corresponds to a line parallel to the ν axis. This implies that w/ξ_0 is a constant, or $w \propto \xi_0$, i.e. the width of the soliton scales as ξ_0. However for $r_e \neq 0.67a$ ($g_2 \neq 0$), the plot of variation of w/ξ_0 with respect to ν is no longer a line parallel to the ν axis. This implies that for $g_2 \neq 0$, the width no longer scales as ξ_0.

The width can be analytically found by putting $f^2 = 1/2$ in Eq.(5.7). This gives us the width to be

$$\frac{w}{\xi_0} = \tanh^{-1}\left(\sqrt{\frac{2\alpha - 1}{\alpha(2 + \gamma)}}\right) + \sqrt{\gamma}\tan^{-1}\left(\sqrt{\frac{\gamma(2\alpha - 1)}{2 + \gamma}}\right).$$

Here, w/ξ_0 is written for the purpose of comparison with soliton solution of LGPE, since ρ (used for LGPE) contains a scaling factor of ξ_0. In the absence of the non-local correction, $\gamma = 0$ and $w/\xi_0 = \tanh^{-1}(\sqrt{\frac{2\alpha-1}{2\alpha}})$, meaning w/ξ_0 is a constant. This implies that the length scale of width of the soliton is ξ_0. However, in the presence of the non-local correction, the width gets modified and the modified length scale is given by $B\xi_0$, where $B = \tanh^{-1}\left(\sqrt{\frac{2\alpha-1}{\alpha(2+\gamma)}}\right) + \sqrt{\gamma}\tan^{-1}\left(\sqrt{\frac{\gamma(2\alpha-1)}{2+\gamma}}\right)$.

Thus, we see that the length scale is not captured by the healing length ξ_0 as the value of ν is increased. As seen previously, in the presence of non-local interactions, the healing length gets modifeid. This modified healing length for BEC with attractive interactions, necessary for generation of bright soliton is given by $\xi = \xi_0\sqrt{1 \mp \gamma}/\sqrt{2}$. We can see that the modified healing length shows an expansion when ν increases. So, qualitatively this feature of soliton width increase is captured by the modified healing length. However, the width of the bright soliton doesn't scale exactly as ξ, but scales as $c\xi$, where c is

a γ dependent function. This is the case because the additional term to the LGPE, although coming from the interaction term, is of a mixed form. That is to say, it has a Laplacian as well as interaction part. However, the soliton solution, as mentioned before arises from a balance of dispersive Laplacian term and the interaction term. This may be the reason for the width of the bright soliton not scaling *exactly* as ξ.

(a) U=0, graph scaled by ξ_0

(b) U=0, graph unscaled

Figure 5.3: Figures show the variation of the width of the bright soliton with change in the gas parameter ν with $\alpha = 1$. In subfigure (a), the width is scaled with the healing length ξ_0, whereas in subfigure (b), the width is not scaled.

Having seen the behaviour of soliton width and energy in the presence of the non-local correction, the next natural step is to check the stability of the bright soliton solution. This stability condition is given by the sign of $dN/d\mu$ [153], where $N = \int |\psi(z,t)|^2$ is the total number of particles in the BEC and $\mu = \alpha g n_0/2$. Here too, for simplifying calculations in the integral, we employ change of variables from ρ to f. Integrating, we get

$$N = \hbar \sqrt{\frac{n_0}{mg}} \left(\sqrt{\alpha} + \frac{1 + \gamma\alpha}{\sqrt{\gamma}} \tan^{-1}(\sqrt{\gamma\alpha}) \right).$$

Bright solitons are stable if $dN/d\mu > 0$. To find if the soliton solution is stable, we differentiate the expression above for N with respect to μ. This gives

$$\frac{dN}{d\mu} \propto \frac{1}{\sqrt{\alpha}} + \sqrt{\gamma} \tan^{-1}(\sqrt{\gamma\alpha}). \tag{5.8}$$

As explained before, $\sqrt{\gamma}$ and $\sqrt{\alpha}$ are positive and hence $\tan^{-1}(\sqrt{\gamma\alpha})$ is also positive, which ensures that $dN/d\mu > 0$. This shows that bright solitons are stable. Fig.(5.4) shows the variation $dN/d\mu$ as a function of γ. This graph corroborates that the bright soliton solution is indeed stable. There has been a proposal of quantifying the stability based on $|dN/d\mu|$ [152]. It says that the soliton stability increases with increase in the magnitude of $|dN/d\mu|$. In this regard, it can be seen from Fig.(5.4) that the soliton stability is enhanced by increasing the non-locality of interactions.
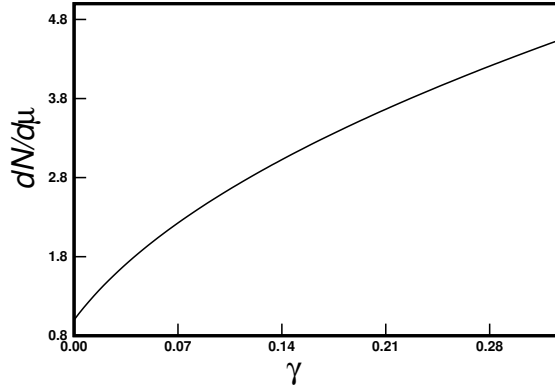
Figure 5.4: The figure shows the variation of $dN/d\mu$ as we change r_e(in scale of a). Here, $\alpha = 1$ and $\nu = 0.1$.

5.4 Dark soliton in a repulsive MGPE

Let us now look at the dark soliton solutions which can be obtained in a repulsive BEC. This corresponds to a self-defocussing non-linearity with non-locality in an optical medium. The 1D MGPE for a repulsive BEC is given as

$$
\begin{aligned}
i\hbar\frac{\partial\psi(z,t)}{\partial t} = &-\frac{\hbar^2}{2m}\frac{\partial^2\psi(z,t)}{\partial z^2} + g|\psi(z,t)|^2\psi(z,t) \\
&+ g\, g_2\psi(z,t)\frac{\partial^2}{\partial z^2}|\psi(z,t)|^2,
\end{aligned}
\tag{5.9}
$$

As for the attractive BEC case in the previous section, let's start by considering N bosons occupying a volume V. The uniform density state has $n_0 = N/V$. The healing at the boundaries may be neglected by assuming that the system is large compared to the healing length. To find moving solutions, it is convenient to consider a moving frame of reference $s = (z - vt)/\sqrt{2}\xi_0$ and write $\psi = \psi(s)e^{-i\mu t/\hbar}$. The form of $\psi(s)$ is taken as $\psi(s) = \sqrt{n_0}\sqrt{\lambda(s)}e^{i\phi(s)}$. Using such a form of ψ, Eq.(5.9) gives two equations for real and imaginary parts as

$$
2\lambda(1-\gamma\lambda)\frac{d^2\lambda}{ds^2} - \left(\frac{d\lambda}{ds}\right)^2 - 8\lambda^2(\lambda-\alpha) - 4\lambda^2\left(\frac{d\phi}{ds}\right)^2 + 8U\lambda^2\frac{d\phi}{ds} = 0;
$$

$$
\tag{5.10}
$$

$$
\frac{d}{ds}\left[\lambda\left(\frac{d\phi}{ds} - U\right)\right] = 0,
$$

where $\gamma = 2g_2/\xi_0^2$ and $U = \sqrt{2}mv\xi_0/\hbar$. To simplify the equations above further, we need to use the boundary conditions for the dark soliton solution. Since, dark soliton

solutions are localized with an intensity minima at $s = 0$, we use the boundary conditions $d\lambda/ds = 0$ for $s = 0$ and $s \to \pm\infty$. Putting these conditions in Eq.(5.10) one gets the central dip $\lambda(0) = U^2$ and the background density $\lambda(s \to \pm\infty) = \alpha$. Further, the lower of the two equations gives, $d\phi/ds = U$ when integrated. This can be used to integrate the upper equation giving

$$\left(\frac{d\lambda}{ds}\right)^2 = \frac{4(\lambda - U^2)(\alpha - \lambda)^2}{1 - \gamma\lambda}.$$

Using the boundary conditions, we have reduced the second order differential equation to a first order differential equation above. However, to obtain a solution, we need to integrate the equation above further. Integrating the equation above gives the following implicit solution for the density profile and phase of a dark soliton [151]

$$\pm s = \frac{1}{\delta_0} \tanh^{-1} \frac{\delta}{\delta_0} + \sqrt{\gamma} \tan^{-1}\left(\delta\sqrt{\gamma}\right)$$

(5.11)

$$\pm\phi(s) = \tan^{-1} \frac{\delta}{U} - U\sqrt{\gamma} \tan^{-1}\left(\delta\sqrt{\gamma}\right).$$

where $\delta^2 = \frac{\lambda(s) - U^2}{1 - \gamma\lambda(s)}$ and $\delta_0^2 = \frac{\alpha - U^2}{1 - \gamma}$. Here, n_0 is the background density over which one observes the dark soliton solution. As for the bright soliton solution, there appears square root of γ which may have $+$ or $-$ sign. As before, only take the $+$ or the $-$ square root of γ can be taken consistently. Taking different signs for two $'\gamma's$ would imply a change of sign between the $\tanh^{-1}$ and $\tan^{-1}$ terms which would no longer be a solution of Eq.(5.10).

Fig.(5.5) shows the density profile for a dark soliton with $U = 0$ for different values of r_e, with the inset showing variation of the width with r_e for $U = 0$. This profile shows that non-locality changes the width of the dark soliton. However, while the width of bright soliton decreases with increasing r_e, the width of the dark soliton increases with an increase in r_e.

As for the bright soliton, energy of a dark soliton can be evaluated using expression for energy functional in Eq.(5.3). The coordinate change in this case is $s \to \lambda$ where $ds = d\lambda \, (\sqrt{1 - \gamma\lambda})/[2(\alpha - \lambda)\sqrt{\lambda - U^2}]$. This gives, by setting $\alpha = 1$ as before, the energy integral as
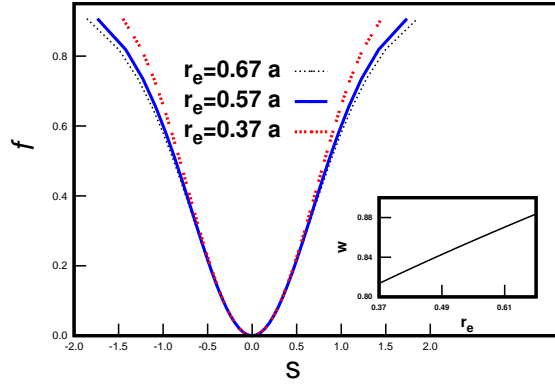
Figure 5.5: The figure shows the density profile of the dark soliton for different values of r_e and $\alpha = 1$ for $U = 0$. The inset shows the variation of the width of dark soliton with variation in r_e(in units of a) for $\nu = 0.1$ for $U = 0$.
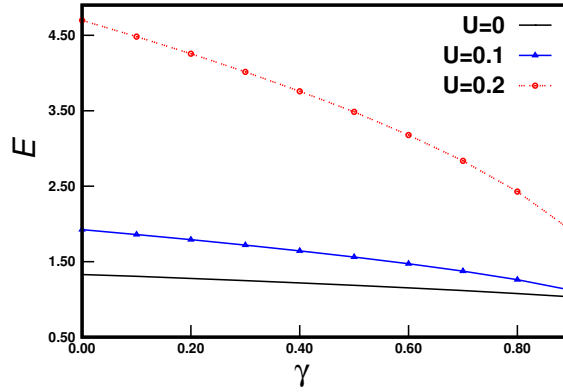
Figure 5.6: The figure shows the variation of the energy over the ground state uniform density of the dark soliton with change in γ, where $\gamma = 2g_2/\xi_0^2$ for some values of U and $\alpha = 1$.

$$E = \sqrt{2}\xi_0 g n_0^2 \int_{U^2}^1 \left\{ \frac{1}{2\lambda}\left[\frac{(1-\lambda)\sqrt{\lambda - U^2}}{\sqrt{1-\gamma\lambda}}\right] + \frac{\lambda U^2\sqrt{1-\gamma\lambda}}{2(1-\lambda)\sqrt{\lambda - U^2})} + \frac{(1-\lambda)\sqrt{1-\gamma\lambda}}{2\sqrt{\lambda - U^2}} \right. $$
$$\left. + \frac{\gamma\lambda}{2}\left(\frac{1 - U^2(\gamma - 2) - \lambda(3 + U^2\gamma) + 2\gamma\lambda^2}{\sqrt{\lambda - U^2}(1-\gamma\lambda)^{3/2}}\right)\right\}d\lambda$$

Fig.(5.6) shows the variation of energy with respect to γ for certain values of U. From this figure, it can be seen that the effect of the non-locality is to decrease the magnitude of energy of the soliton.

Fig.(5.7) shows the effect of non-locality on the width of the dark soliton for $U = 0$. The incomplete graphs for $r_e < 0.67a$ beyond certain values of ν are due to the fact that $\delta_0^2 = \frac{1}{1-\gamma}$ becomes negative and hence δ_0 becomes imaginary. This indicates that the implicit dark soliton solutions given by Eq.(5.11) exist only till a certain value of ν for a given value of r_e.
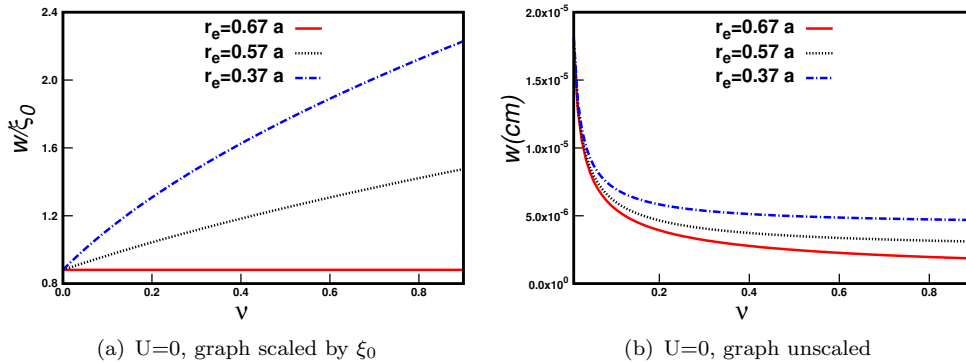
(a) U=0, graph scaled by ξ_0
(b) U=0, graph unscaled
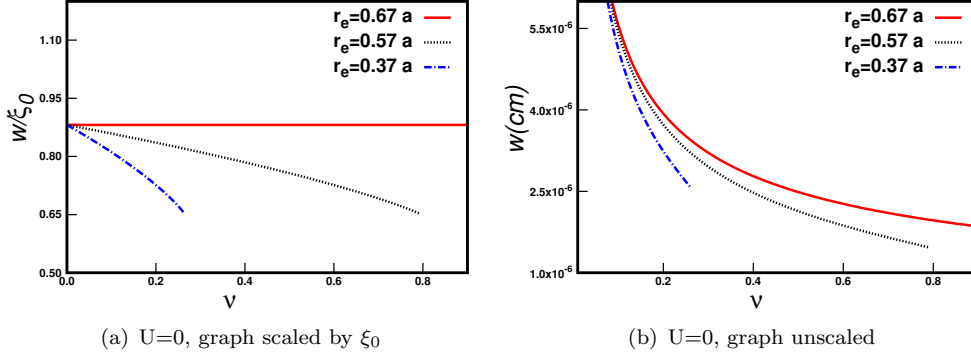
Figure 5.7: Figures show the variation of the width of the black soliton with change in the gas parameter ν for $\alpha = 1$. In subfigure (a), the width is scaled with the healing length ξ_0, whereas in subfigure (b), the width is not scaled.

The change in width for a stationary dark soliton($U = 0$) can be looked at analytically as follows. For the sake of simplicity, let us consider $r_e \propto a$, such that $g_2 = ca^2$. Since $g_2 = \frac{a^2}{3} - \frac{ar_e}{2}$, $0 \le c \le 1/3$ because $g_2 > 0$ for a repulsive BEC. Further, since $\xi_0 = 1/\sqrt{8\pi an_0}$, we can write γ as, $\gamma = 2g_2/\xi_0^2 = 16\pi c\nu$. With $U = 0$, $\delta^2 = \frac{\lambda}{1-\gamma\lambda}$ and $\delta_0^2 = \frac{1}{1-\gamma}$. Let us define the width to the point where the soliton density is half of the density at the point far off from the central dip. That is, the width of the soliton is the value of s(say w/ξ_0) when $\lambda = 1/2$. This gives the width of the black soliton as

$$\frac{w}{\xi_0} = \sqrt{\frac{1-\gamma}{\alpha}} \tanh^{-1}\left(\sqrt{\frac{1-\gamma}{\alpha(2-\gamma)}}\right) + \sqrt{\gamma} \tan^{-1}\left(\sqrt{\frac{\gamma}{2-\gamma}}\right), \qquad (5.12)$$

where α corresponds to the background density as stated before.

Had it been the local GP equation i.e., $\gamma = 0$, one would have obtained $w/\xi_0 = \tanh^{-1}\left(\sqrt{\frac{1}{2}}\right)$. This implies that w/ξ_0 is a constant, meaning that ξ_0 is the length scale for solitons, in the case of local GP dynamics. However, when $\gamma \neq 0$, it can be seen that the scale is different from ξ_0 and depends on γ. Let us say that due to a finite γ, $w/(A \times \xi_0)$ is a constant now instead of w/ξ_0. Then the new length scale for the width is $A\xi_0$. To find this new length scale, we can use Eq.(5.12) and demand that $w/(A \times \xi_0)$ be a constant. This demand gives us the value of A as $A = \sqrt{1-\gamma} \tanh^{-1}\left(\sqrt{\frac{1-\gamma}{2-\gamma}}\right) + \sqrt{\gamma} \tan^{-1}\left(\sqrt{\frac{\gamma}{2-\gamma}}\right)$. This gives us the new length scale $A\xi_0$.

Having obtained the expression for width of dark soliton solution of MGPE, let us compare it with the healing length. As shown previously, doing a small amplitude oscillation analysis around the uniform density ground state gives the dispersion relation for small amplitude oscillations as $\omega = \pm k\sqrt{\frac{gn}{m} + \frac{\hbar^2 k^2}{4m^2}}$ for the LGPE. Note here that since the repulsive is stable, ω is real. The healing length as before is ξ_0. Doing such

an analysis for the MGPE with repulsive interactions gives the modified healing length as $\xi = \xi_0\sqrt{1-\gamma}/\sqrt{2}$. This change in the healing length indicates that there has to be a shrinking in the width of the dark soliton in the presence of non-local interactions which can be observed here, as for the bright soliton. Hence, for dark solitons too, the width of the dark soliton somewhat follows the modified healing length in the presence of non-local interactions. However, the width of the soliton in the presence of non-local interactions although qualitatively follows the modified healing length ξ, the width is not exactly scaled by ξ. It scales with $c\xi$, where c is a γ-dependent function.

One of the popular methods of obtaining dark solitons experimentally is the phase imprinting method [61, 131]. From Eq.(5.11), it is evident that along with the spatial density variation, dark solitons are accompanied by a spatial variation of phase of the wave function, given by $\phi(s)$. The phase imprinting method, as the name suggests, uses a laser which is off-resonant with regards to the excitations in an atomic BEC and imprints the required phase for the generation of dark soliton. For a stationary soliton ($U = 0$), it can be seen from Eq.(5.11) that there is a sudden phase jump at $s = 0$ from $-\pi/2$ for $s < 0$ to $\pi/2$ for $s > 0$. It is phase jumps like these which have to be imprinted. For $U = 0$, the factor γ doesn't play a role. However, as U increases, the variation of the phase with respect to s is significantly altered by γ and hence the phase to be imprinted for soliton generation changes with γ. Fig.(5.8) shows the phase variation of the dark soliton as a function of s for few different values of r_e, with $U = 0.8$.

As for the bright soliton, the stability of the dark soliton solution of the MGPE is of interest. The stability of dark solitons is provided by the Vakhitov-Kolokolov(VK) conditions which determine the stability based on the sign of dQ/dU, where Q is the normalized momentum of the soliton given by

$$Q = \frac{i}{2}\int_{-\infty}^{\infty}\left[\psi(z,t)\partial_z\psi^*(z,t) - \psi^*(z,t)\partial_z\psi(z,t)\right]$$
$$\times\left[1 - \frac{n_0}{|\psi(z,t)|^2}\right]dz$$

Dark solitons are stable if $dQ/dU > 0$ according to the VK condition. Further, as for the bright soliton, there is a proposal for a stability quantifier using the magnitude of dQ/dU. It states that the stability is enhanced as the value of dQ/dU increases beyond 0 [152].

Using the dark soliton solution, the expression for Q is given by
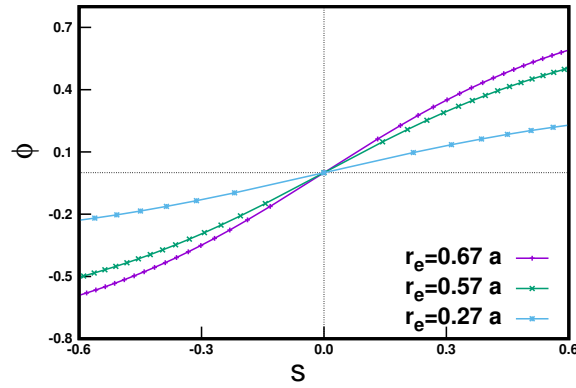
Figure 5.8: The figure shows the variation of phase of the dark soliton $\phi(s)$ as a function of s for a few values of r_e. The gas parameter is fixed at $\nu = 0.1$, $\alpha = 1$ and $U = 0.8$.

$$Q = -2\alpha \tan^{-1}\left(\frac{\delta_0}{U}\right) + (\alpha - U^2)\frac{U}{\delta_0}$$
$$+ \frac{U}{\sqrt{\gamma}}\{1 + \gamma(2\alpha - U^2)\}\tan^{-1}(\delta_0\sqrt{\gamma}).$$

The integration is done by using the change of coordinates from $z \to \lambda$ as before.

Using this expression for Q, one can evaluate dQ/dU, which is given by

$$\frac{dQ}{dU} = \frac{2U^4\gamma - 2U^2\alpha - \alpha U^2\gamma + 3\alpha^2}{\delta_0(\alpha - U^2\gamma)}$$
$$+ \frac{U^2(1 - U^2\gamma + 2\alpha\gamma)}{\delta_0[-1 + (1 + U^2 - \alpha)\gamma]} \tag{5.13}$$
$$+ \left(\frac{1 - 3U^2\gamma + 2\alpha\gamma}{\sqrt{\gamma}}\right)\tan^{-1}(\delta_0\sqrt{\gamma}).$$

To bear in mind is the fact that δ_0 is a function of U.

Fig.(5.9) shows the variation of dQ/dU with respect to U for different values of the effective range r_e. This graph is plotted for $\nu = 0.5$ and $\alpha = 1$. It shows that the solitons are stable even for such large values of ν. Note that even for higher and lower value of ν, one can use Eq.(5.13) to draw plots similar to Fig.(5.9) to show that solitons are stable for a range of ν values. However, at larger values of ν, the higher order corrections would come into picture. For lower values of ν, only the lower order correction used in MGPE is sufficient and as such the solitons are stable using the VK conditions.

Fig.(5.9) shows that the VK stability condition is satisfied for all U for $\alpha = 1$. A simple check can be done to show that $dQ/dU > 0$ for all α for $U = 0$. This can be done by

putting $U = 0$ in Eq.(5.13), which gives $dQ/dU = (3\alpha/\delta_0) + [(1 + 2\alpha\sqrt{\gamma}\tan^{-1}(\delta_0\sqrt{\gamma}))/\sqrt{\gamma}]$, which is > 0.
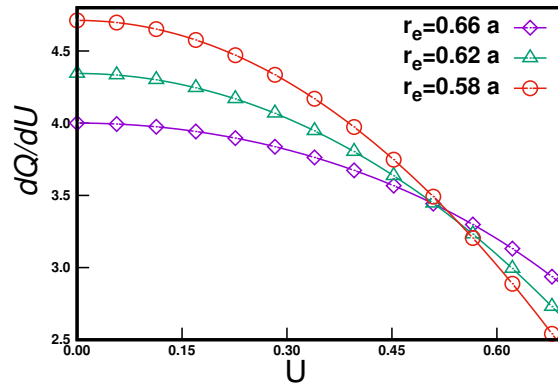
Figure 5.9: The figure shows the value of dQ/dU as a function of U for a few values of r_e . The gas parameter is fixed at $\nu = 0.5$ and $\alpha = 1$.

As for the bright solitons, $|dQ/dU|$ increases for a fixed value of gas parameter as we increase γ (i.e. decrease r_e) for $U = 0$. However, from Fig.(5.9) one can say with certainty that the increased nonlocality provides additional stability to the dark soliton [152] for U close to $U = 0$.

Bright and dark soliton generation in BEC has been achieved by several groups [59, 128]. Bright solitons are generated by trapping a BEC with repulsive interactions and then using Feshbach resonance to modify the scattering length from positive values (repulsive BEC) to negative values (attractive BEC). On the other hand, dark solitons are generated in a repulsive BEC by using methods like phase-imprinting and density engineering. Both these solitons require strong anisotropic confinement in order to freeze out the instability modes perpendicular to the 1D soliton. As shown in our analysis, the non-locality of the interactions manifest upon increasing the gas parameter ν ($:= a^3 n_0$). Experimentally, ν can be increased by tuning the s-wave scattering length, using the Feshbach resonance. As mentioned in the introduction, high values of ν have been achieved in trapped condensates [41, 42]. However, its effect on solitons in a BEC has not been experimentally studied to the best of our knowledge. Thus, after generation of a bright or dark soliton in a BEC, the s-wave scattering length can be tuned to increase ν and its effect on the width of the soliton can be observed by using imaging techniques. By studying the variation of the soliton versus ν, the parameter r_e can be evaluated. Thus, studying the effect of non-local interactions on the soliton width provides for a measure of the effective range parameter r_e.

5.5 Discussion

In this chapter, we have shown the analysis of 1D soliton solutions for a modified Gross-Pitaevskii equation(MGPE). The MGPE takes into account the non-locality of s-wave interactions in a Bose-Einstein Condensate(BEC). Using the exact solutions obtained by Krolikowski *et al.*, we have studied the behaviour of these solutions for a BEC. As the soliton solution is obtained due to a balance between dispersion and non-linearity, the introduction of correction term to the GP equation changes the length scale of the solitons. Consequently, the width of the solitons change as well. This change in the length scale of soliton width shows a similar behaviour to the modified healing length for the MGPE. The change in the width can be experimentally verified as a confirmation of the existence of non-locality of interactions in a BEC. An important consequence of it is that the value of effective range of interactions r_e can be experimentally determined. We have also studied the energetics of the soliton solution and further explored their stability.

The effective range of interactions r_e depends on the details of the interaction potential which is system specific. However, the strength of the non-local interactions depends not only on r_e, but also on the s-wave scattering length (a). The scattering length can be tuned using Feshbach resonance to amplify the effects of change in soliton width. This would lead to a considerable shift of the width from that of the healing length ξ_0. The width of the soliton can then be compared with ξ_0 to determine the value of r_e.

Do note that the change in the width of the dark and bright solitons are opposite in nature and that readily provides one with a qualitative verification of the existence of change in healing length due to non-locality of interactions. Moreover, in this chapter we have also given exact quantitative measure for the change in width as a function of r_e for the dark and bright solitons. In an experiment, if one uses similar condensates for positive as well as negative scattering lengths, obtained using Feshbach resonance, one can actually measure r_e of the system in two different ways, i.e. from the shrinking and from the broadening of the respective solitons.

The spectrum of elementary excitations for the local GP equation shows a phonon-like behaviour $\omega \propto k$ for small wave-numbers (k) and particle-like behaviour $\omega \propto k^2$ for large k. The healing length is the length scale where there is a transition of this spectrum from phonon-like behaviour to particle-like behaviour. In the local GP equation the width of the soliton solution scales as $\xi_0 = 1/\sqrt{8\pi a n_0}$. For the MGPE, there is a change in the healing length and this modified healing length ξ shrinks with increasing non-locality [62] for a BEC with repulsive interactions. Whereas, it is shown in this chapter that for an attractive BEC, the modified healing length ξ is bigger than the ξ_0. Solitons are the

structures whose width scales as the healing length of the system and therefore solitons should capture this modification in the healing length resulting from the non-locality of inter-particle interactions. We show that the width of the soliton shows qualitatively similar behaviour as ξ.

An exact solution provides with the opportunity of analyzing the energetics of the structure and we have fully utilized this opportunity to explore the stability of solitons in the presence of non-local interactions. The soliton solutions of the MGPE are stable even as one increases the gas parameter (ν) to small but finite values. The non-locality of interactions in a BEC imparts additional stability to the solitons, considering the proposal of quantifying soliton stability [152]. However, as seen from Fig.(5.9), beyond a certain value of U, the stability of solitons with stronger non-local interactions decreases. It would be interesting to analyze such a behaviour with respect to the proposal quantifying soliton stability. Such a behaviour might arise due to the modified behaviour of dispersive and focussing effects in a MGPE. However, a detailed study of such a behaviour might throw more light on the stability of solitons in 1D.

Chapter 6

Roton mode softening in multi-component BEC due to finite range of interactions

In the previous chapters, we have considered first order corrections to the LGPE and studied the vortex and soliton in a BEC. For the vortex solution, the new class of vortex solution arose due to the tight confinement of the condensate along the radial direction. The soliton solution showed deviation in length scale for increase of gas parameter a^3n. In this chapter, we will study the dispersion relation of small amplitude oscillation modes. Instead of considering only the first order correction to the LGPE, we shall consider the entire interaction integral with a non-local pseudopotential. This is because the higher order corrections would involve terms of the form k^{2l}, for the l-th order correction. As the value of k increases, the higher order corrections would become prominent. Hence, it doesn't make sense to truncate this series. Instead, the exact features of the dispersion relation would be captured if we keep the entire interaction integral while doing the small amplitude oscillation mode analysis.

The small amplitude oscillation modes arise as fluctuations on top of the uniform density ground state of a BEC in the absence of an external potential. For the LGPE, the dispersion relation of these modes show a phonon like $\omega \propto k$ behaviour for small momentum (k) modes and particle like $\omega \propto k^2$ behaviour for large k. This is for the LGPE, which has a contact pseudopotential. However, for an extended pseudopotential, there appear roton modes in the dispersion relation [66]. The lowering of these roton modes usually is a prescribed way to obtain the so-called supersolid state [154]. However, obtaining such a supersolid state would involve high values of $\nu := a^3n > 1$. This regime would involve

high three body losses [34]. To lower the three body losses and enhance the lifetime of the supersolid state, it is desirable to obtain roton mode softening at a lower value of ν.

Among the many variations obtained in a BEC is the variation of obtaining a BEC with multiple components. Such a BEC with multiple-components has been realized experimentally [19, 155]. The miscibility of the many components is defined by the miscibility criteria relating the density of the species and the inter-species scattering length [20]. For a multi-component BEC in a miscible state, one obtains a coupled GP equation, where the wave-function of one species affects the dynamics of all other species. A small amplitude mode analysis can be done for a BEC with multiple components as well. In this chapter we shall precisely do this. We will show that as for the single-component BEC, in the presence of an extended pseudopotential, multi-component BEC also manifests roton mode in the dispersion relation. We show that as we go on increasing the number of components in a multi-component BEC, the roton mode softening appears at progressively lower values of ν [156]. Thus, obtaining roton mode softening in a multi-component BEC would lower three body losses and enhance lifetime. This mainly happens due to coupling of different components of the multi-component BEC.

We start by revisiting the roton minimum appearing in the elementary excitation spectrum of a single component BEC with extended pseudopotential which has been studied previously [66, 68]. This roton minimum can be lowered by increasing the gas parameter $a^3 n$. We then study the effect of non-locality of s-wave scattering on the appearance and lowering of the roton minimum for a BEC with multiple components. We investigate whether we can soften the roton minimum in a multi-component BEC at a lower value of the gas parameter $\sqrt{n_i n_j} a_{ij}^3$ as compared to that for a single-component BEC, where a_{ij} is the inter-species scattering length and n_i and n_j represent the densities of the ith and jth components. We show that for multi-component BECs, the appearance and lowering of roton minimum can be achieved at a lower value of the gas parameter as we go on increasing the number of distinct components. We observe that even for a two-component BEC, the roton mode softening can be achieved at a significantly lower value of the gas parameter. We shall only be discussing small amplitude modes for a BEC with repulsive interactions.

Positive interaction strength implies a repulsive BEC, while negative interaction strength implies an attractive BEC. Positive scattering length ($a > 0$) would give us a stable condensate where we can have high degree of controllability over the BEC parameters. On the other hand for $a < 0$, the BEC is inherently unstable and we have to tune parameters to stabilize it in the first place. As regards the finite range expansion presented in Chapter.3, it is valid for both positive and negative value of a. However, while discussing the small amplitude oscillation modes, we strictly consider $a > 0$. The reason for it is that

since with single-component and multicomponent BECs, we talk of achieving high values of gas parameter $(a^3 n)$, it would only be appropriate to talk of a repulsive BEC since increasing $a^3 n$ for an attractive BEC would quickly render it unstable. This instability of a BEC for $a < 0$ is also reflected in the dispersion relation, where taking attractive interactions would give us instabilities in the small amplitude oscillation modes.

6.1 Single component BEC

6.1.1 Excitations with local interactions

Let us discuss briefly the dispersion relation for a single component BEC with δ-function inter-particle pseudopotential given by $V_{eff}(\mathbf{r} - \mathbf{r}') = g \, \delta(\mathbf{r} - \mathbf{r}')$. This is a standard textbook calculation [37]. In the absence of an external potential, the Gross-Pitaveskii(GP) equation with such contact interactions is given by

$$i\hbar \frac{\partial \psi(\mathbf{r}, t)}{\partial t} = -\frac{\hbar^2}{2m} \nabla^2 \psi(\mathbf{r}, t) + g|\psi(\mathbf{r}, \mathbf{t})|^2 \psi(\mathbf{r}, \mathbf{t}). \tag{6.1}$$

This equation admits a solution with uniform density. This uniform density state of a BEC is given by $\psi(\mathbf{r}, t) = \sqrt{n} e^{-i\mu t/\hbar}$, where $|\psi(\mathbf{r}, t)|^2$ gives the uniform density and μ is the chemical potential. Small amplitude oscillations on top of this uniform density ground state are taken to be of the form $\theta(\mathbf{r}, t) = \sum_l [u_l(\mathbf{r})e^{\frac{-i\omega_l t}{\hbar}} + v_l^*(\mathbf{r})e^{\frac{i\omega_l t}{\hbar}}]e^{-i\mu t/\hbar}$. The calculation of the small amplitude oscillations over a uniform density state will be done in the same fashion as was done in Sec.(5.2.1). In this case we drop the subscript l and take $u(\mathbf{r}) = ue^{i\mathbf{k}.\mathbf{r}}$, $v(\mathbf{r}) = ve^{i\mathbf{k}.\mathbf{r}}$ and collect terms which evolve in time identically. This procedure gives us the dispersion relation for excitations as $\omega = \sqrt{(\hbar^2 k^4/(4m^2)) + (k^2 gn/m)}$. This relation tells us that for small k, the dispersion is phonon like, whereas for large k it is particle like. To keep in mind is the fact that the current approach uses the δ-function approximation for the pseudopotential, which is equivalent to taking the range of a rectangular barrier pseudopotential tending to zero.

Next we briefly describe the extended pseudopotential used in literature and then use it to study the dispersion relation for a single component and then multi-component BECs in the presence of non-local s-wave scattering.

6.1.2   Excitations with non-local interactions

Let us now look at the effect of non-local interactions on the small amplitude oscillation modes on top of the uniform density state of a BEC. As mentioned before, the uniform density state of a BEC is given by $\psi(\mathbf{r}, t) = \sqrt{n}e^{-i\mu t/\hbar}$. Let us take the non-local interaction pseudopotential as $V_{eff}(\mathbf{r} - \mathbf{r}') = 3g/[4\pi(\sigma a)^3]$ for $|\mathbf{r} - \mathbf{r}'| \leq \sigma a$ and zero otherwise, where σ is an order unity proportionality factor. Thus the width of the scattering pseudopotential is of the order of the s-wave scattering length.

The non-local GP equation in presence of the pseudopotential mentioned above can be derived from the full non-local GP equation, given by [37]

$$i\hbar\frac{\partial\psi(\mathbf{r}, t)}{\partial t} = -\frac{\hbar^2}{2m}\nabla^2\psi(\mathbf{r}, t)$$
$$+ \psi(\mathbf{r}, t)\int\psi^*(\mathbf{r}', t)V_{eff}(\mathbf{r} - \mathbf{r}')\psi(\mathbf{r}', t)d\mathbf{r}',$$

Inserting the pseudopotential mentioned above, we get,

$$i\hbar\frac{\partial\psi(\mathbf{r}, t)}{\partial t} = -\frac{\hbar^2}{2m}\nabla^2\psi(\mathbf{r}, t)$$
$$+ \frac{3g}{(\sigma a)^3}\psi(\mathbf{r}, t)\int_0^{\sigma a}|\psi(\boldsymbol{\phi}, t)|^2 d\boldsymbol{\phi}, \tag{6.2}$$

where, $\boldsymbol{\phi} = \mathbf{r} - \mathbf{r}'$ and $d\boldsymbol{\phi}$ represents the infinitesimal volume element. The integral limits are so taken since we have taken the width of the scattering barrier to be of the order of the s-wave scattering length. We further set the dimensionless constant σ to unity for brevity. This we do while mentioning the caveat that the range of the pseudopotential is not exactly the scattering length, but is of the order of the scattering length.

Once again, we take the form of excitations on top of the uniform density state as $\theta(\mathbf{r}, t) = \sum_l [u_l(\mathbf{r})e^{\frac{-i\omega_l t}{\hbar}} + v_l^*(\mathbf{r})e^{\frac{i\omega_l t}{\hbar}}]e^{-i\mu t/\hbar}$ and treat u and v as excitations with small amplitudes and hence neglect their higher powers. As for the local interactions case, taking $u(\mathbf{r}) = ue^{i\mathbf{k}\cdot\mathbf{r}}$, $v(\mathbf{r}) = ve^{i\mathbf{k}\cdot\mathbf{r}}$ and collecting terms which evolve in time identically, we get now equations similar to ones in Sec.(5.2.1)

$$\hbar\omega u = \frac{\hbar^2 k^2}{2m} u + \frac{gn}{ka} \sin(\sigma ka) [u + v]$$

$$-\hbar\omega v = \frac{\hbar^2 k^2}{2m} v + \frac{gn}{ka} \sin(\sigma ka) [u + v].$$

These equations can be written in the matrix form as

$$\begin{pmatrix} -\hbar\omega + \frac{\hbar^2 k^2}{2m} + \frac{gn}{ka} \sin(\sigma ka) & \frac{gn}{ka} \sin(\sigma ka) \\ \frac{gn}{ka} \sin(\sigma ka) & \hbar\omega + \frac{\hbar^2 k^2}{2m} + \frac{gn}{ka} \sin(\sigma ka) \end{pmatrix} \begin{pmatrix} u \\ v \end{pmatrix} = \begin{pmatrix} 0 \\ 0 \end{pmatrix}.$$

For the matrix equation above to have a non-zero solution in u and v, the determinant of the square matrix on the LHS has to be zero. This condition gives us the following dispersion relation

$$\omega = \pm \frac{\hbar}{m} \sqrt{\frac{k^4}{4} + (4\pi kn) \sin \sigma ka}.$$

which can be equivalently written as

$$\omega = \pm \frac{\hbar}{a^2 m} \sqrt{\frac{\lambda^4}{4} + (4\pi a^3 n \lambda) \sin \sigma \lambda}, \tag{6.3}$$

where $\lambda = ka$. The gas parameter $a^3 n$ appearing in the equation above should be small in order for the three body interactions to be noticeably small. Particularly, the well known diluteness limit is given by $a^3 n \ll 1$. However, there have been recent experiments which have explored the limits of the gas parameter, trying to push it towards the strongly interacting regime $a^3 n \sim 1$ [41, 140].

The dispersion relation given by Eq.(6.3) exhibits a roton minimum which can be lowered as we increase $a^3 n$ as shown in Fig.(6.1). The roton minimum touches the ak axis at a value of $a^3 n \sim 1.5$ which is beyond the $a^3 n \ll 1$ limit. This would take us well into the strongly interacting regime. Nonetheless, we see that it is possible to pull the roton minimum down in principle. Thus we get a hint that it might be possible to pull the roton minimum down, at a lower value of $a^3 n$, by introducing additional interactions such as those in multi-component BEC. Since the macroscopic wave-function of different components in a multi-component BEC is different, there occur cross terms between the wave-functions in the GP equation, due to the inter-species scattering. Thus for multi-component BEC, there exist additional interaction terms than the ones in the GP equation for a single component BEC. In the following section, we consider
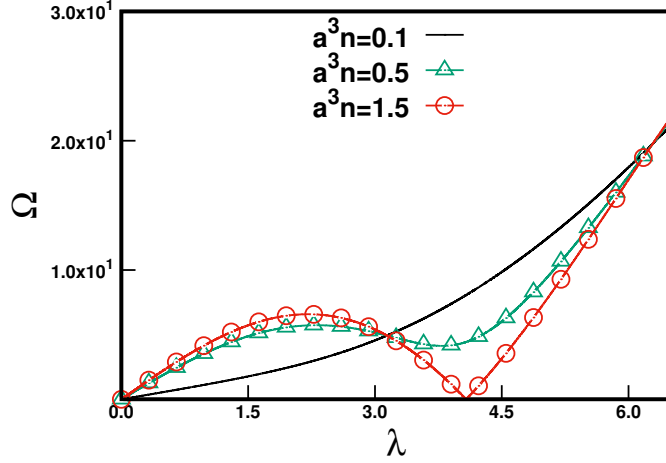
Figure 6.1: Figure shows the dispersion relation for single component BEC in the presence of non-local inter-particle interaction pseudopotential for certain values of the parameter a^3n. Here, $\Omega = m\omega a^2/\hbar$ and $\sigma = 1$ for the sake of comparison.

multi-component BEC and study the manifestation of inter-species interactions in the dispersion relation of small amplitude oscillations.

6.2 Multi-component BEC

BECs with more than one components, in the absence of an external potential, can be analysed by taking into account the inter-particle interaction in the GP energy functional. This can be written as [77]

$$
E = \frac{\hbar^2}{2m} \sum_j \int d\mathbf{r}\, |\nabla\psi_j(\mathbf{r})|^2 + \sum_j \int d\mathbf{r}\, \frac{|\psi_j(\mathbf{r})|^2}{2} \int d\mathbf{r}'\, \psi_j^*(\mathbf{r}')V_{jj}(\mathbf{r}-\mathbf{r}')\psi_j(\mathbf{r}')
$$
$$
+ \sum_{j,l}^{j>l} \int\int d\mathbf{r}'d\mathbf{r}\, \left(\frac{\psi_j(\mathbf{r})\psi_j^*(\mathbf{r})V_{jl}(\mathbf{r}-\mathbf{r}')\psi_l(\mathbf{r}')\psi_l^*(\mathbf{r}')}{2}\right).
$$
(6.4)

where g_{ij} represents the inter-species s-wave scattering strength, $g_{ij} = 4\pi\hbar^2 a_{ij}(m_i + m_j)/(m_i m_j)$, m_i and m_j represent the mass of the atoms of different species whose wavefunctions are ψ_i and ψ_j respectively. The inter-particle scattering length is given by a_{ij}. If the scattering pseudopotential is taken to be δ-function as before with $V_{ii}^{eff}(\mathbf{r} - \mathbf{r}') = g_{ii}\delta(\mathbf{r} - \mathbf{r}')$ for intra-species scattering and $V_{ij}^{eff}(\mathbf{r} - \mathbf{r}') = g_{ij}\delta(\mathbf{r} - \mathbf{r}')$, we get the local GP equation for multi-component BEC as

$$i\hbar\frac{\partial\psi_j(\mathbf{r},t)}{\partial t} = -\frac{\hbar^2}{2m}\nabla^2\psi_j(\mathbf{r},t) + g_{jj}|\psi_j(\mathbf{r},t)|^2\psi_j(\mathbf{r},t) + \psi_j(\mathbf{r},t)\sum_l^{j\neq l} g_{jl}|\psi_l(\mathbf{r},t)|^2, \quad (6.5)$$

for each of the several components, denoted by the subscript j.

Now, as for the single component case, these equations admit solutions with uniform density for each component given by $\psi_j(\mathbf{r},t) = \sqrt{n_j}e^{-i\mu_j t/\hbar}$. Such BEC might exist stably in many configurations with regards to the miscibility. The general miscibility condition for two components i and j is given by $a_{ij} < \sqrt{a_i a_j}$ [157]. The miscibility condition can be obtained using a simple energy calculation as follows.

6.2.1   Miscibility criterion

Let us see this miscibility criterion for a two-component BEC. The same logic can be extended to multi-component BEC.

The energy of a two-component BEC, occupying a volume V, with N_1 particles of species 1 and N_2 particles of species 2 in a homogeneous state (mixed phase) can be evaluated using the energy functional in Eq.(6.4) as

$$E_{mis} = \frac{1}{2}\left[g_{11}\frac{N_1^2}{V} + g_{22}\frac{N_2^2}{V} + 2g_{12}\frac{N_1 N_2}{V}\right].$$

Now, for a segregated phase, the interaction term g_{12} would be absent. Let us then consider the species 1 occupying a volume V_1 and species 2 occupying the volume V_2, such that $V_1 + V_2 = V$. This energy would be $E = \frac{1}{2}\left(g_{11}N_1^2/V_1 + g_{22}N_2^2/V_2\right)$. Now, the volumes V_1 and V_2 occupied can be fixed by minimizing the energy, subject to the condition $V_1 + V_2 = V$. This gives us the energy as

$$E_{seg} = \frac{1}{2}\left[g_{11}\frac{N_1^2}{V} + g_{22}\frac{N_2^2}{V} + 2\sqrt{g_1 g_2}\frac{N_1 N_2}{V}\right].$$

Now, for the BEC to be present in the miscible phase, $E_{mis} < E_{seg}$. This condition gives $g_{12} < \sqrt{g_1 g_2}$. Writing $g = 4\pi\hbar^2 a/m$, we get this miscibility condition as $a_{12} < \sqrt{a_1 a_2}$. This calculation can be extended to multiple components and we may obtain the condition for miscible state to prevail as $a_{ij} < \sqrt{a_i a_j}$.

6.2.2 Excitations with local interactions

We shall consider here a uniform, homogeneous mixture state of the many components, i.e. we consider a state where the miscibility criterion holds for all components. We shall first look at the dispersion relation of small amplitude oscillations for the local GP equation given by Eq.(6.5) and then look at the non-local case in the next section.

We take the small amplitude excitations over the state $\psi_j(\mathbf{r}, t) = \sqrt{n_j} e^{-i\mu_j t/\hbar}$ of the form $\theta_j(\mathbf{r}, t) = \sum_q [u_{qj}(\mathbf{r}) e^{\frac{-iw_q t}{\hbar}} + v_{qj}^*(\mathbf{r}) e^{\frac{iw_q t}{\hbar}}] e^{-i\mu_j t/\hbar}$. Further, as for the single component case, we take the form of u_j and v_j as $u_{qj}(\mathbf{r}) = u_{qj} e^{i\mathbf{k_q} \cdot \mathbf{r}}$, $v_{qj}(\mathbf{r}) = v_{qj} e^{i\mathbf{k_q} \cdot \mathbf{r}}$. For a two component BEC, this dispersion relation has two distinct branches [158]. In general for a multicomponent BEC we may get a complicated dispersion relation for excitations. To simplify the system, we assume that all the intra-species scattering lengths are equal (a_1 say), so are the inter-species scattering lengths (a_2 say). This simplification enables us to look particularly into the effects of the presence of multiple components in a BEC on the roton mode softening. This simplification also brings out the role of inter-species interaction on roton mode softening, which is our core interest here.

Further, taking species with equal densities (n) and comparable masses (m) we get the following matrix structure for excitations

$$
\begin{pmatrix}
U_- & X & c & c & \text{........} & & & & \\
X & U_+ & c & c & \text{........} & & & & \\
c & c & U_- & X & c & c & \text{....} & & \\
c & c & X & U_+ & c & c & \text{....} & & \\
 & & & . & & & & & \\
 & & & & . & & & & \\
 & & & & & . & & & \\
 & & & & & & . & & \\
 & \text{........} & & c & c & U_- & X \\
 & \text{........} & & c & c & X & U_+
\end{pmatrix}
\begin{pmatrix}
u_1 \\ v_1 \\ . \\ . \\ . \\ . \\ . \\ . \\ u_s \\ v_s
\end{pmatrix}
=
\begin{pmatrix}
0 \\ 0 \\ . \\ . \\ . \\ . \\ . \\ . \\ 0 \\ 0
\end{pmatrix},
\tag{6.6}
$$

where

$$
U_\pm := \pm w\hbar - \frac{\hbar^2 k^2}{2m} - g_1 n
$$

$$
X := -g_1 n
$$

$$
c := -g_2 n,
$$

with s as the total number of distinct components in the multi-component BEC.

To get a non-trivial solution for excitations u and v on top of the uniform density ground state, the determinant of the $2s \times 2s$ square matrix in Eq.(6.6) must be zero. This condition gives us

$$\left[w^2 - \frac{\hbar^2}{m^2}\left(\frac{k^4}{4} + 4\pi na_1 k^2 + (s-1)4\pi na_2 k^2\right)\right] \times \left[w^2 - \frac{\hbar^2}{m^2}\left(\frac{k^4}{4} + 4\pi na_1 k^2 - 4\pi na_2 k^2\right)\right]^{(s-1)} = 0.$$

This equation gives us two branches of the dispersion relation as,

$$w = \frac{\hbar}{m}\left[\frac{k^4}{4} + 4\pi na_1 k^2 + (s-1)4\pi na_2 k^2\right]^{\frac{1}{2}}$$

$$or/and \hspace{12em} (6.7)$$

$$w = \frac{\hbar}{m}\left[\frac{k^4}{4} + 4\pi na_1 k^2 - 4\pi na_2 k^2\right]^{\frac{1}{2}}.$$

6.2.3 Excitations with non-local interactions

Let us now consider non-local pseudopotential for both intra-species and inter-species interactions in a multi-component BEC. Let the interaction pseudopotential be given by $V_{jj}^{eff}(\mathbf{r} - \mathbf{r}') = 3g_{jj}/4\pi(\sigma a_{jj})^3$ for $|\mathbf{r} - \mathbf{r}'| \leq \sigma a_{jj}$ and zero otherwise for the intra-species interaction. For the inter-species interaction, we take the interaction psuedopotential as $V_{ij}^{eff}(\mathbf{r} - \mathbf{r}') = 3g_{ij}/4\pi(\sigma a_{ij})^3$ for $|\mathbf{r} - \mathbf{r}'| \leq \sigma a_{ij}$ and zero otherwise. We shall like to re-emphasize the fact that we do not claim the range of the pseudopotential to be exactly equal to that of the scattering length, but it is of the order of the scattering length, which is what is considered here to simplify the model.

Now, we write the non-local GP equation which can be derived from the energy functional in Eq.(6.4) by considering the interaction pseudopotential to be non-local, as given above. It is of the form

$$i\hbar\frac{\partial\psi_j(\mathbf{r},t)}{\partial t} = -\frac{\hbar^2}{2m}\nabla^2\psi_j(\mathbf{r},t) + \frac{3g_{jj}}{(\sigma a_{jj})^3}\psi_j(\mathbf{r},t)\int_0^{\sigma a_{jj}}|\psi_j(\boldsymbol{\phi},t)|^2 d\boldsymbol{\phi}$$
$$+\sum_l^{j\neq l}\Big[\frac{3g_{jl}}{(\sigma a_{jl})^3}\psi_j(\mathbf{r},t)\int_0^{\sigma a_{jl}}\psi_l^*(\boldsymbol{\phi},t)\cdot\psi_l(\boldsymbol{\phi},t)d\boldsymbol{\phi}\Big]. \tag{6.8}$$

As for the single component case, $\boldsymbol{\phi}=\mathbf{r}-\mathbf{r}'$ and $d\boldsymbol{\phi}$ represents the infinitesimal volume element. The above equation admits a solution where each of the species have a uniform density, same as that for the local case. This can be verified by plugging in the form for different ψ_j as $\psi_j(\mathbf{r},t)=\sqrt{n_j}e^{-i\mu_j t/\hbar}$. As before, considering small amplitude oscillations $\theta_j(\mathbf{r},t)$ on top of this uniform density state, we get the following matrix by mode matching.

$$\begin{pmatrix} A_- & B & D & D & .... & & & \\ B & A_+ & D & D & .... & & & \\ D & D & A_- & B & D & D & .... & \\ D & D & B & A_+ & D & D & .... & \\ & & & . & & & & \\ & & & . & & & & \\ & & & . & & & & \\ & & & & . & & & \\ & & .... & D & D & A_- & B \\ & & .... & D & D & B & A_+ \end{pmatrix}\begin{pmatrix} u_1 \\ v_1 \\ . \\ . \\ . \\ . \\ . \\ . \\ u_s \\ v_s \end{pmatrix} = \begin{pmatrix} 0 \\ 0 \\ . \\ . \\ . \\ . \\ . \\ . \\ 0 \\ 0 \end{pmatrix}, \tag{6.9}$$

where

$$A_\pm := \pm\,\omega\hbar - \frac{\hbar^2 k^2}{2m} - g_1 n\frac{\sin\sigma a_1 k}{a_1 k}$$
$$B := -\,g_1 n\frac{\sin\sigma a_1 k}{a_1 k}$$
$$D := -\,g_2 n\frac{\sin\sigma a_2 k}{a_2 k}.$$

Here too we have considered the simplification that all intra-species scattering lengths are equal(a_1) and so are the inter-species scattering lengths(a_2).

As before, to get a non-trivial solution for excitations u and v on top of the uniform density ground state, the determinant of the $2s\times 2s$ square matrix in Eq.(6.9) must be

(a) $\beta = 0.49$, $a_1^3 n = 0.5$ (b) $\beta = 0.49$, $a_1^3 n = 0.55$ (c) $\beta = 0.49$, $a_1^3 n = 0.616$

Figure 6.2: Figures shows the dispersion relation for small amplitude excitations of a BEC, in the presence of non-local interaction pseudopotential between atoms, for the common branch of elementary excitations for multi-component BEC. The plots are for different values of the intra-species gas parameter $a_1^3 n$. Here, $\Omega = m\omega a_1^2/\hbar$ and $\sigma = 1$ for the sake of comparison.

zero. Since the matrix structure is similar to the one for the local multi-component case, we get the following equation

$$\left[\omega^2 - \frac{\hbar^2}{m^2}\left(\frac{k^4}{4} + 4\pi n a_1 k^2 \left(\frac{\sin \sigma a_1 k}{a_1 k}\right) + (s-1)4\pi n a_2 k^2 \left(\frac{\sin \sigma a_2 k}{a_2 k}\right)\right)\right]$$
$$\times \left[\omega^2 - \frac{\hbar^2}{m^2}\left(\frac{k^4}{4} + 4\pi n a_1 k^2 \left(\frac{\sin \sigma a_1 k}{a_1 k}\right) - 4\pi n a_2 k^2 \left(\frac{\sin \sigma a_2 k}{a_2 k}\right)\right)\right]^{(s-1)} = 0.$$

This condition gives us two branches of the dispersion relation for excitations as

$$\omega = \frac{\hbar}{m}\left[\frac{k^4}{4} + 4\pi n a_1 k^2 \left(\frac{\sin \sigma a_1 k}{a_1 k}\right) + (s-1)4\pi n a_2 k^2 \left(\frac{\sin \sigma a_2 k}{a_2 k}\right)\right]^{\frac{1}{2}}$$

$$or/and \tag{6.10}$$

$$\omega = \frac{\hbar}{m}\left[\frac{k^4}{4} + 4\pi n a_1 k^2 \left(\frac{\sin \sigma a_1 k}{a_1 k}\right) - 4\pi n a_2 k^2 \left(\frac{\sin \sigma a_2 k}{a_2 k}\right)\right]^{\frac{1}{2}}.$$

The above equations exhibit a roton minimum, similar to the one for a single component BEC with non-local pseudopotential. However, there is a crucial difference, since now the factor s in the above equation means that the dispersion relation would depend on the number of distinct species in the multi-component BEC. Also, for a single component BEC there was just one length scale for the scattering length. However, for a multi-component BEC, on top of the intra-species scattering length there exist inter-species scattering length as well.

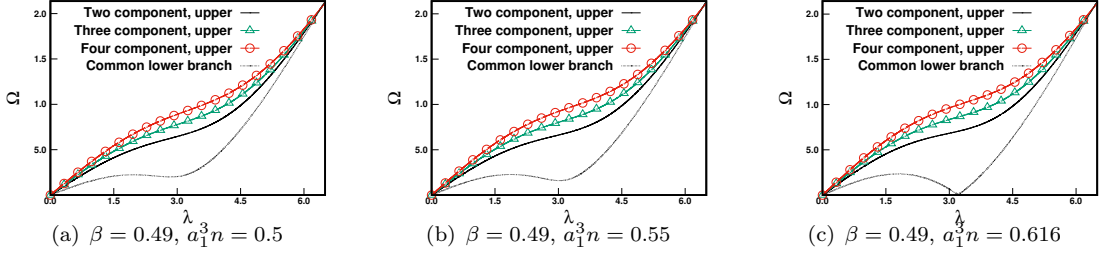We write the dispersion relation in Eq.(6.10) in a form similar to that of Eq.(6.3) as
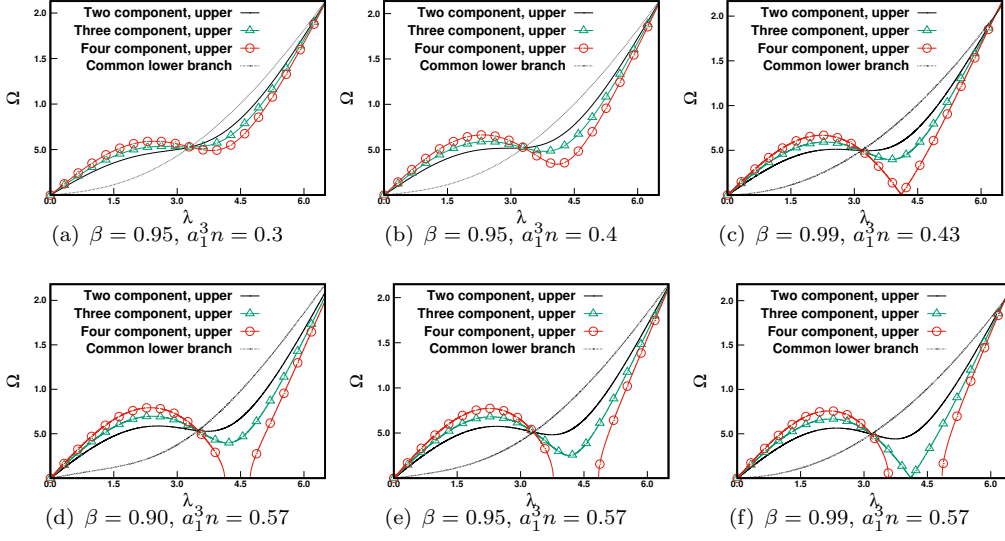
Figure 6.3: Figures shows the dispersion relation for small amplitude excitations of a BEC, in the presence of non-local interaction pseudopotential between atoms, with various number of distinct components as labelled in the graphs. The plots are for different values of the intra-species gas parameter $a_1^3 n$ and $\beta = a_2/a_1$. Here, $\Omega = m\omega a_1^2/\hbar$ and $\sigma = 1$ for the sake of comparison.

$$\omega = \frac{\hbar}{a_1^2 m}\left[\frac{\lambda^4}{4} + 4\pi a_1^3 n\lambda \sin\sigma\lambda + (s-1)4\pi a_1^3 n\lambda \sin\sigma\beta\lambda\right]^{\frac{1}{2}}$$

$$or/and \tag{6.11}$$

$$\omega = \frac{\hbar}{a_1^2 m}\left[\frac{\lambda^4}{4} + 4\pi a_1^3 n\lambda \sin\sigma\lambda - 4\pi a_1^3 n\lambda \sin\sigma\beta\lambda\right]^{\frac{1}{2}}$$

where $\lambda = a_1 k$ and $\beta = a_2/a_1$. As the miscibility criteria states, we should stay in the limit $a_2 < a_1$, implying $\beta < 1$ [157]. Also, as we have taken the densities of each component to be the same, the gas parameter takes the form na_2^3 and na_1^3 for the inter-species and intra-species scattering length respectively [20]. Since $a_2 < a_1$, $na_2^3 < na_1^3$.

As we had seen in the single component case with non-local interactions, roton lowering was possible due to the $\sin ak$ term, since it attains negative values. Here too, the roton minimum is obtained due to $\sin a_1 k$ and $\sin \beta a_1 k$ terms. However, the behaviour of the upper and lower branches of Eq.(6.11) is different due to the opposite sign of $\sin a_1 k$ and $\sin \beta a_1 k$, and the absence of s in the lower branch. Also, notice that the lower branch is common to all the multi-component BEC with $s \geq 2$. In Fig.(6.2) we plot this common branch for various values of the gas parameter. The lowest value of the gas parameter for which the roton mode of this branch may be pulled down to the $\omega = 0$

axis is $a_1^3 n \sim 0.616$. Notice here that since $\sin \lambda$ and $\sin \beta\lambda$ have opposite sign, the roton minimum would be lowered when $\sin \beta\lambda$ is positive and $\sin \lambda$ is negative. This is in contrast to the upper branch both the terms being negative will enhance the roton lowering. Hence, for the common branch, the value of $\beta = a_2/a_1$ for which the roton mode softening is enhanced is $\beta \sim 0.49$. For the upper branch, as we shall see, the roton lowering would be enhanced for β very close to 1. Having discussed the common branch, we next discuss the behaviour of the upper branch of Eq.(6.11).

In Fig.(6.3) we plot the dispersion relation of elementary excitations for a two, three and four component BEC for the upper branch in Eq.(6.11). This figure shows that, for a fixed value of the parameter $a_1^3 n$, the roton minimum is lowered as we increase the number of distinct components in a BEC. From the figure we also see that the lower branch of ω in Eq.(6.11) does not show any instability in the regime of parameters considered. The values taken in the figure are such that $a_2 < a_1$ such that the miscibility limit is satisfied. For the single component BEC (Fig.(6.1)) the roton lowering was achieved at $a^3 n \sim 1.5$. However, here the roton lowering is achieved at a value of $a_1^3 n \sim a_2^3 n \sim 0.43$ for a four component BEC and $a_1^3 n \sim a_2^3 n \sim 0.57$ for a three component BEC. Upon further varying the value of $a_1^3 n$ we may observe roton lowering for a two-component BEC in the upper branch. The value of gas parameter for this to happen is $a_1^3 n \sim 0.85$. However, we have already seen that the common branch of excitation for multi-component BEC gives us roton mode softening at a lower value of gas parameter, viz., $a_1^3 n \sim 0.616$. Since, this branch is present for $s \geq 2$, it is present for a two-component BEC as well. Hence the common(lower)branch would give roton lowering for a two component BEC at a smaller value of the gas parameter than the upper branch.

The condition for three body losses to be negligible in a BEC is given by the diluteness condition $a^3 n \ll 1$. As the parameter $a^3 n \rightarrow 1$ or beyond one, loss of atoms from the condensate occurs. Nonetheless, BEC in such strongly interacting regimes have been obtained and studied [140]. This is achieved by tuning the s-wave scattering length [159]. The lifetime of such a strongly interacting BEC would depend on the gas parameter and hence it is important to obtain the roton lowering at a lower value of the gas parameter.

The loss rate for a BEC is given by the equation $dN(t)/dt = -K_3^{tot} < n^2 > N(t)/6$, where $N(t)$ is the number of atoms at time t, $< n^2 >$ is the mean square density of the condensate and K_3^{tot} is the total 3 body loss rate constant[160]. The factor K_3^{tot} is dependent on the gas parameter $a^3 n$. From Feshbach resonance experiments for commonly used atomic BEC components like rubidium, caesium, potassium, lithium and sodium [160–164], one can see that obtaining values of $a^3 n$ near 1 requires working very close to the resonance. These experiments have also measured value of K_3^{tot} for a

range of values of the scattering lengths. One can see from these experiments that K_3^{tot} increases very sharply near the resonance. Hence, an increase in the value of a^3n from 0.6 to 1.5 would increase the loss rate K_3^{tot} by two to three orders of magnitude. Thus, it can be seen that the reduction in the value of a^3n for roton mode softening that we have shown is quite significant.

We can see that for finite k, setting the width of the pseudopotential interaction tending to zero, as is done for local interactions, would mean setting the scattering length tending to zero. One can set $a \to 0$ in Eq.(6.10). This would essentially give us back the multi-component dispersion relation in Eq.(6.7), which we had got by neglecting the non-locality of the pseudopotential in the multi-component BEC.

The phenomenon seen in Fig.(6.3) of the roton mode softening at a lower value of gas parameter, arises mainly because the inter-species interaction. The lower value of gas parameter ensures that the three body losses reduce as we increase the number of components. As the strongly interacting regime $a^3n \to 1$ has been achieved experimentally, such a roton lowering is realizable for a multi-component BEC by tuning the scattering lengths involved at lower loss rates.

6.3 Discussion

In this chapter, we have studied elementary excitations in a BEC in the presence of non-local s-wave interactions for multi-component BECs. We started by studying the effect of non-local interactions on the spectrum of elementary excitations in a single component BEC. We considered these elementary excitations on top of the uniform density ground state. The consideration of finite range of inter-boson interactions gives us a roton mode in the spectrum of elementary excitations. This roton mode can be lowered by increasing the gas parameter (a^3n). The roton energy becomes zero for a value of $a^3n > 1$ for a single component BEC. We then have studied elementary excitations on top of a ground state of multi-component BEC, where each of the components has a uniform density. We work in the limit where the various components are miscible. Consideration of finite range of inter-boson interactions gives us a roton mode for multi-component BEC as well. We investigated to find the lowest value of the gas parameter a_1^3n for which we get zero energy roton modes. We have shown that for BEC with two components and above, zero energy roton modes can be obtained for $a_1^3n < 1$. Furthermore, we have shown that as we go on increasing the disticnt components of a multi-component BEC, zero energy roton modes are obtained for lower and lower values of a_1^3n.

Note that we have just considered the s-wave scattering and not any other form of long range interactions. The non-local s-wave scattering pseudopotential is taken to be a rectangular barrier with width of the order of the s-wave scattering length. Previous works have shown that in the presence of non-local interaction pseudopotential, there appears a roton minimum in the dispersion relation, for a single component BEC. This roton minimum can be lowered by modifying the width of interactions, which can be taken to be of the order of the scattering length. However, for achieving this roton mode softening, one has to go beyond the diluteness limit ($a^3 n \ll 1$) and into the strongly interacting regime.

The experimental progress in obtaining strongly interacting BEC is substantial with the gas parameter being pushed very close to $a^3 n \sim 1$. This is achieved by tuning the s-wave scattering length. However, as we go near the strongly interacting BEC regime $a^3 n \sim 1$ value, three body losses become significant. The magnitude of such losses would increase with the increase of the gas parameter. Hence it is necessary to obtain zero energy roton modes at a lower value of the gas parameter and this is where multi-component BEC helps. We have shown that even using just a two-component BEC, we are able to push the value of gas parameter for obtaining zero energy roton modes from 1.5 to 0.616. As we increase the number of components further, we get zero energy roton modes for even lower values of the gas parameters.

As the roton mode exhibits itself in a single-component BEC, it is but natural to expect such a roton minimum in a multi-component BEC as well. What is peculiar to the multi-component BEC is the softening of roton mode, at a certain value of gas parameter, just by increasing the number of distinct components. This roton mode softening comes about mainly because of the fact that every species in a multi-component BEC is represented by a particular wave-function. This brings about presence of cross-coupling terms in the GP equation used to describe the multi-component system. Due to such terms, the small amplitude oscillation modes of one component couple to the ground state of other component at the expense of energy which helps lower the roton energy. This is seen as roton mode softening in the dispersion relation. Since the strongly interacting regime of a BEC is achieved experimentally, the technique suggested by us would help realize zero energy roton modes at a lower value of gas parameter, thus reducing losses.

Chapter 7

Conclusion and future works

In this thesis, we have studied the effect of finite range of interactions on the excitations in a BEC. We started by considering the corrections to the GP equation with contact interactions, due to the finite range of the interactions. We found the energy functional for such a GP equation with corrections up to an arbitrary order. The term by term correspondence between correction terms added to the GP equation and its energy functional, with its applicability restricted to corrections with even symmetry was a characteristic feature of this correspondence. We then studied the effect of corrections to the LGPE (GP equation with contact interactions) on the vortex solution in a BEC. Here, it was shown that there exists a new class of vortex solution whose width is of the order of microscopic length scale of interactions. This solution was shown to manifest itself in the presence of tight trapping. This is important in the context of obtaining low filling fractions in the context of obtaining analogous Quantum hall effect in BECs. Next, we studied the effect of corrections to the LGPE on the soliton solution. The change in the length scale, its relation to the modified healing length and the enhanced stability of the soliton solution due to the finite range corrections were important features here. Finally, we looked at the effect of finite range interactions on the elementary excitation spectrum in BECs. We showed here that adding distinct components helps to lower the roton minimum at lower loss rates.

The LGPE neglects the range of inter-boson interactions and as such this range doesn't appear in the LGPE. As we progressively increase the gas parameter, this finite range of interactions would begin to show up. Hence, it only makes sense for the finite range of interactions to show up in the equation governing BECs in the regime of non-negligible values of gas parameter. The simplest way to account for this range is to assume that the GP equation holds and to add perturbative corrections to the LGPE.

From the experimental point of view, since the discovery of BECs and attainment of Feshbach resonance in BECs, strongly interacting BECs have been obtained [41, 42]. As the diluteness limit is breached, it is but natural to expect a modified equation for the BEC dynamics and this is what we have considered in this thesis. With progressively higher values of gas parameter obtained in experiments, the results presented in this thesis are open to experimental verification.

Neglecting the contribution of higher order terms depends upon the problem at hand. For example, in the case of small amplitude oscillation modes, we have taken the entire series because the nth order contribution of the series goes as k^{2n} . As a result the series cannot be truncated for large k. However, for the case of vortex solution and solitons, the situation is different. For the case of vortex solution, we have shown that for the vortex of order s, the solution near the core scales as $R^{|s|}$ and hence the corrections to the local GP equation above the $2s$th order in derivative is zero. Thus there is a natural truncation for the vortex solution. Lastly, for the case of soliton solution, the scenario becomes clear when we consider the width of the interaction pseudopotential to be of the order of s-wave scattering length. Doing so gives us that the qth order correction to the local GP equation is multiplied by a factor of $(a^3 n)^q$. Thus, as long as we stay in the limit $a^3 n < 1$, we are assured that the higher order terms fall fast. This accompanied by the fact that the higher derivatives of density fall off enables us to safely truncate the series of corrections at the first order. Having stated these conditions, it is essential to re-state that the truncation of the series of corrections depends on the problem in question. Hence in Chapter.3, we have presented corrections to the energy functional up to an arbitrary order since the problem at hand may require corrections above the first order to be included.

The results presented in this thesis can be extended in many directions. Firstly, the new class of single vortex solution presented by us can be studied in the presence of various trapping potentials. Its dynamics in three dimensions is also of interest. More importantly, study of a lattice of such thin vortices can be undertaken in view of obtaining lower vortex filling fractions to achieve analogous quantum hall effect. This may be studied by starting with two thin vortices and studying their interaction. Their mutual interaction potential can be thus obtained. This interaction potential can then be extended to study the formation of vortex lattice as the angular frequency of rotation of the BEC is increased. This thin vortex may also be studied with respect to formation of a vortex tangle to study superfluid turbulence. Transport phenomenon in a BEC with a tangle of thin vortices would be of interest in this direction.

The 1D LGPE has been solved using the inverse scattering problem and is known to have infinitely many conserved quantities [165]. A crucial step for solving this problem is

obtaining what are called as *'Lax pairs'* for the problem. However, this inverse scattering problem has not been solved for corrections to the LGPE, nor have the Lax pairs for such a system been found. In this direction, the discovery of Lax pairs for the 1D LGPE with corrections is important. Even the discovery of Lax pairs for the first order correction would open a new line of inquiry into the problem. There may then exist a pattern for Lax pairs of corrections up to an arbitrary order. In any case, the Lax pairs for LGPE with first order correction would be crucial.

We have shown that roton minimum can be obtained and lowered at a lower value of gas parameter by adding additional components to the BEC. Lowering this roton minimum would lead to a solid order on top of the superfluid BEC. The nature of the order can be further explored. For a single component BEC, various phases of solid order have been proposed, which includes the 1D stripe phase [68] and various lattice structures [67]. However, such a study for more than one components has not been done to the best of our knowledge. In this direction the type of structure favoured by a multi-component system is of interest.

Finally, the effect of finite range of interactions can be studied in finite temperature models of BEC. The effect of temperature on BEC has been studied in literature and various finite temperature models have been proposed [166]. The applicability of these models depend on the system under consideration. However, the simultaneous effect of finite range of interactions and finite temperature has not been considered to the best of our knowledge. Such finite temperature models are usually proposed for exciton-polariton condensate where the temperature and dissipative effects become important. As such, the effect of finite range of interactions in such systems would be interesting to see. The interplay between the strengths of finite temperature corrections and finite range corrections might give an interplay between different phases in such systems.

We thus conclude our discussion on the results presented in the thesis and possible future works that may stem out of it. We sincerely hope that our work would kindle a lot of experimental interest towards the study of finite range effects in a BEC.

Bibliography

[1] Ganesan Venkataraman. *Bose and his Statistics*. Universities Press, 1992.

[2] SN Bose. Plancks law and light quantum hypothesis. *Z. Phys*, 26(1):178, 1924.

[3] A Einstein. Quantum theory of the monoatomic ideal gas. *Sitzungsber. Preuss. Akad. Wiss*, 1:3, 1925.

[4] Fritz London. On the Bose-Einstein condensation. *Physical Review*, 54(11):947, 1938.

[5] Harald F Hess. Evaporative cooling of magnetically trapped and compressed spin-polarized hydrogen. *Physical Review B*, 34(5):3476, 1986.

[6] William D Phillips and Harold J Metcalf. Cooling and trapping atoms. *Scientific American*, 256(3):50–57, 1987.

[7] William D Phillips. Nobel lecture: Laser cooling and trapping of neutral atoms. *Reviews of Modern Physics*, 70(3):721, 1998.

[8] Harold J Metcalf and Peter Van der Straten. *Laser cooling and trapping*. Springer Science & Business Media, 2012.

[9] Mike H Anderson, Jason R Ensher, Michael R Matthews, Carl E Wieman, and Eric A Cornell. Observation of Bose-Einstein condensation in a dilute atomic vapor. *Science*, 269(5221):198–201, 1995.

[10] Dale G Fried, Thomas C Killian, Lorenz Willmann, David Landhuis, Stephen C Moss, Daniel Kleppner, and Thomas J Greytak. Bose-Einstein condensation of atomic hydrogen. *Phys. Rev. Lett.*, 81(18):3811, 1998.

[11] Eugene P Gross. Quantum theory of interacting bosons. *Annals of Physics*, 9(2):292–324, 1960.

[12] LP Pitaevskii. Vortex lines in an imperfect Bose gas. *Sov. Phys. JETP*, 13(2):451–454, 1961.

[13] Eugene P Gross. Structure of a quantized vortex in boson systems. *Il Nuovo Cimento Series 10*, 20(3):454–477, 1961.

[14] Toshio Tsuzuki. Nonlinear waves in the pitaevskii-gross equation. *Journal of Low Temperature Physics*, 4(4):441–457, 1971.

[15] Philip G Drazin and Robin S Johnson. *Solitons: an introduction*, volume 2. Cambridge university press, 1989.

[16] William P Reinhardt and Charles W Clark. Soliton dynamics in the collisions of Bose-Einstein condensates: an analogue of the josephson effect. *Journal of Physics B: Atomic, Molecular and Optical Physics*, 30(22):L785, 1997.

[17] Richard P Feynman. Simulating physics with computers. *International journal of theoretical physics*, 21(6-7):467–488, 1982.

[18] Oliver Morsch and Markus Oberthaler. Dynamics of Bose-Einstein condensates in optical lattices. *Reviews of modern physics*, 78(1):179, 2006.

[19] David C Roberts and Masahito Ueda. Stability analysis for n-component Bose-Einstein condensate. *Physical Review A*, 73(5):053611, 2006.

[20] VI Yukalov and EP Yukalova. Stratification of moving multicomponent Bose-Einstein condensates. *Laser Physics Letters*, 1(1):50–53, 2004.

[21] Daniele Faccio, Francesco Belgiorno, Sergio Cacciatori, Vittorio Gorini, Stefano Liberati, and Ugo Moschella. *Analogue gravity phenomenology: analogue spacetimes and horizons, from theory to experiment*, volume 870. Springer, 2013.

[22] Carlos Barcelo, Stefano Liberati, and Matt Visser. Analogue gravity from Bose-Einstein condensates. *Classical and Quantum Gravity*, 18(6):1137, 2001.

[23] Luis Javier Garay, JR Anglin, J Ignacio Cirac, and P Zoller. Sonic analog of gravitational black holes in Bose-Einstein condensates. *Physical Review Letters*, 85(22):4643, 2000.

[24] Oren Lahav, Amir Itah, Alex Blumkin, Carmit Gordon, Shahar Rinott, Alona Zayats, and Jeff Steinhauer. Realization of a sonic black hole analog in a Bose-Einstein condensate. *Phys. Rev. Lett.*, 105(24):240401, 2010.

[25] V Bolpasi, NK Efremidis, MJ Morrissey, PC Condylis, D Sahagun, M Baker, and W von Klitzing. An ultra-bright atom laser. *New Journal of Physics*, 16(3):033036, 2014.

[26] William Guerin, J-F Riou, John P Gaebler, Vincent Josse, Philippe Bouyer, and Alain Aspect. Guided quasicontinuous atom laser. *Phys. Rev. Lett.*, 97(20):200402, 2006.

[27] NP Robins, PA Altin, JE Debs, and JD Close. Atom lasers: Production, properties and prospects for precision inertial measurement. *Physics Reports*, 529(3):265–296, 2013.

[28] Wolfgang Ketterle. Nobel lecture: When atoms behave as waves: Bose-Einstein condensation and the atom laser. *Reviews of Modern Physics*, 74(4):1131, 2002.

[29] D Kadio and YB Band. Analysis of a magnetically trapped atom clock. *Phys. Rev. A*, 74(5):053609, 2006.

[30] H Müntinga, H Ahlers, M Krutzik, A Wenzlawski, S Arnold, D Becker, K Bongs, H Dittus, H Duncker, N Gaaloul, et al. Interferometry with Bose-Einstein condensates in microgravity. *Phys. Rev. Lett.*, 110(9):093602, 2013.

[31] Ying-Ju Wang, Dana Z Anderson, Victor M Bright, Eric A Cornell, Quentin Diot, Tetsuo Kishimoto, Mara Prentiss, RA Saravanan, Stephen R Segal, and Saijun Wu. Atom michelson interferometer on a chip using a Bose-Einstein condensate. *Physical review letters*, 94(9):090405, 2005.

[32] Lene Vestergaard Hau, Stephen E Harris, Zachary Dutton, and Cyrus H Behroozi. Light speed reduction to 17 metres per second in an ultracold atomic gas. *Nature*, 397(6720):594–598, 1999.

[33] Oliver Zobay, Elena V Goldstein, and Pierre Meystre. Atom holography. *Phys. Rev. A*, 60(5):3999, 1999.

[34] C.J. Pethick and H. Smith. *Bose-Einstein Condensation in Dilute Gases*. Cambridge University Press, 2001.

[35] Haixiang Fu, Yuzhu Wang, and Bo Gao. Beyond the fermi pseudopotential: A modified gross-pitaevskii equation. *Phys. Rev. A*, 67:053612, 2003.

[36] A Collin, P Massignan, and CJ Pethick. Energy-dependent effective interactions for dilute many-body systems. *Physical Review A*, 75(1):013615, 2007.

[37] L. Pitaevskii and S. Stringari. *Bose-Einstein Condensation*. Oxford Science Publications, 2003.

[38] Jun John Sakurai and Jim Napolitano. *Modern quantum mechanics*. Addison-Wesley, 2011.

[39] Keith Burnett, Mark Edwards, and Charles W Clark. The theory of Bose-Einstein condensation of dilute gases. *Physics Today*, 52(12):37–42, 1999.

[40] Franco Dalfovo, Stefano Giorgini, Lev P Pitaevskii, and Sandro Stringari. Theory of Bose-Einstein condensation in trapped gases. *Reviews of Modern Physics*, 71 (3):463, 1999.

[41] SB Papp, JM Pino, RJ Wild, S Ronen, Carl E Wieman, Deborah S Jin, and Eric A Cornell. Bragg spectroscopy of a strongly interacting rb 85 bose-einstein condensate. *Physical review letters*, 101(13):135301, 2008.

[42] Neil R Claussen, Elizabeth A Donley, Sarah T Thompson, and Carl E Wieman. Microscopic dynamics in a strongly interacting Bose-Einstein condensate. *Physical review letters*, 89(1):010401, 2002.

[43] Tsin D Lee, Kerson Huang, and Chen N Yang. Eigenvalues and eigenfunctions of a Bose system of hard spheres and its low-temperature properties. *Physical Review*, 106(6):1135, 1957.

[44] D.B.M. Dickerscheid H.T.C. Stoof, K.B. Gubbels. *Ultracold Quantum Fields*. Springer, 2009.

[45] Abhijit Pendse. Long-range s-wave interactions in Bose-Einstein condensates: An exact correspondence between truncated free energy and dynamics. *International Journal of Theoretical Physics*, 56(7):2081–2085, 2017.

[46] Marvin E Cage, Kv Klitzing, AM Chang, F Duncan, M Haldane, Robert B Laughlin, AMM Pruisken, and DJ Thouless. *The quantum Hall effect*. Springer Science & Business Media, 2012.

[47] A Rozhkov and D Stroud. Quantum melting of a two-dimensional vortex lattice at zero temperature. *Physical Review B*, 54(18):R12697, 1996.

[48] FA Lindemann. Fa lindemann, phys. z. 11, 609 (1910). *Phys. Z.*, 11:609, 1910.

[49] Jasper Willem Reijnders. *Quantum Phases for rotating bosons*. 2005.

[50] Nigel R Cooper, Nicola K Wilkin, and JMF Gunn. Quantum phases of vortices in rotating Bose-Einstein condensates. *Physical review letters*, 87(12):120405, 2001.

[51] NR Cooper and NK Wilkin. Composite fermion description of rotating Bose-Einstein condensates. *Physical Review B*, 60(24):R16279, 1999.

[52] Nicolas Regnault and Th Jolicoeur. Quantum hall fractions in rotating Bose-Einstein condensates. *Physical review letters*, 91(3):030402, 2003.

[53] Erich J Mueller and Tin-Lun Ho. Two-component Bose-Einstein condensates with a large number of vortices. *Physical review letters*, 88(18):180403, 2002.

[54] Nicholas Read and E Rezayi. Beyond paired quantum hall states: Parafermions and incompressible states in the first excited landau level. *Physical Review B*, 59 (12):8084, 1999.

[55] V. Schweikhard, I. Coddington, P. Engels, V. P. Mogendorff, and E. A. Cornell. Rapidly rotating Bose-Einstein condensates in and near the lowest landau level. *Phys. Rev. Lett.*, 92:040404, Jan 2004.

[56] Alexander L Fetter, B Jackson, and S Stringari. Rapid rotation of a Bose-Einstein condensate in a harmonic plus quartic trap. *Physical Review A*, 71(1):013605, 2005.

[57] Susanne Viefers. Quantum hall physics in rotating Bose-Einstein condensates. *Journal of Physics: Condensed Matter*, 20(12):123202, 2008.

[58] Alexander L. Fetter. Rotating trapped Bose-Einstein condensates. *Rev. Mod. Phys.*, 81:647–691, 2009.

[59] DJ Frantzeskakis. Dark solitons in atomic Bose-Einstein condensates: from theory to experiments. *Journal of Physics A: Mathematical and Theoretical*, 43(21): 213001, 2010.

[60] S. Burger, K. Bongs, S. Dettmer, W. Ertmer, K. Sengstock, A. Sanpera, G. V. Shlyapnikov, and M. Lewenstein. Dark solitons in Bose-Einstein condensates. *Phys. Rev. Lett.*, 83:5198–5201, Dec 1999.

[61] J Denschlag, JE Simsarian, DL Feder, Charles W Clark, LA Collins, J Cubizolles, L Deng, EW Hagley, K Helmerson, William P Reinhardt, et al. Generating solitons by phase engineering of a Bose-Einstein condensate. *Science*, 287(5450):97–101, 2000.

[62] Supratik Sarkar and A Bhattacharyay. Non-local interactions in a bec: an analogue gravity perspective. *Journal of Physics A: Mathematical and Theoretical*, 47(9): 092002, 2014.

[63] J Steinhauer, R Ozeri, N Katz, and N Davidson. Excitation spectrum of a Bose-Einstein condensate. *Physical review letters*, 88(12):120407, 2002.

[64] M-O Mewes, MR Andrews, NJ Van Druten, DM Kurn, DS Durfee, CG Townsend, and W Ketterle. Collective excitations of a Bose-Einstein condensate in a magnetic trap. *Phys. Rev. Lett.*, 77(6):988, 1996.

[65] Sandro Stringari. Collective excitations of a trapped Bose-condensed gas. *Phys. Rev. Lett.*, 77(12):2360, 1996.

[66] Yves Pomeau and Sergio Rica. Dynamics of a model of supersolid. *Physical review letters*, 72(15):2426, 1994.

[67] Francesco Ancilotto, Maurizio Rossi, and Flavio Toigo. Supersolid structure and excitation spectrum of soft-core bosons in three dimensions. *Physical Review A*, 88(3):033618, 2013.

[68] Tommaso Macri, Fabian Maucher, Fabio Cinti, and Thomas Pohl. Elementary excitations of ultracold soft-core bosons across the superfluid-supersolid phase transition. *Physical Review A*, 87(6):061602, 2013.

[69] L Santos, GV Shlyapnikov, and M Lewenstein. Roton-maxon spectrum and stability of trapped dipolar Bose-Einstein condensates. *Physical review letters*, 90(25): 250403, 2003.

[70] PB Blakie, D Baillie, and RN Bisset. Roton spectroscopy in a harmonically trapped dipolar Bose-Einstein condensate. *Physical Review A*, 86(2):021604, 2012.

[71] N Henkel, R Nath, and T Pohl. Three-dimensional roton excitations and supersolid formation in rydberg-excited Bose-Einstein condensates. *Physical review letters*, 104(19):195302, 2010.

[72] Si-Cong Ji, Long Zhang, Xiao-Tian Xu, Zhan Wu, Youjin Deng, Shuai Chen, and Jian-Wei Pan. Softening of roton and phonon modes in a Bose-Einstein condensate with spin-orbit coupling. *Physical review letters*, 114(10):105301, 2015.

[73] Jun-Ru Li, Jeongwon Lee, Wujie Huang, Sean Burchesky, Boris Shteynas, Furkan Çağrı Top, Alan O Jamison, and Wolfgang Ketterle. A stripe phase with supersolid properties in spin–orbit-coupled Bose-Einstein condensates. *Nature*, 543 (7643):91, 2017.

[74] Yun Li, Giovanni I Martone, Lev P Pitaevskii, and Sandro Stringari. Superstripes and the excitation spectrum of a spin-orbit-coupled Bose-Einstein condensate. *Physical review letters*, 110(23):235302, 2013.

[75] R Mottl, F Brennecke, K Baumann, R Landig, T Donner, and T Esslinger. Roton-type mode softening in a quantum gas with cavity-mediated long-range interactions. *Science*, 336(6088):1570–1573, 2012.

[76] L.Landau. *Journal of Physics*, XI, No.1, 1947.

[77] Robert William Pattinson. *Two-component Bose-Einstein condensates: equilibria and dynamics at zero temperature and beyond.* Newcastle University, 2014.

[78] W. Ketterle et al. *Phys. Rev. Lett.*, 75, 3969, 1995.

[79] Frederick Reif. *Fundamentals of statistical and thermal physics.* Waveland Press, 2009.

[80] R.K. Pathria. *Statistical Mechanics.* Elsevier, 2011.

[81] Herbert B Callen. *Thermodynamics and an Introduction to Thermostatistics.* AAPT, 1998.

[82] VI Yukalov. Principal problems in Bose-Einstein condensation of dilute gases. *Laser Physics Letters*, 1(9):435–461, 2004.

[83] Leonard Sidney Rodberg and Raphael Morton Thaler. *Introduction to the quantum theory of scattering.* Academic Press, 1967.

[84] David J Griffiths and Darrell F Schroeter. *Introduction to quantum mechanics.* Cambridge University Press, 2018.

[85] Cheng Chin, Rudolf Grimm, Paul Julienne, and Eite Tiesinga. Feshbach resonances in ultracold gases. *Reviews of Modern Physics*, 82(2):1225, 2010.

[86] Eddy Timmermans, Paolo Tommasini, Mahir Hussein, and Arthur Kerman. Feshbach resonances in atomic Bose-Einstein condensates. *Physics Reports*, 315(1-3): 199–230, 1999.

[87] Kenichi Kasamatsu and Makoto Tsubota. Static and dynamic properties of multicomponent Bose-Einstein condensates of ytterbium atoms. *Journal of Low Temperature Physics*, 150(3-4):599–604, 2008.

[88] Yuki Kawaguchi and Masahito Ueda. Spinor Bose-Einstein condensates. *Physics Reports*, 520(5):253–381, 2012.

[89] Alexander L Fetter and Daniel Rokhsar. Excited states of a dilute Bose-Einstein condensate in a harmonic trap. *Phys. Rev. A*, 57(2):1191, 1998.

[90] Y Castin and R Dum. Bose-Einstein condensates in time dependent traps. *Physical Review Letters*, 77(27):5315, 1996.

[91] Victor M Perez-Garcia, Humberto Michinel, and Henar Herrero. Bose-Einstein solitons in highly asymmetric traps. *Physical Review A*, 57(5):3837, 1998.

[92] Anthony J. Leggett. Bose-Einstein condensation in the alkali gases: Some fundamental concepts. *Rev. Mod. Phys.*, 73:307–356, Apr 2001.

[93] Augusto Smerzi, Stefano Fantoni, Stefano Giovanazzi, and SR Shenoy. Quantum coherent atomic tunneling between two trapped Bose-Einstein condensates. *Physical Review Letters*, 79(25):4950, 1997.

[94] H Kamerlingh Onnes. The liquefaction of helium. *Koninklijke Nederlandse Akademie van Wetenschappen Proceedings Series B Physical Sciences*, 11:168–185, 1908.

[95] Pyotr Kapitza. Viscosity of liquid helium below the λ-point. *Nature*, 141(3558): 74, 1938.

[96] HR Glyde. Bose-Einstein condensation measurements and superflow in condensed helium. *Journal of Low Temperature Physics*, 172(5-6):364–387, 2013.

[97] Theodore H Maiman et al. Stimulated optical radiation in ruby. 1960.

[98] E. R. I. Abraham, W. I. McAlexander, C. A. Sackett, and Randall G. Hulet. Spectroscopic determination of the *s*-wave scattering length of lithium. *Phys. Rev. Lett.*, 74:1315–1318, 1995.

[99] Tino Weber, Jens Herbig, Michael Mark, Hanns-Christoph Nägerl, and Rudolf Grimm. Bose-Einstein condensation of cesium. *Science*, 299(5604):232–235, 2003.

[100] Giovanni Modugno, Gabriele Ferrari, Giacomo Roati, Robert J Brecha, A Simoni, and Massimo Inguscio. Bose-Einstein condensation of potassium atoms by sympathetic cooling. *Science*, 294(5545):1320–1322, 2001.

[101] Axel Griesmaier, Jörg Werner, Sven Hensler, Jürgen Stuhler, and Tilman Pfau. Bose-Einstein condensation of chromium. *Physical Review Letters*, 94(16):160401, 2005.

[102] Y. Castin, H. Wallis, and J. Dalibard. Limit of doppler cooling. *J. Opt. Soc. Am. B*, 6(11):2046–2057, 1989.

[103] Wolfgang Ketterle, Dallin S Durfee, and DM Stamper-Kurn. Making, probing and understanding Bose-Einstein condensates. *arXiv preprint cond-mat/9904034*, 1999.

[104] Wolfgang Petrich, Michael H Anderson, Jason R Ensher, and Eric A Cornell. Stable, tightly confining magnetic trap for evaporative cooling of neutral atoms. *Physical Review Letters*, 74(17):3352, 1995.

[105] David E Pritchard. Cooling neutral atoms in a magnetic trap for precision spectroscopy. *Physical Review Letters*, 51(15):1336, 1983.

[106] GM Tino and M Inguscio. Experiments on Bose-Einstein condensation. *La Rivista del Nuovo Cimento (1978-1999)*, 22(4):1, 1999.

[107] Cl C Bradley, CA Sackett, JJ Tollett, and Randall G Hulet. Evidence of Bose-Einstein condensation in an atomic gas with attractive interactions. *Physical review letters*, 75(9):1687, 1995.

[108] JE Simsarian, J Denschlag, Mark Edwards, Charles W Clark, Lu Deng, Edward W Hagley, Kristian Helmerson, SL Rolston, and William D Phillips. Imaging the phase of an evolving Bose-Einstein condensate wave function. *Physical review letters*, 85(10):2040, 2000.

[109] Stefan Schmid, Arne Härter, and Johannes Hecker Denschlag. Dynamics of a cold trapped ion in a Bose-Einstein condensate. *Physical review letters*, 105(13):133202, 2010.

[110] Curtis Charles Bradley, CA Sackett, and RG Hulet. Bose-Einstein condensation of lithium: Observation of limited condensate number. *Physical Review Letters*, 78(6):985, 1997.

[111] R Meppelink, RA Rozendaal, SB Koller, JM Vogels, and P Van der Straten. Thermodynamics of Bose-Einstein condensed clouds using phase-contrast imaging. *Physical Review A*, 81(5):053632, 2010.

[112] Jacob F Sherson, Christof Weitenberg, Manuel Endres, Marc Cheneau, Immanuel Bloch, and Stefan Kuhr. Single-atom-resolved fluorescence imaging of an atomic mott insulator. *Nature*, 467(7311):68, 2010.

[113] EAL Henn, JA Seman, G Roati, Kilvia Mayre Farias Magalhães, and Vanderlei Salvador Bagnato. Emergence of turbulence in an oscillating Bose-Einstein condensate. *Physical review letters*, 103(4):045301, 2009.

[114] JR Abo-Shaeer, C Raman, JM Vogels, and Wolfgang Ketterle. Observation of vortex lattices in Bose-Einstein condensates. *Science*, 292(5516):476–479, 2001.

[115] C Raman, JR Abo-Shaeer, JM Vogels, K Xu, and W Ketterle. Vortex nucleation in a stirred Bose-Einstein condensate. *Physical review letters*, 87(21):210402, 2001.

[116] KW Madison, F Chevy, W Wohlleben, and J Dalibard. Vortex formation in a stirred Bose-Einstein condensate. *Phys. Rev. Lett.*, 84(5):806, 2000.

[117] PC Haljan, I Coddington, Peter Engels, and Eric A Cornell. Driving Bose-Einstein condensate vorticity with a rotating normal cloud. *Physical review letters*, 87(21): 210403, 2001.

[118] AE Leanhardt, A Görlitz, AP Chikkatur, D Kielpinski, Y-i Shin, DE Pritchard, and W Ketterle. Imprinting vortices in a Bose-Einstein condensate using topological phases. *Physical review letters*, 89(19):190403, 2002.

[119] Nigel R Cooper, Nicola K Wilkin, and JMF Gunn. Quantum phases of vortices in rotating Bose-Einstein condensates. *Phys. Rev. Lett.*, 87(12):120405, 2001.

[120] Seji Kang, J Choi, SW Seo, WJ Kwon, and Y Shin. Rotating a Bose-Einstein condensate by shaking an anharmonic axisymmetric magnetic potential. *Phys. Rev. A*, 91(1):013603, 2015.

[121] BP Anderson, PC Haljan, CA Regal, DL Feder, LA Collins, Charles W Clark, and Eric A Cornell. Watching dark solitons decay into vortex rings in a Bose-Einstein condensate. *Physical Review Letters*, 86(14):2926, 2001.

[122] AE Muryshev, HB van Linden van den Heuvell, and GV Shlyapnikov. Stability of standing matter waves in a trap. *Physical Review A*, 60(4):R2665, 1999.

[123] P Öhberg and L Santos. Dark solitons in a two-component Bose-Einstein condensate. *Physical review letters*, 86(14):2918, 2001.

[124] Chad N Weiler, Tyler W Neely, David R Scherer, Ashton S Bradley, Matthew J Davis, and Brian P Anderson. Spontaneous vortices in the formation of Bose-Einstein condensates. *Nature*, 455(7215):948, 2008.

[125] Kali E Wilson, Zachary L Newman, Joseph D Lowney, and Brian P Anderson. In situ imaging of vortices in Bose-Einstein condensates. *Physical Review A*, 91(2):023621, 2015.

[126] Michael Robin Matthews, Brian P Anderson, PC Haljan, DS Hall, CE Wieman, and Eric A Cornell. Vortices in a Bose-Einstein condensate. *Physical Review Letters*, 83(13):2498, 1999.

[127] Joachim Brand and William P Reinhardt. Solitonic vortices and the fundamental modes of the snake instability: Possibility of observation in the gaseous Bose-Einstein condensate. *Physical Review A*, 65(4):043612, 2002.

[128] KE Strecker, GB Partridge, AG Truscott, and Randall G Hulet. Bright matter wave solitons in Bose-Einstein condensates. *New Journal of Physics*, 5(1):73, 2003.

[129] J Denschlag, JE Simsarian, DL Feder, Charles W Clark, LA Collins, J Cubizolles, Lu Deng, Edward W Hagley, Kristian Helmerson, William P Reinhardt, et al. Generating solitons by phase engineering of a Bose-Einstein condensate. *Science*, 287(5450):97–101, 2000.

[130] LD Carr, J Brand, S Burger, and A Sanpera. Dark-soliton creation in Bose-Einstein condensates. *Physical Review A*, 63(5):051601, 2001.

[131] Biao Wu, Jie Liu, and Qian Niu. Controlled generation of dark solitons with phase imprinting. *Physical review letters*, 88(3):034101, 2002.

[132] GA El, A Gammal, and AM Kamchatnov. Oblique dark solitons in supersonic flow of a Bose-Einstein condensate. *Physical review letters*, 97(18):180405, 2006.

[133] J Stenger, S Inouye, Ananth P Chikkatur, DM Stamper-Kurn, DE Pritchard, and Wolfgang Ketterle. Bragg spectroscopy of a Bose-Einstein condensate. *Physical Review Letters*, 82(23):4569, 1999.

[134] Roger G Newton. *Scattering theory of waves and particles.* Springer Science & Business Media, 2013.

[135] Abhijit Pendse and Arijit Bhattacharyay. Effect of non-local interactions on the vortex solution in Bose-Einstein condensates. *The European Physical Journal B*, 90(12):244, 2017.

[136] Makoto Tsubota, Kenichi Kasamatsu, and Masahito Ueda. Vortex lattice formation in a rotating Bose-Einstein condensate. *Physical Review A*, 65(2):023603, 2002.

[137] R Srinivasan. Vortices in Bose-Einstein condensates: A review of the experimental results. *Pramana*, 66(1):3–30, 2006.

[138] Marios C Tsatsos, Pedro ES Tavares, André Cidrim, Amilson R Fritsch, Mônica A Caracanhas, F Ednilson A dos Santos, Carlo F Barenghi, and Vanderlei S Bagnato. Quantum turbulence in trapped atomic Bose-Einstein condensates. *Physics Reports*, 622:1–52, 2016.

[139] Bogdan Damski and Wojciech H Zurek. Soliton creation during a Bose-Einstein condensation. *Physical review letters*, 104(16):160404, 2010.

[140] Scott E Pollack, D Dries, Mark Junker, YP Chen, TA Corcovilos, and RG Hulet. Extreme tunability of interactions in a li 7 Bose-Einstein condensate. *Physical Review Letters*, 102(9):090402, 2009.

[141] MA Helal. Soliton solution of some nonlinear partial differential equations and its applications in fluid mechanics. *Chaos, Solitons & Fractals*, 13(9):1917–1929, 2002.

[142] James Roy Taylor. *Optical solitons: theory and experiment*, volume 10. Cambridge University Press, 1992.

[143] Peter Ciblis and Irena Cosic. The possibility of soliton/exciton transfer in proteins. *Journal of Theoretical Biology*, 184(3):331–338, 1997.

[144] Sigeo Yomosa. Soliton excitations in deoxyribonucleic acid (dna) double helices. *Physical Review A*, 27(4):2120, 1983.

[145] Lyubov V Doronina, Aleksandr A Voronin, Olga I Ivashkina, Marina A Zots, Konstantin V Anokhin, Ekaterina Rostova, Andrei B Fedotov, and Aleksei M Zheltikov. Tailoring the soliton output of a photonic crystal fiber for enhanced two-photon excited luminescence response from fluorescent protein biomarkers and neuron activity reporters. *Optics letters*, 34(21):3373–3375, 2009.

[146] Stefan Burger, K Bongs, S Dettmer, W Ertmer, K Sengstock, A Sanpera, GV Shlyapnikov, and M Lewenstein. Dark solitons in Bose-Einstein condensates. *Phys. Rev. Lett.*, 83(25):5198, 1999.

[147] S Inouye, MR Andrews, J Stenger, H-J Miesner, DM Stamper-Kurn, and W Ketterle. Observation of feshbach resonances in a Bose-Einstein condensate. *Nature*, 392(6672):151–154, 1998.

[148] Wenlong Wang and PG Kevrekidis. Two-component dark-bright solitons in three-dimensional atomic Bose-Einstein condensates. *Physical Review E*, 95(3):032201, 2017.

[149] Ian B Spielman, Lauren M Aycock, Dina Genkina, Hsin I Lu, Hilary Hurst, and Victor Galitski. Impurity driven brownian motion of solitons in elon-gated Bose-Einstein condensates. *Nature Physics*, 2017.

[150] Wieslaw Krolikowski, Ole Bang, Jens Juul Rasmussen, and John Wyller. Modulational instability in nonlocal nonlinear kerr media. *Physical Review E*, 64(1):016612, 2001.

[151] Wiesław Królikowski and Ole Bang. Solitons in nonlocal nonlinear media: Exact solutions. *Physical Review E*, 63(1):016610, 2000.

[152] Y Sivan, G Fibich, B Ilan, and MI Weinstein. Qualitative and quantitative analysis of stability and instability dynamics of positive lattice solitons. *Physical Review E*, 78(4):046602, 2008.

[153] K.H. Spatschek E.W. Ladtke and L. Stenflo. *Journal of Math. Phys.*, 24.

[154] GV Chester. Speculations on Bose-Einstein condensation and quantum crystals. *Phys. Rev. A*, 2(1):256, 1970.

[155] DJ McCarron, HW Cho, DL Jenkin, MP Köppinger, and SL Cornish. Dual-species Bose-Einstein condensate of rb 87 and cs 133. *Physical Review A*, 84(1):011603, 2011.

[156] Abhijit Pendse. Effect of finite range interactions on roton mode softening in a multi-component bec. *Journal of Physics B: Atomic, Molecular and Optical Physics*, 51(8):085303, 2018.

[157] P Ao and ST Chui. Binary Bose-Einstein condensate mixtures in weakly and strongly segregated phases. *Physical Review A*, 58(6):4836, 1998.

[158] AS Alexandrov and Viktor V Kabanov. Excitations and phase segregation in a two-component Bose-Einstein condensate with an arbitrary interaction. *Journal of Physics: Condensed Matter*, 14(18):L327, 2002.

[159] Cheng Chin and V. V. Flambaum. Enhanced sensitivity to fundamental constants in ultracold atomic and molecular systems near feshbach resonances. *Phys. Rev. Lett.*, 96:230801, 2006.

[160] G Smirne, RM Godun, D Cassettari, V Boyer, CJ Foot, Thomas Volz, Niels Syassen, Stephan Dürr, Gerhard Rempe, MD Lee, et al. Collisional relaxation of feshbach molecules and three-body recombination in rb 87 Bose-Einstein condensates. *Physical Review A*, 75(2):020702, 2007.

[161] Elmar Haller, Mohamed Rabie, Manfred J Mark, Johann G Danzl, Russell Hart, Katharina Lauber, Guido Pupillo, and H-C Nägerl. Three-body correlation functions and recombination rates for bosons in three dimensions and one dimension. *Physical review letters*, 107(23):230404, 2011.

[162] Matteo Zaccanti, Benjamin Deissler, Chiara DErrico, Marco Fattori, Mattia Jona-Lasinio, Stefan Müller, Giacomo Roati, Massimo Inguscio, and Giovanni Modugno. Observation of an efimov spectrum in an atomic system. *Nature Physics*, 5(8):586–591, 2009.

[163] Noam Gross, Zav Shotan, Servaas Kokkelmans, and Lev Khaykovich. Observation of universality in ultracold li 7 three-body recombination. *Physical review letters*, 103(16):163202, 2009.

[164] J Stenger, S Inouye, MR Andrews, H-J Miesner, DM Stamper-Kurn, and W Ketterle. Strongly enhanced inelastic collisions in a Bose-Einstein condensate near feshbach resonances. *Physical review letters*, 82(12):2422, 1999.

[165] A Shabat and V Zakharov. Exact theory of two-dimensional self-focusing and one-dimensional self-modulation of waves in nonlinear media. *Soviet physics JETP*, 34(1):62, 1972.

[166] Nick P Proukakis and Brian Jackson. Finite-temperature models of Bose-Einstein condensation. *Journal of Physics B: Atomic, Molecular and Optical Physics*, 41 (20):203002, 2008.